

SYNTHESIS AND ELECTROPOLYMERIZATION OF PHTHALOCYANINE DERIVATIVES FOR
ELECTROCHEMICAL REDUCTION OF CARBON DIOXIDE



A Dissertation Submitted in Partial Fulfillment of the Requirements
for the Degree of Doctor of Philosophy in Chemistry

Department of Chemistry

Faculty of Science

Chulalongkorn University

Academic Year 2019

Copyright of Chulalongkorn University

การสังเคราะห์และอิเล็กโทรพอลิเมอไรเซชันของอนุพันธ์เทโไลซานินสำหรับรีดักชันเชิงเคมีไฟฟ้า
ของคาร์บอนไดออกไซด์



วิทยานิพนธ์นี้เป็นส่วนหนึ่งของการศึกษาตามหลักสูตรปริญญาวิทยาศาสตรดุษฎีบัณฑิต
สาขาวิชาเคมี ภาควิชาเคมี
คณะวิทยาศาสตร์ จุฬาลงกรณ์มหาวิทยาลัย
ปีการศึกษา 2562
ลิขสิทธิ์ของจุฬาลงกรณ์มหาวิทยาลัย

จรรยาบรรณ : การสังเคราะห์และอิเล็กโทรพอลิเมอร์ไรเซชันของอนุพันธ์ไทโ
 ไชยานินสำหรับรีดักชันเชิงเคมีไฟฟ้าของคาร์บอนไดออกไซด์. (SYNTHESIS AND
 ELECTROPOLYMERIZATION OF PHTHALOCYANINE DERIVATIVES FOR
 ELECTROCHEMICAL REDUCTION OF CARBON DIOXIDE) อ.ที่ปรึกษาหลัก : ศ. ดร.
 พัชณิตา ธรรมรงค์กิจ

งานวิจัยนี้อธิบายการสังเคราะห์และพอลิเมอร์ไรเซชันทางไฟฟ้าเคมีของไทโ
 ไชยานินชนิดใหม่ ที่มีหมู่แทนที่ไบโทอีนเพื่อให้ได้ฟิล์มพอลิเมอร์ที่มีความสามารถในการเร่งปฏิกิริยาทางรีดักชันของ
 คาร์บอนไดออกไซด์ (CO₂) มอนอเมอร์ไทโไชยานินเป้าหมายสังเคราะห์ขึ้นโดยกระบวนการสองขั้นตอน
 ผ่านปฏิกิริยาซุซูกิและไซโคลเซชันของไทโไชยานินไตรล์ที่ได้ หลังจากนั้นปฏิกิริยาพอลิเมอร์ไรเซชันทางไฟฟ้า
 ของมอนอเมอร์เป้าหมายบนกระจกที่เคลือบด้วยอินเดียมทินออกไซด์และกระดาษคาร์บอนถูกดำเนินการ
 ด้วยเทคนิคไซคลิกโวลแทมเมตรี ฟิล์มพอลิเมอร์ที่ได้ถูกนำมาพิสูจน์เอกลักษณ์ด้วยวิธีทางสเปกโตรสโคปี
 หลากหลายวิธี ประสิทธิภาพการเร่งปฏิกิริยารีดักชันทางไฟฟ้าเคมีของ CO₂ ของพอลิเมอร์เหล่านี้ถูก
 ตรวจสอบด้วยเทคนิคไซคลิกโวลแทมเมตรีและการวัดอิเล็กโทรไลซิสแบบควบคุมศักย์ไฟฟ้า ผลการ
 ทดลองแสดงให้เห็นว่าฟิล์มพอลิเมอร์ของอนุพันธ์โคบอลต์ไทโไชยานินบนกระดาษคาร์บอนแสดง
 ประสิทธิภาพในการเร่งเชิงไฟฟ้าทางการรีดักชันของ CO₂ ที่โดดเด่นในบรรดาพอลิเมอร์ทั้งหมดโดยให้
 คาร์บอนมอนอกไซด์ (CO) เป็นผลิตภัณฑ์หลักที่ประสิทธิภาพฟาราเดย์ (FE) 94 เปอร์เซ็นต์ โดยการให้
 ศักย์ไฟฟ้า -1.30 โวลต์เทียบกับขั้วไฟฟ้าอ้างอิงแบบซิลเวอร์/ซิลเวอร์คลอไรด์ (3 โมลาร์ โพแทสเซียมคลอ
 ไรด์) และสารละลายในน้ำของ 0.5 โมลาร์โพแทสเซียมโบคาร์บอเนตในเซลล์แบบสองห้องสามอิเล็กโทรด
 หลังจากอิเล็กโทรไลซิสเป็นเวลา 2 ชั่วโมง ในการทำการอิเล็กโทรไลซิส 20 ชั่วโมงภายใต้ภาวะเดียวกัน
 โดยการติดตามด้วยเทคนิคออนไลน์แก๊สโครมาโทกราฟี ฟิล์มพอลิเมอร์นี้มีความเสถียรตลอดการทดลอง
 และให้ CO ที่ความหนาแน่นกระแสคงที่และ FE 72 เปอร์เซ็นต์ ซึ่งสอดคล้องกับจำนวนการหมุนเวียน
 สะสมและความถี่การหมุนเวียนเฉลี่ย 12,359 และ 0.17 วินาที⁻¹ ตามลำดับ

สาขาวิชา เคมี
 ปีการศึกษา 2562

ลายมือชื่อนิสิต
 ลายมือชื่อ อ.ที่ปรึกษาหลัก

5771942923 : MAJOR CHEMISTRY

KEYWORD: phthalocyanine derivatives, electrochemical polymerization,
electrochemical reduction of carbon dioxide

Jirapong Luangchaiyaporn : SYNTHESIS AND ELECTROPOLYMERIZATION OF
PHTHALOCYANINE DERIVATIVES FOR ELECTROCHEMICAL REDUCTION OF
CARBON DIOXIDE. Advisor: Prof. PATCHANITA THAMYONGKIT, Dr.rer.nat.

This research describes synthesis and electrochemical polymerization of novel bithiophenyl-substituted phthalocyanines in order to get polymeric films that have electrocatalytic activities towards reduction of carbon dioxide (CO₂). The target phthalocyanine monomers are synthesized by a two-step procedure including Suzuki reaction and cyclization of the resulting phthalonitrile. After that, electropolymerization of the target monomers on an indium tin oxide-coated glasses or carbon papers is performed by a cyclic voltammetry technique. The resulting polymer films are characterized by various spectroscopic methods. Catalytic performance towards the electrochemical reduction of CO₂ of these polymers is investigated by the cyclic voltammetry and controlled potential electrolysis measurements. The results show that the polymer film of the cobalt(II) phthalocyanine derivative on the carbon papers exhibits remarkable electrocatalytic performance among all polymers by giving carbon monoxide (CO) with faradaic efficiency (FE) 94% as a major product by applying potential of -1.30 V vs. Ag/AgCl (3M KCl) and a 0.5 M KHCO₃ aqueous solution in a three-electrode two-compartment cell after 2-h electrolysis. Upon 20-h electrolysis under the same condition by using online gas chromatography monitoring, this polymer film is found to be stable throughout the experiment and afforded CO at constant current density and FE of 72%, corresponding to accumulated turnover number and average turnover frequency of 12,359 and 0.17 s⁻¹, respectively.

Field of Study: Chemistry

Student's Signature

Academic Year: 2019

Advisor's Signature

ACKNOWLEDGEMENTS

Firstly, I would like to express my gratitude to Prof. Dr. Patchanita Thamyongkit who is my advisor for supporting, encouraging, advising, trusting and giving me many opportunities during my PhD study. Without her valuable guidance, my dissertation would not have been possible. I also would like to thank Assoc. Prof. Dr. Vudhichai Parasuk for serving as a chairman, Prof. Dr. Thawatchai Tuntulani and Assoc. Prof. Dr. Buncha Pulpoka for serving as examiners, and Assoc. Prof. Dr. Nantanit Wanichacheva for serving as an external examiner, and for their profound suggestions and comments in this dissertation.

Secondly, I would like to sincerely thank o.Univ. Prof. Mag. Dr. DDr. h.c. Niyazi Serdar Sariciftci and Prof. Dr. Dr. h. c. Dietrich R.T. Zahn for providing me the opportunities to do my research and access a lot of analytical and spectroscopic instruments in their laboratories at JKU Institute of Physical Chemistry / Linz Institute of Organic Solar Cells (LIOS) in Austria and at Technische Universität Chemnitz in Germany, respectively. Besides, I also thank all members in these groups for their valuable friendship and great helpfulness.

Additionally, I would like to thank financial supports for my PhD study provided by Science Achievement Scholarship of Thailand (SAST), Graduate School of Chulalongkorn University (The 90th Anniversary of Chulalongkorn University Fund, Ratchadaphiseksomphot Endowment Fund, and Overseas Research Experience Scholarship for Graduate Students) and International Promovieren an der Technischen Universität Chemnitz (InProTUC).

Finally, I would like to express my deepest appreciation to my family (my father, my mother and my younger brothers), my friends and my colleagues for their love, understanding, great support and encouragement throughout my PhD study.

Jirapong Luangchaiyaporn

TABLE OF CONTENTS

	Page
ABSTRACT (THAI).....	iii
ABSTRACT (ENGLISH).....	iv
ACKNOWLEDGEMENTS.....	v
TABLE OF CONTENTS.....	vi
LIST OF FIGURES.....	ix
LIST OF SCHEMES.....	xvi
LIST OF TABLES.....	xvii
CHAPTER 1 INTRODUCTION.....	1
1.1 Objectives of this research.....	4
1.2 Scopes of this research.....	4
CHAPTER 2 THEORY AND LITERATURE REVIEWS.....	5
2.1 Electrochemical reduction of CO ₂	5
2.2 Free base phthalocyanine (H ₂ Pc) and metallophthalocyanine (MPc).....	7
2.2.1 Optical properties of Pc and MPc.....	8
2.2.2 Redox properties of MPc.....	9
2.3 Electrochemical polymerization techniques.....	10
2.4 Electrochemical methods ⁶⁶	12
2.4.1 Cyclic voltammetry (CV).....	12
2.2.2 Chronoamperometry (CA) or controlled potential electrolysis (CPE).....	14
2.5. Gas Chromatography (GC) ^{79, 80}	15
2.6. Ion Chromatography (IC) ⁸¹	15

2.7 Raman spectroscopy ^{84, 85}	16
2.8 X-ray photoelectron spectroscopy (XPS) ⁸⁹	18
CHAPTER 3 EXPERIMENTS	19
3.1 Chemicals.....	19
3.2 Analytical Instruments	19
3.3 Synthesis Procedures	20
3.3.1 4-([2,2'-bithiophen]-5-yl)phthalonitrile (1).....	20
3.3.2 2,9,16,23-tetra([2,2'-bithiophen]-5-yl)phthalocyaninato-zinc(II) (ZnPc-2T). 21	
3.3.3 2,9,16,23-tetra([2,2'-bithiophen]-5-yl)phthalocyaninato-cobalt(II) (CoPc-2T)	
.....	22
3.3.4 2,9,16,23-tetra([2,2'-bithiophen]-5-yl)phthalocyaninato-copper(II) (CuPc-2T)	
.....	23
3.3.5 2,9,16,23-tetra([2,2'-bithiophen]-5-yl)phthalocyaninato-nickel(II) (NiPc-2T)	
.....	24
3.3.6 2,9,16,23-tetra([2,2'-bithiophen]-5-yl)phthalocyanine (H ₂ Pc-2T)	25
3.4 Electrochemistry.....	26
3.4.1 Electropolymerization	26
3.4.2 CPE in a one-compartment electrochemical cell	27
3.4.3 CPE in a two-compartment electrochemical cell	28
CHAPTER 4 RESULTS AND DISCUSSION.....	31
4.1 Synthesis and characterization of the target compounds	31
4.1.1 Synthesis and characterization of MPc-2Th	31
4.1.2 Investigation of photophysical properties of the target compounds	34
4.2 Preparation and characterization of the target polymers	38
4.2.1 Electrochemical polymerization of ZnPc-2T.....	38

4.2.2 Electrochemical polymerization of CoPc-2T.....	39
4.2.3 Investigation of the photophysical properties of the polymer films.....	41
4.3 Investigation of the electrocatalytic performance of the target polymers towards the CO ₂ reduction	48
4.3.1 Cyclic voltammetry (CV) studies and controlled potential electrolysis (CPE) measurements in a one-compartment cell and organic medium. .	48
4.3.2 Cyclic voltammetry (CV) studies and controlled potential electrolysis (CPE) measurements in a two-compartment cell and aqueous medium.	52
4.4 Comparison to other literatures	65
CHAPTER 5 CONCLUSION.....	67
REFERENCES	69
APPENDIX.....	82
VITA.....	99

LIST OF FIGURES

	Page
Figure 1-1. Amount of CO ₂ (dark line) and temperature change (blue line) for the past 800,000 years, based on EPICA (ice core) data.....	1
Figure 1-2. Systematic artificial carbon cycle.....	2
Figure 1-3. A general structure of target compounds.....	3
Figure 2-1. Schematic diagrams of ECR of CO ₂ under (a) homogenous (b) heterogenous catalysis.....	6
Figure 2-2. typical spectra of H ₂ Pc and MPc.....	8
Figure 2-3. Gouteman's four-orbital linear combination of atomic orbital model. ²⁶ ...	9
Figure 2-4. Molecular structures of some H ₂ Pc and MPc derivatives bearing electrochemically polymerizable peripheral units.....	11
Figure 2-5. A schematic diagram of a three-electrode one-compartment electrochemical cell.....	13
Figure 2-6. Excitation signals of cyclic voltammetry.....	13
Figure 2-7. Cyclic voltammograms of the first electrochemical a) reduction and b) oxidation.....	13
Figure 2-8. a) An excitation signal for CA and b) a chronoamperometric response. ⁶⁶	14
Figure 2-9. A schematic diagram of a GC setup.....	15
Figure 2-10. Schematic diagram of an ion chromatography setup.....	16
Figure 2-11. Energy diagrams of resonance Raman scattering and non-resonance Raman scattering spectroscopies, comparing with other spectroscopic techniques...	17
Figure 2-12. A schematic diagram of a photoelectron emission process.....	18

Figure 3-1. A one-compartment three-electrode electrochemical set up for electropolymerization.	27
Figure 3-2. A one-compartment three-electrode electrochemical set up for CPE experiments.	28
Figure 3-3. A two-compartment three-electrode electrochemical cell.	29
Figure 3-4. A two-compartment three-electrode electrochemical setup connected with online GC.....	30
Figure 4-1. Absorption spectra and solution of (a) ZnPc , (b) CoPc and (C) H₂Pc derivatives having no substituent (black solid line and left flasks) and bearing bithiophenyl β -groups (red dashed lines and right flasks).....	35
Figure 4-2. Emission spectra of ZnPc (black solid line) and ZnPc-2T (red dashed line) solutions upon excitation at their (a) B and (b) Q bands, and H₂Pc (black solid line) and H₂Pc-2T (red dashed line) solutions upon excitation at their (c) B and (d) Q bands.....	36
Figure 4-3. Cyclic voltammograms and films obtained from electrochemical polymerization of ZnPc-2T at the first cycle (black solid line), the 2 nd -9 th cycles (red dotted lines) and the 10 th cycle (blue dashed line) on (a) an ITO/glass and (b) a carbon paper.	39
Figure 4-4. Cyclic voltammograms and films obtained from electrochemical polymerization of CoPc-2T at the first cycle (black solid line), (a) the 2 nd -19 th cycles (red dotted lines) and 20 th (blue dashed line) on an ITO/glass and (b) 2 nd -39 th (red dotted lines) and the 40 th cycles (blue dashed line) on a carbon paper.	40
Figure 4-5. Absorption spectra of (a) a ZnPc-2T solution in THF (black solid line), a drop-casted film of ZnPc-2T (red dashed line) and a poly(ZnPc-2T) film on an ITO/glass (blue dotted line), and (b) a CoPc-2T solution in THF (black solid line), a drop-casted film of CoPc-2T (red dashed line) and a poly(CoPc-2T) film on the ITO/glass (blue dotted line).	42

Figure 4–6. Raman spectra of **2T** (black line), **ZnPc** (red line), **ZnPc-2T** (blue line) and **poly(ZnPc-2T)** (green line) upon laser excitation at (a) 514.7 nm and (b) 633 nm, as well as Raman spectra of **2T** (black line), **CoPc** (red line), **CoPc-2T** (blue line) and **poly(CoPc-2T)** (green line) at laser excitation at (c) 514.7 nm and (d) 633 nm. 44

Figure 4–7. ATR FT-IR spectra of bithiophene (**2T**) (black line), unsubstituted **MPc** (red line), **MPc-2T** (blue line) and **poly(MPc-2T)** (green line) when M is (a) Zn and (b) Co. 45

Figure 4–8. (a) a Microscopic image, (b) a SEM image, and EDX maps showing (c) sulfur (S) and (d) zinc (Zn) atoms of a **poly(ZnPc-2T)** film on a carbon paper. 47

Figure 4–9. (a) a Microscopic image, (b) a SEM image, and EDX maps showing (c) sulfur (S) and (d) cobalt (Co) atoms of a **poly(CoPc-2T)** film on a carbon paper. 47

Figure 4–10. Cyclic voltammogram of a **poly(ZnPc-2T)**-modified carbon paper under N_2 - (thick black solid line) and CO_2 -saturated (thick red dashed line) conditions, compared with those of bare carbon papers under the N_2 - (thin black solid line) and CO_2 -saturated (thin red dashed line) conditions recorded in a 0.1 M TBAPF₆ in ACN solution in a one-compartment three-electrode cell. 49

Figure 4–11. Cyclic voltammograms of a **poly(CoPc-2T)**-modified carbon paper under N_2 - (thick black solid line) and CO_2 -saturated (thick red dashed line) conditions compared with those of bare carbon papers under the N_2 - (thin black solid line) and CO_2 -saturated (thin red dashed line) conditions recorded in a 0.1 M TBAPF₆ in ACN solution in a one-compartment three-electrode cell. 50

Figure 4–12. Chronoamperometric responses of the ECR of CO_2 in a 0.1 M TBAPF₆ solution in ACN at the potential of -1.70 V vs. Ag/AgCl QRE for (a) 3 h and (b) 12 h of a bare carbon paper (square symbol with black line), a **poly(ZnPc-2T)**-modified carbon paper (circle symbol with red line) and a **poly(CoPc-2T)**-modified carbon paper (triangle symbol with blue line) in a one-compartment three-electrode cell. . 51

Figure 4–13. Cyclic voltammograms of (a) **poly(ZnPc-2T)**- and (b) **poly(CoPc-2T)**-modified carbon papers under N_2 - (thick black solid line) and CO_2 -saturated (thick red dashed line) condition, compared with those of bare carbon papers under the N_2 -

(thin black solid line) and CO₂-saturated (thin red dashed line) conditions recorded in a 0.5 M KHCO₃ solution in a two-compartment three-electrode cell. 53

Figure 4–14. (a) Chronoamperometric responses of a CPE experiment at the potential of –1.20 V vs. Ag/AgCl (3M KCl) for 2 h of a bare carbon paper under N₂- (black line) or CO₂- (red line) saturated conditions, a **poly(ZnPc-2T)**-modified carbon paper under CO₂-saturated condition (square symbol with black line) and a **poly(CoPc-2T)**-modified carbon paper under N₂-(cycle symbol with red line) or CO₂- (triangle symbol with blue line) saturated condition in a 0.5 M KHCO₃ electrolyte b) % Faradaic efficiencies of CO and H₂ production from the CPE at the potential of –1.20 V vs. Ag/AgCl (3M KCl) for 2 h in presence of a bare carbon paper, and a **poly(ZnPc-2T)**- and a **poly(CoPc-2T)**-modified carbon papers in a N₂- or CO₂-saturated 0.5 M KHCO₃ electrolyte solution and a two-compartment three-electrode cell. 55

Figure 4–15. a) Chronoamperometric responses of 2-h CPE using a **poly(CoPc-2T)**-modified carbon paper as a WE in a N₂-saturated 0.5 M KHCO₃ solution at the applied potential of –1.20 V (square symbol with black line) and at –1.30 V vs. Ag/AgCl (3M KCl) (circle symbol with red line) and in a CO₂-saturated one under applied potential at –1.20 V (up-pointing triangle symbol with blue line) and at –1.30 V vs. Ag/AgCl (3M KCl) (down-pointing triangle symbol with green line) in a two-compartment three-electrode electrochemical cell. 57

Figure 4–16. a) % FE of CO and H₂ formation from 2-h CPE at applied potentials of –1.20 V and –1.30 V vs. Ag/AgCl (3M KCl) in the absence and presence of a **poly(CoPc-2T)** film on carbon paper and in a N₂- or CO₂-saturated 0.5 M KHCO₃ solution. b) Quantitative analysis of gas products from 2-h CPE using the **poly(CoPc-2T)**-modified carbon paper as a WE at the potentials of –1.20 V and –1.30 V vs. Ag/AgCl (3M KCl) a in N₂- or CO₂- saturated 0.5 M KHCO₃ solution and a two-compartment three-electrode electrochemical cell. 58

Figure 4–17. Cyclic voltammograms of a **poly(CoPc-2T)**-modified carbon paper under N₂- (thin black line) and CO₂-saturated conditions (thin red dashed line), compared with those of a bare carbon paper under the N₂- (thick solid black line)

and CO₂-saturated conditions (thick red dashed line) recorded in a 0.1 M KH₂PO₄/K₂HPO₄ electrolyte solution..... 60

Figure 4–18. a) Chronoamperometric responses of 2-h using a **poly(CoPc-2T)**-modified carbon paper as a WE at potential of –1.30 V vs. Ag/AgCl (3M KCl) under N₂-saturated condition in a 0.5 M KHCO₃ (square symbol with black line) and in a 0.1 M KH₂PO₄/K₂HPO₄ (circle symbol with red line) and under CO₂-saturated condition in a 0.5 M KHCO₃ (up-pointing triangle symbol with blue line) and in a 0.1 M KH₂PO₄/K₂HPO₄ (down-pointing triangle symbol with blue green) in a two-compartment three-electrode electrochemical cell..... 60

Figure 4–19. a) % FE of CO and H₂ formations from 2-h CPE at applied potential of –1.30 V vs. Ag/AgCl (3M KCl) in the absence and presence of a **poly(CoPc-2T)** film on carbon paper electrode under a N₂- or CO₂- saturated condition of 0.5 M KHCO₃ or 0.1 M KH₂PO₄/K₂HPO₄ solution. b) Quantitative analysis of gas products from 2-h CPE using the **poly(CoPc-2T)**-modified carbon paper as a WE at the potentials of –1.30 V vs. Ag/AgCl (3M KCl) in a N₂- or CO₂- saturated conditions of 0.5 M KHCO₃ or 0.1 M KH₂PO₄/K₂HPO₄ solution in a two-compartment three-electrode electrochemical cell..... 62

Figure 4–20. Catalysis performance of a **poly(CoPc-2T)**-modified carbon papers for ECR of CO₂ studied by an online GC technique over 20 h at potential of –1.20 V, –1.30 V and –1.40 V vs. Ag/AgCl (3M KCl) in a CO₂-saturated 0.5 M KHCO₃ solution in terms of a) current density, b) % FE of CO formation and c) an accumulated amount of CO product..... 64

Figure A–1. A ¹H-NMR spectrum of compound **1** in CDCl₃..... 83

Figure A–2. A ¹³C-NMR spectrum of compound **1** in CDCl₃..... 83

Figure A–3. HR-ESI mass spectrum of compound **1**..... 84

Figure A–4. Crystal Data for C₃₂N₄S₄ (**1**): triclinic, space group P-1 (no. 2), $a = 7.6076$ (14) Å, $b = 12.529(2)$ Å, $c = 15.757(3)$ Å, $\alpha = 105.655(5)^\circ$, $\beta = 100.619(5)^\circ$, $\gamma = 104.030(5)^\circ$, $V = 1352.0(4)$ Å³, $Z = 2$, $T = 296.15$ K, $\mu(\text{MoK}\alpha) = 0.381$ mm⁻¹, $D_{\text{calc}} = 1.397$ g/cm³, 16102 reflections measured ($2.786^\circ \leq 2\Theta \leq 48.478^\circ$), 4322 unique ($R_{\text{int}} =$

0.0520, $R_{\text{sigma}} = 0.0669$) which were used in all calculations. The final R_1 was 0.1516 ($l > 2\sigma(l)$) and wR_2 was 0.4738 (all data).....	85
Figure A-5. A $^1\text{H-NMR}$ spectrum of ZnPc-2T in $(\text{CD}_3)_2\text{SO}$	86
Figure A-6. A $^{13}\text{C-NMR}$ spectrum of ZnPc-2T in $(\text{CD}_3)_2\text{SO}$	86
Figure A-7. A HR-MALDI-TOF mass spectrum and an isotopic pattern of a molecular ion peak of ZnPc-2T	87
Figure A-8. Absorption spectra of ZnPc-2T in THF.....	87
Figure A-9. A calibration curve for absorption at 362 nm of ZnPc-2T in THF.....	88
Figure A-10. A calibration curve for absorption at 637 nm of ZnPc-2T in THF.....	88
Figure A-11. A calibration curve for absorption at 707 nm of ZnPc-2T in THF.....	89
Figure A-12. Absorption and photoluminescence spectra of ZnPc-2T in THF.....	89
Figure A-13. A HR-MALDI-TOF mass spectrum and an isotopic pattern of a molecular ion peak of CoPc-2T	90
Figure A-14. Absorption spectra of CoPc-2T in THF.....	90
Figure A-15. A calibration curve for absorption at 351 nm of CoPc-2T in THF.....	91
Figure A-16. A calibration curve for absorption at 692 nm of CoPc-2T in THF.....	91
Figure A-17. A MALDI-TOF mass spectrum and an isotopic pattern of a molecular ion peak of H₂Pc-2T	92
Figure A-18. Absorption and photoluminescence spectra of H₂Pc-2T in THF.....	92
Figure A-19. A MALDI-TOF mass spectrum and an isotopic pattern of a molecular ion peak of CuPc-2T	93
Figure A-20. Absorption spectra of CuPc-2T in THF.....	93
Figure A-21. A MALDI-TOF mass spectrum and an isotopic pattern of a molecular ion peak of NiPc-2T	94

Figure A-22. a) Cyclic voltammogram (CV) of the **poly(CoPc-2T)**-modified carbon paper in N_2 -saturated 0.1 M TBAPF₆ DMF solution with scan rate of 50 mV·s⁻¹ b) a Current density vs. time curve, corresponding with CV curve..... 95



LIST OF SCHEMES

	Page
Scheme 2-1. A molecular structure of H_2Pc and metalation process of H_2Pc	8
Scheme 2-2. (a) Oxidation and (b) reduction of the inactive MPc	10
Scheme 2-3. Oxidation and reduction of the active MPc	10
Scheme 4-1. Synthesis of $ZnPc-2T$, $CoPc-2T$, $CuPc-2T$, $NiPc-2T$ and H_2Pc-2T	33



LIST OF TABLES

	Page
Table 2-1. Possible reduction pathways on cathode and anode during the reduction of CO ₂	5
Table 4-1. Photophysical properties of the target phthalocyanines compared with their unsubstituted analogs.	37
Table 4-2. XPS analysis data of poly(ZnPc-2T) , poly(CoPc-2T) and their monomers.	46
Table 4-3 Catalysis performance of poly(ZnPc-2T) and poly(CoPc-2T) -modified carbon papers for ECR of CO ₂ performed in a 0.1 M TBAPF ₆ /ACN solution at the applied potential of -1.70 V vs. Ag/AgCl QRE with one-compartment three-electrode cell.	52
Table 4-4. Catalytic activity of the Poly(CoP-2T) films for the 20-hour ECR of CO ₂ . 65	
Table 4-5 Comparison of the catalytic performance of the poly(CoPc-2T) -modified carbon paper develop from this work with other reported high-performance catalysts for the ECR of CO ₂ to CO in aqueous media.	66

CHAPTER 1

INTRODUCTION

According to the European project for ice coring in Antarctica (EPICA) during 1996–2005, information about amount of carbon dioxide (CO₂) and temperature change have been uncovered for 800,000 years ago as shown in **Figure 1-1**.^{1, 2} The data came from ice core in Antarctica, which was cut and analyzed by an isotopic method and a gas chromatography technique. The results showed that the amount of the CO₂ and temperature change have cycled up and down and tend to move together. The amount of CO₂ had been in a range of approximately 180 to 280 parts per million (ppm) with average temperature around -0.2 °C. However, after industrial evolution in 1950, the amount of CO₂ has increased to around 2 ppm per year. Until now, the amount of CO₂ is around 415 ppm with the increase in the temperature by 1 °C, comparing with the time before the industrial evolution. There are some predictions that the amount of CO₂ and temperature change will increase to 550 ppm and +3 °C in 2050, respectively,^{3, 4} causing climate change, global warming and a lot of environmental problems.^{5, 6}

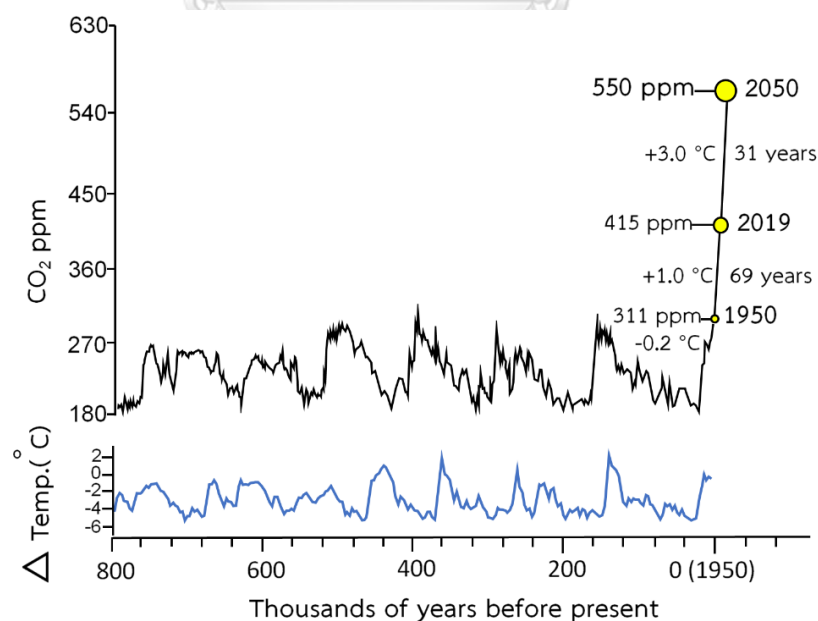


Figure 1-1. Amount of CO₂ (dark line) and temperature change (blue line) for the past 800,000 years, based on EPICA (ice core) data.^{1, 2}

Among several methods proposed to relieve these problems, electrochemical reduction of CO₂ (ECR) is one of the most popular approaches to reduce and convert CO₂ into various kinds of value-added products, such as carbon monoxide (CO), formic acid (HCOOH), methanol (CH₃OH), ethanol (C₂H₅OH), methane (CH₄), ethane (C₂H₆), etc.⁷⁻¹⁰ Moreover, this method does not only support renewable energy exploitation to create an artificial carbon-neutral cycle as shown in **Figure 1-2**,¹¹ but also can be easily done in water media, atmospheric pressure and room temperature.¹² However, direct electrochemical conversion of CO₂ in the water media is very hard to achieve because of high stability of a CO₂ molecule¹³ and competitive hydrogen evolution in the water media.¹⁴ To overcome this obstacle, electrocatalysts have been used to provide alternative pathways and gain selective activity for the conversion of CO₂. Due to high stability and good redox properties, metallophthalocyanine (MPC) derivatives have been of interest as promising electrocatalysis,¹⁵⁻¹⁸ photocatalysis,^{19, 20} and photoelectrocatalysis.^{21, 22} for conversion of CO₂. However, inevitable aggregation of phthalocyanine macrocycles²³⁻²⁵ often causes complication in film and electrode preparation.²⁶ Normally, the electrodes can be modified by these compounds by using binder, such as polystyrene¹⁵ or nafion^{27, 28}, to enhance attachment of these materials on electrode surface and increase the stability. However, the binders allow penetration of only photons and some ions, leading to suppressing of the CO₂ at surrounding catalysts site.²⁹

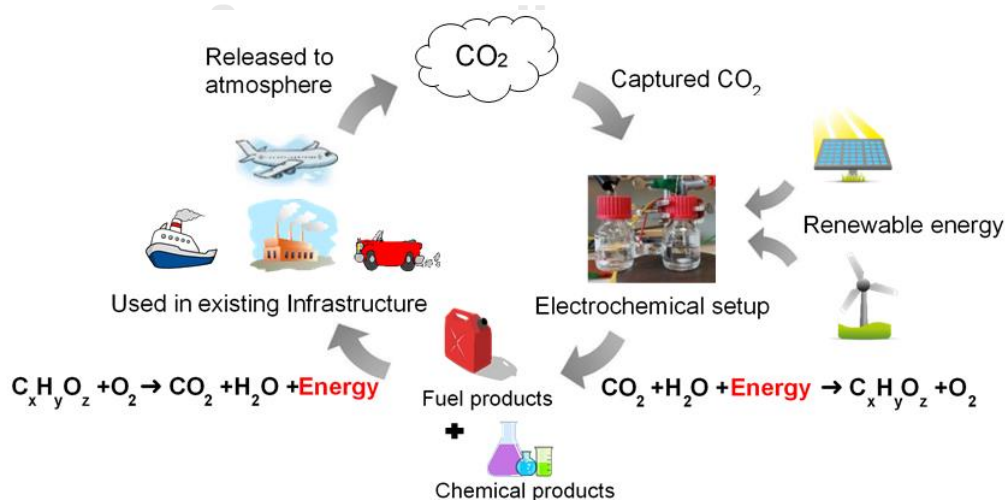


Figure 1-2. Systematic artificial carbon cycle.¹¹

To overcome this problem, we introduced electrochemical polymerization method for preparing the **MPC**-modified electrode by using **MPC** monomers bearing electropolymerizable peripheral units. This method could not only directly graft **MPC** polymer films onto the electrode surface without using binder, but also control film thickness with well-defined film morphology.³⁰ Recently, several groups reported the electropolymerization of the **MPC** bearing heterocyclic moieties such as thiophene,³¹ pyrrole,³² and 3,4-ethylenedioxythiophene (EDOT)³³ for optoelectronic applications and heterogeneous electrocatalytic chemical processes. Nevertheless, to the best of our knowledge, there are only few reports describing the use of the **MPC**-based polymers for the heterogeneous ECR of CO₂.³⁴

In this work, our target **MPC** and free base phthalocyanine (**H₂Pc**) derivatives contain bithiophenyl β -substituents as shown in **Figure 1–3**. We hypothesize that these β -substituents can enhance solubilities of the target **H₂Pc** and **MPC** compounds, compared with that of the unsubstituted analog and be electrochemically polymerized to create the corresponding polymer-modified electrodes. Moreover, resulting modified electrodes are expected to have high stability and high active surface area for using as electrocatalysts for the ECR of CO₂ because the electropolymerization of these kinds of compounds could create the two-dimensional polymeric network with high exposure to the CO₂ molecules and suppressed aggregation effect of the macrocyclic phthalocyanine.³⁰

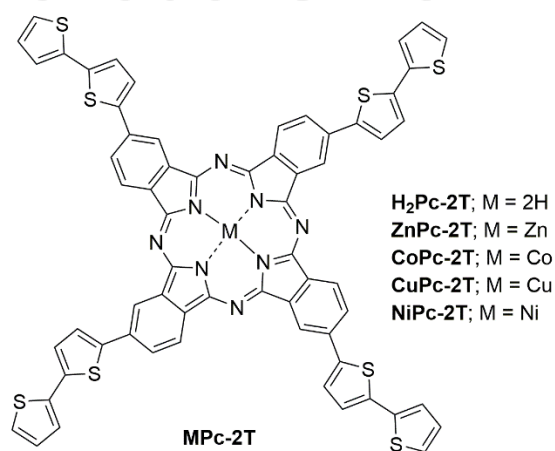


Figure 1–3. A general structure of target compounds.

1.1 Objectives of this research

To synthesize and investigate new bithiophenyl-substituted **H₂Pc** and **MPc** compounds and their polymers for the heterogenous ECR of CO₂.

1.2 Scopes of this research

H₂Pc and **MPc** derivatives bearing bithiophenyl β -substituents, whose structures are shown in **Figure 1-2**, will be synthesized and characterized by means of spectroscopic methods consisting of proton-1 and carbon-13 nuclear magnetic resonance (¹H and ¹³C-NMR) spectroscopy, mass spectrometry (MS), UV-visible and photoluminescence spectrophotometry, attenuated total reflectance-Fourier transform infrared spectroscopy (ATR-FTIR), and X-ray photoelectron spectroscopy (XPS). After that, the obtained target compounds will be polymerized by the electrochemical technique on indium tin oxide coated glass (ITO/glass) and carbon paper. The resulting polymer-modified electrodes will be characterized by cyclic voltammetry and spectroscopic methods including UV-visible spectrophotometry, ATR-FTIR spectroscopy, XPS analysis, scanning electron microscope (SEM) and energy dispersive X-ray spectroscopy (EDX). The catalytic activities of the polymer-modified electrodes for the heterogeneous ECR of CO₂ will be investigated by the cyclic voltammetry (CV) technique in organic or aqueous electrolyte media. Qualitative and quantitative analyses of product(s) from the ECR of CO₂ will be performed by chronoamperometry (CA) or controlled-potential electrolysis (CPE), gas chromatography (GC) and ion chromatography (IC).

CHAPTER 2

THEORY AND LITERATURE REVIEWS

2.1 Electrochemical reduction of CO₂

In principle, CO₂ is a stable molecule having a linear structure. Electrochemically, the reduction of CO₂ usually requires high potential, such as at -1.97 V in DMF,^{13, 35} -1.90 V in water^{13, 36} vs. normal hydrogen electrode (NHE), for a one-electron reduction process to change the CO₂ structure molecule from a linear to a bent reactive radical species, which can accept another electron to form primary products such as CO and HCOOH.³⁷ By thermodynamic calculation, the ECR of CO₂ requires less potential in the multi-electron and multi-proton transfer process, compared to the one-electron reduction process as shown in **Table 2-1**.^{38, 39}

Table 2-1. Possible reduction pathways on cathode and anode during the reduction of CO₂.³⁹

Product	Reaction	E° redox / V vs. NHE
CO ₂ radical anion in DMF	$\text{CO}_2 + \text{e}^- \rightarrow \text{CO}_2^{\cdot-}$	-1.97 ^{13, 35}
CO ₂ radical anion in water	$\text{CO}_2 + \text{e}^- \rightarrow \text{CO}_2^{\cdot-}$	-1.90 ^{13, 36}
Hydrogen gas	$2\text{H}^+ + 2\text{e}^- \rightleftharpoons \text{H}_2$	0 ^a
HCOOH	$\text{CO}_2 + 2\text{H}^+ + 2\text{e}^- \rightleftharpoons \text{HCOOH}$	-0.58 ^a
Formaldehyde	$\text{CO}_2 + 4\text{H}^+ + 4\text{e}^- \rightleftharpoons \text{HCHO} + \text{H}_2\text{O}$	-0.55 ^a
CO (gas)	$\text{CO}_2 + 2\text{H}^+ + 2\text{e}^- \rightleftharpoons \text{CO} + \text{H}_2\text{O}$	-0.51 ^a
CH ₃ OH	$\text{CO}_2 + 6\text{H}^+ + 6\text{e}^- \rightleftharpoons \text{CH}_3\text{OH} + \text{H}_2\text{O}$	-0.39 ^a
C ₂ H ₅ OH	$2\text{CO}_2 + 12\text{H}^+ + 12\text{e}^- \rightleftharpoons \text{C}_2\text{H}_5\text{OH} + 3\text{H}_2\text{O}$	-0.33 ^a
CH ₄	$\text{CO}_2 + 8\text{H}^+ + 8\text{e}^- \rightleftharpoons \text{CH}_4 + 2\text{H}_2\text{O}$	-0.24 ^a
CH ₂ CH ₆	$2\text{CO}_2 + 14\text{H}^+ + 14\text{e}^- \rightleftharpoons \text{C}_2\text{H}_6 + 4\text{H}_2\text{O}$	-0.27 ^a

^aReduction potentials are calculated by using Gibbs free energy of formation from thermodynamic data at pH 7.

Moreover, in the presence of several protons and electrons, more valuable fuel products, such as CH_3OH , $\text{C}_2\text{H}_5\text{OH}$, CH_4 and CH_2CH_6 , can be obtained. However, in fact, the ECR of CO_2 in presence of proton is hard to achieve due to complete hydrogen (H_2) evolution occurring at 0 V vs. NHE.³⁹ Therefore, rate of reaction and activation energy of the reduction play importance role in the conversion of CO_2 in this case and hence electrocatalysts are required.¹³

In general, there are two types of the electrocatalysts for the ECR of CO_2 consisting of homogenous and heterogenous catalysts,^{13, 40} mechanistic operation of which are illustrated in **Figures 2-1a** and **2-1b**, respectively. In the homogeneous catalytic process, the catalyst is in the same phase as electrolyte and the ECR occurs mainly on an electrode surface. An advantage of the homogenous electrochemical condition is high turnover number (TON) of the catalyst because the catalyst from the solution can act as the new catalyst the electrode surface. Nevertheless, this process requires high overvoltage due to resistance of the electrolyte created in a gap between the electrode surface and the catalyst molecules. Moreover, the remaining catalyst cannot be conveniently separated from the process after use. To overcome these problems, the use of the heterogeneous catalysts has been proposed. In this approach, the catalyst is deposited on a working electrode (WE) by several appropriate techniques such as drop casting, spin coating, physical vapor deposition (PVD) and electrochemical deposition. However, in this method, high stability of electrocatalyst is required due to limited surface coverage of the electrocatalyst on the electrode.

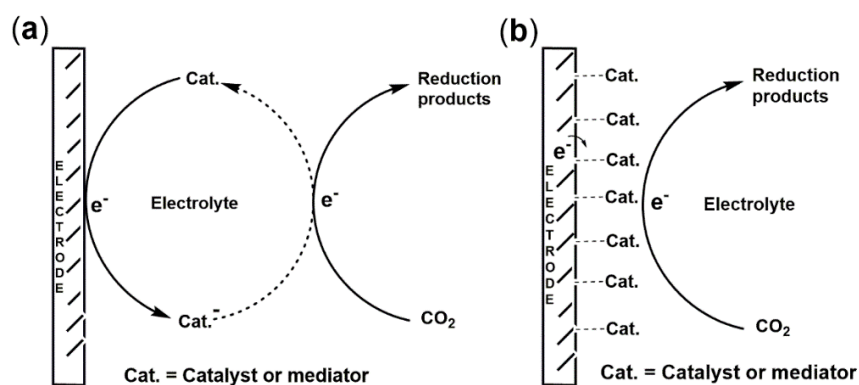


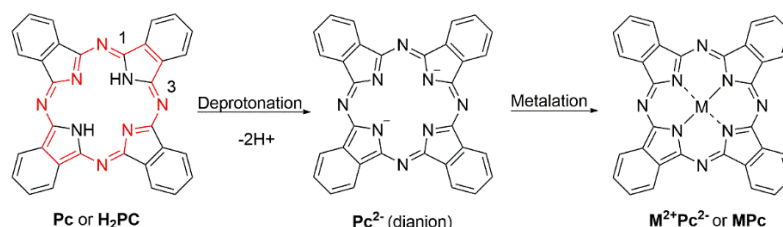
Figure 2-1. Schematic diagrams of ECR of CO_2 under (a) homogenous (b) heterogenous catalysis.^{3,5}

In the past decades, many literatures have showed that **MPC** compounds have been good candidates as highly efficient electrocatalysts for the heterogeneous ECR of CO₂ in terms of high stability, reversible redox properties and selective binding with CO₂. The ECR of CO₂ catalyzed by **MPC** (M= Co, Ni) was firstly described by Meshitsuka *et al.*¹⁵ The studies showed that dip-coated **MPC** films on graphite electrodes could serve as very active catalysts for the ECR of CO₂. Kapusta and Hackerman studied **MPC** (M= Co, Ni, Fe, Cu, Cr, Sn) deposited on glassy carbon rod electrodes¹⁶ and found that the efficiency of the ECR of CO₂ in an aqueous solution was defined as **CoPc** > **NiPc** >> **FePc** = **CuPc** > **CrPc**, **SnPc**. **CoPc** and **NiPc** gave formate at pH > 5 and methanol at lower pH values. In addition, the **MPC** compounds became less active in less acidic condition due to irreversibility of the catalysts. Tanabe and Ohno used a plasma-assisted vacuum deposition technique to prepare films of **MPC** compounds on glassy carbon electrodes.⁴¹ Reactivity order of the catalysts for the ECR of CO₂ was found to be **CoPc** >> **NiPc** > **FePc** ~ **MgPc** ~ **MnPc** ~ **ZnPc** in the aqueous solution. Furuya and Matsui studied 17 kinds of **MPC** compounds deposited on porous carbon gas-diffusion electrodes.⁴² **CoPc** and **NiPc** showed the highest catalytic activity for the ECR of CO₂ in the aqueous solution with current efficiency of 100% and gave carbon monoxide as a product. Abe *et al.* reported that butoxy-substituted **CoPc** coated on basal-plane pyrolytic graphite (BPG) electrodes exhibited higher catalytic activity and selective for the ECR of CO₂, compared with **CoPc** due to the presence of electron donor substituents.¹⁷ Isaacs *et al.* performed the polymerization of amino-substituted **H₂Pc** and **MPC** (M= Co, Ni, Fe) on the glassy carbon electrodes using the cyclic voltammetry.³⁴ The polymeric **CoPc**-modified electrode exhibited electrochemical conversion of CO₂ into formic acid as a major product in the aqueous solution. Spectroelectrochemical experiments indicated the reduction of Co(II) to Co(I) following by the reduction of the macrocyclic phthalocyanine in this process.

2.2 Free base phthalocyanine (H₂Pc) and metallophthalocyanine (MPC)

H₂Pc is a heterocyclic molecule having a conjugated system of 18 π -electrons.^{26, 43} The **H₂Pc** macrocycle is based on porphine rings consisting of four

isoindole rings bridged to each other at 1 and 3 positions by imine (=N-) linkers (Scheme 2-1). H_2Pc can be deprotonated to generate dianionic ligand which was able to coordinate with various metals to obtain MPc .



Scheme 2-1. A molecular structure of H_2Pc and metalation process of H_2Pc .

2.2.1 Optical properties of Pc and MPc

H_2Pc and MPc exhibit two intense absorption bands at 300–400 nm and > 600 nm, which are called Soret band (B-band) and Q-band, respectively (Figure 2-2), with high extinction coefficient value ($>10^5 M^{-1}\cdot cm^{-1}$) originating from a Gouterman's four-orbital LCAO model (Figure 2-3).^{26, 43} In the presence of central metals, the extra transition band between 400–600 nm can appear when metal to ligand charge transfer (MLCT) or ligand to metal charge transfer (LMCT) occur, depending on matching energy levels between metal and ligand.^{26, 43, 44} Due to these interesting properties, the H_2Pc and MPc have attracted great attention in optoelectronic applications, such as photovoltaic cells,⁴⁵ photocatalysis,^{19, 20} and photoelectrocatalysis.^{21, 22, 46}

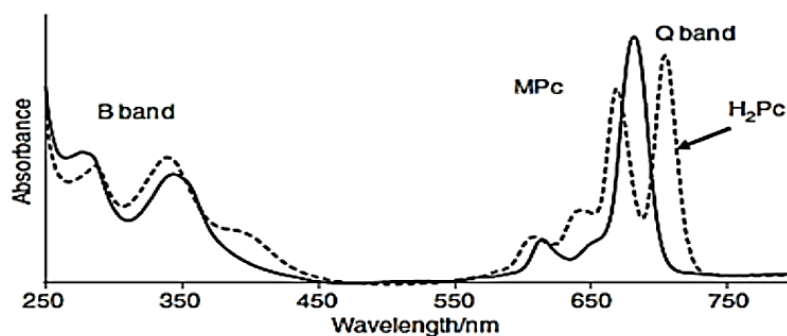


Figure 2-2. typical spectra of H_2Pc and MPc .²⁶

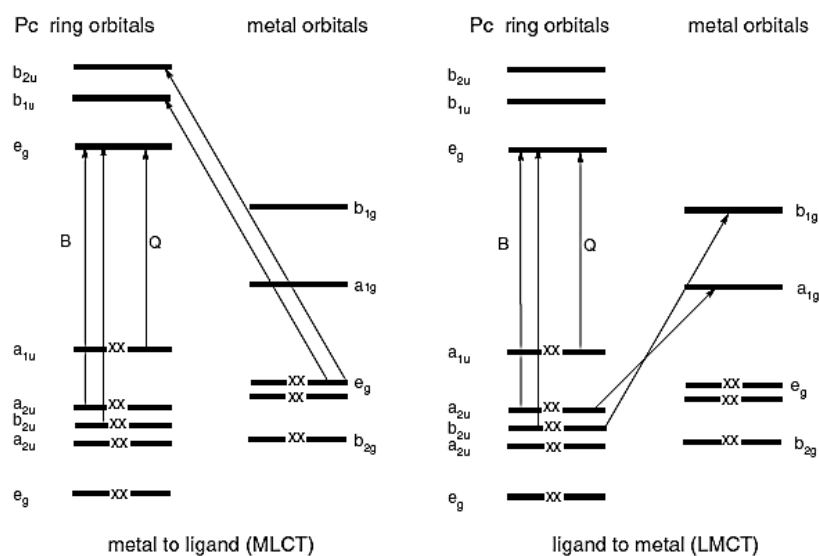
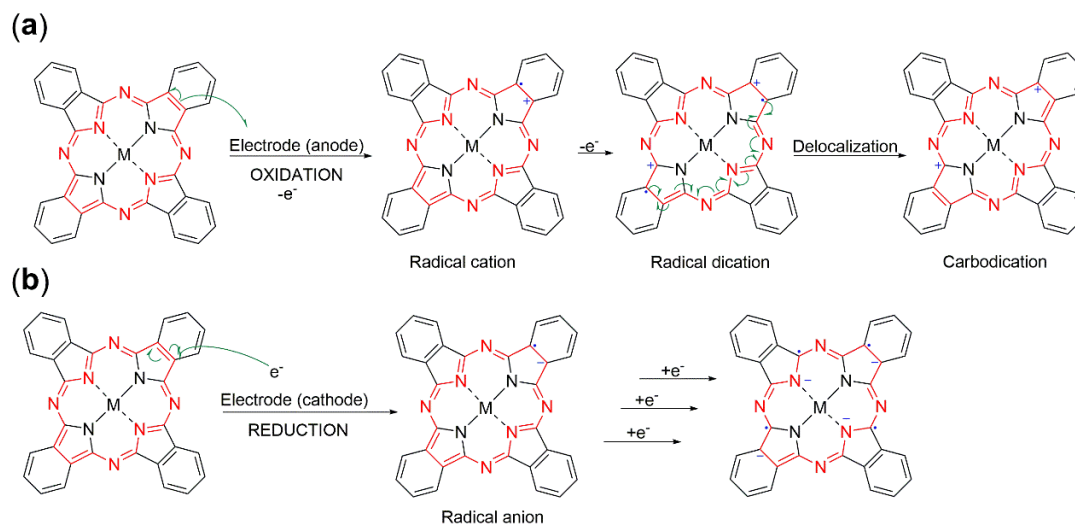


Figure 2-3. Gouteman's four-orbital linear combination of atomic orbital model.²⁶

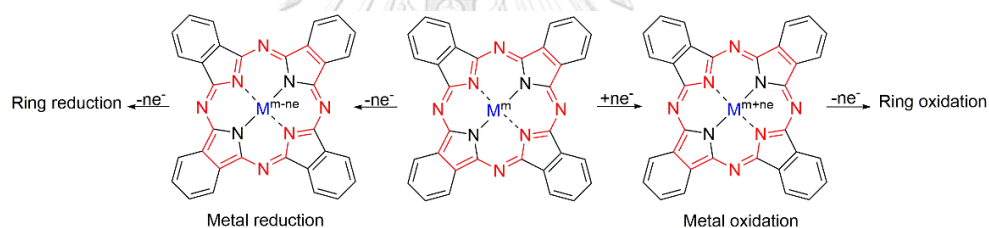
2.2.2 Redox properties of MPC

In principle, the redox properties of MPC derivatives can be classified into two groups^{47, 48} comprising active and inactive MPC compounds. The redox processes of the inactive MPC derivatives, such as ZnPC, Li₂PC and MgPC analogs, are involved by the 18 π -conjugated system of the macrocycle. In Scheme 2-2a, oxidation reaction of the inactive group can provide a maximum of two electron from conjugated backbone by an oxidative doping process, leading to a radical cation and a radical dication,²⁶ Moreover, these free radicals from the radical dication can be recombined to form a spinless of carbodication, which is a stable state like a quinones structure.^{49, 50} This quinone-like state of quinones structure exhibits high electron mobility because electron can delocalize more fluently, favorable for optoelectronic or electronic applications.⁵¹⁻⁵³ In Scheme 2-2b, the reduction of the inactive MPC compounds can accept maximum of four electrons into their macrocycles to generate radical anions.²⁶ On the other hand, the active MPC derivatives, such as the one having M= Co, Ni, Cu, and Mn undergo first oxidation or reduction at their metal centers due to the presence of paramagnetic electrons as shown in Scheme 2-3, resulting in the possible additional extra redox processes and axial coordination at the metal centers.^{44, 48, 54} Moreover, this kind of MPC derivatives can undergo further oxidation or reduction at the macrocycles, leading to great potential of the active

MPC compounds in the electrocatalysis, such as oxidation of L-cysteine,³² the H₂ evolution,^{55, 56} the ECR of CO₂,⁵⁷ etc.



Scheme 2-2. (a) Oxidation and (b) reduction of the inactive MPC.



Scheme 2-3. Oxidation and reduction of the active MPC.

2.3 Electrochemical polymerization techniques

There are many approaches to deposit the H₂Pc and MPC derivatives on the substrates, such as ⁵⁸, drop casting,⁵⁹ spray coating,⁶⁰ dip coating,⁶¹ electrochemical coating⁶², etc. Among these techniques, electrochemical deposition has unique advantages in term of controlled film thickness, well-defined film morphology, operating condition and high surface coverage on the substrate, even on the porous one. Optimization of the electrodeposition can be achieved by adjusting various parameters, such as concentration of deposited compound, applied potential, type of electrode, type of electrolyte, etc. Moreover, the electrochemical polymerization is one of the most popular polymerization methods providing selective transformation of several kinds of monomers into corresponding polymers. To achieve the electrochemical polymerization, electrochemically active units have to

present in the monomer molecules, such as thiophene,³¹ pyrrole,³² and EDOT,³³ etc. According to many literatures, there are many successful synthesis and electrochemical polymerization of the **MPC** materials bearing the electropolymerizable units. Trombach et al.⁶³ and Obirai et al.³² synthesized **H₂Pc** and **MPC** derivatives bearing pyrrol-1-yl groups (**1A** and **1B**, respectively, **Figure 2-4**) and successfully polymerized them on the ITO/glass surface by means of the cyclic voltammetry and spectroelectrochemical measurement was used to investigate the oxidation-reduction processes on the macrocycle and metal centers. In addition, a film of a cobalt-chelated derivative was found to have the catalytic activity towards the oxidation of L-cysteine to create disulfide bonds.³² Yavuz et al. synthesized a **NiPc** derivative substituted with 4-(2,5-di-2-thiophen-2-yl-pyrrol-1-yl) groups (**1C**, **Figure 2-4**) and polymerized it on the ITO/glass electrodes.⁶⁴ The polymers of another series of the **H₂Pc** and **MPC** derivatives containing thiophene-based peripheral substituents (**1D-F**, **Figure 2-4**) were prepared and studied for

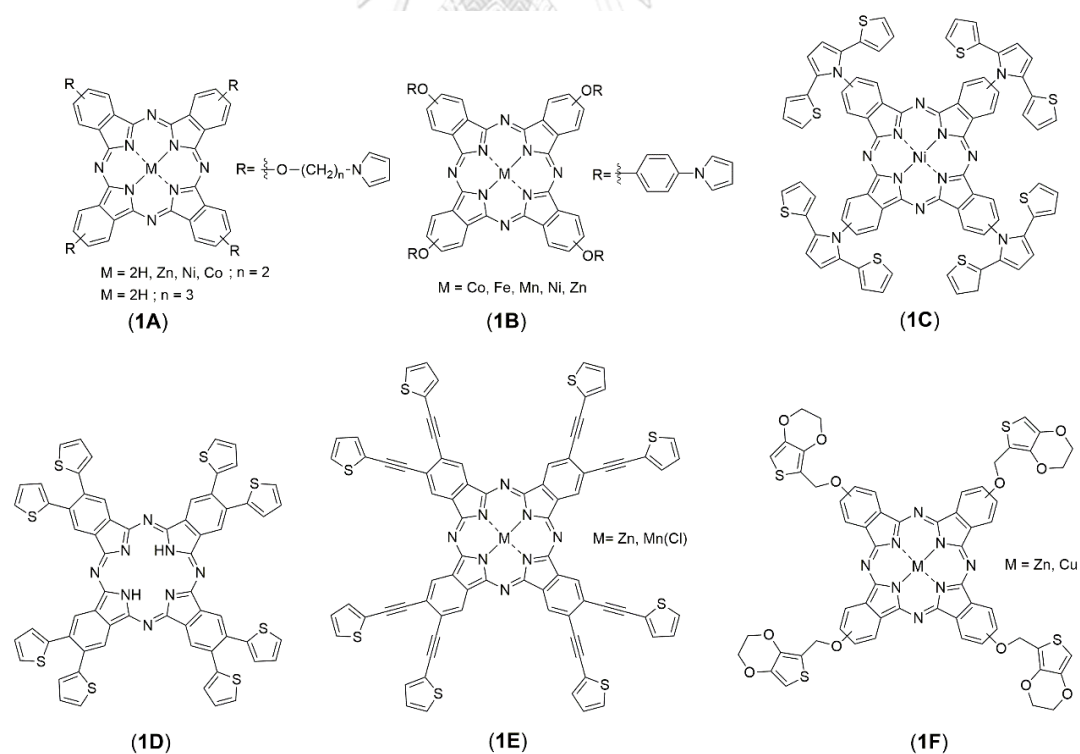


Figure 2-4. Molecular structures of some **H₂Pc** and **MPC** derivatives bearing electrochemically polymerizable peripheral units.

electrochromic applications.^{31, 33, 65} According to these research works, the electrochemical polymerization seems to be the promising technique for preparing the polymer films of our target **H₂Pc** and **MPc** derivatives.

2.4 Electrochemical methods⁶⁶

2.4.1 Cyclic voltammetry (CV)

The CV is an electrochemical technique widely used to provide information about electroactive species, such as number of electron transfer, redox potential, catalytic activity, doping/dedoping effect, and electrochemical stability.⁶⁷⁻⁶⁹ An electrochemical cell consists of the WE, a reference electrode (RE) and a counter electrode (CE), which are immersed in an electrolyte solution, as shown in **Figure 2-5**. The potential of the WE are applied against the RE in an unstirred solution, while the CE works as an assistant electrode where an opposite reaction to the WE occur. In this technique, the input potential against time is in a triangle wave form, which is called an excitation signal, as shown in **Figure 2-6**. One the triangle wave form or one cycle consists of a forward scan and a reverse scan, corresponding with oxidation reaction and then reversed reaction of electroactive species, respectively, or vice versa, depending on a direction of the sweeping potential. If the potential is swept from high potential to low potential, the reduction of the electroactive species will occur first as shown in **Figure 2-7a**. In contrast, if the potential is swept from low potential to high potential, the oxidation of the electroactive species will occur first as shown in **Figure 2-7b**. When the redox reaction of the electroactive species under the applied potential occur, enhancement of current intensity will be observed, leading to peak current in a cyclic voltammogram. In the cyclic voltammogram, important parameters are initial potential (E_{init}), final potential (E_{final}), cathodic peak potential (E_{pc}), anodic peak potential (E_{pa}), cathodic peak current (i_{pc}), anodic peak current (i_{pa}) and half wave potential ($E_{1/2}$). These parameters can give information on the electrochemical behavior of analysts that are useful for many studies and applications.

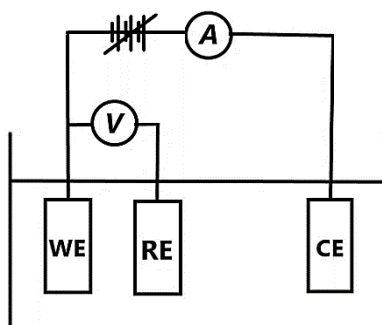


Figure 2-5. A schematic diagram of a three-electrode one-compartment electrochemical cell.⁷⁰

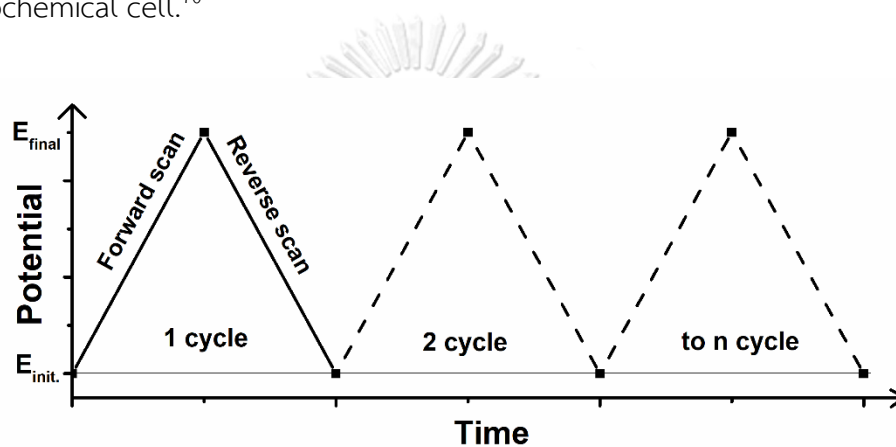


Figure 2-6. Excitation signals of cyclic voltammetry.⁶⁸

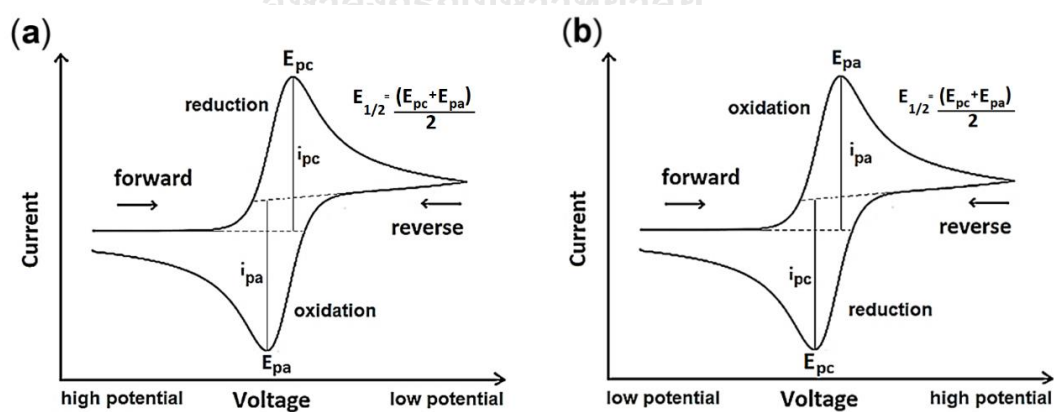


Figure 2-7. Cyclic voltammograms of the first electrochemical a) reduction and b) oxidation.⁷¹

2.2.2 Chronoamperometry (CA) or controlled potential electrolysis (CPE)

The CA or CPE is another kind of voltammetry that is performed in the same three-electrode system as that used in CV.⁷² The principle of this technique is to apply the constant potential to the WE against potential of the RE. The excitation signal plotted between the potential and the time is depicted in **Figure 2–8a**. When the electrochemical reaction of the electroactive species occurs at the certain potential, current response will be measured against the time as shown in **Figure 2–8b**. This technique offers useful tools for many applications, such as investigation of the stability of the catalyst,⁷³ measurement of total charge (Q) for Faradaic efficiency (FE) calculation,⁷³ activation of electrode and deposition of metallic or non-metallic compounds on the electrodes,^{74, 75} etc.

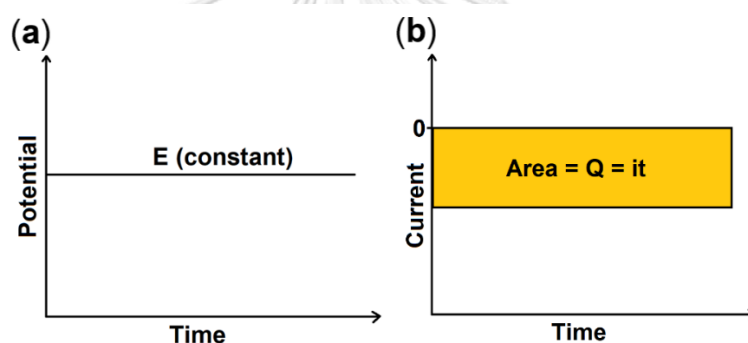


Figure 2–8. a) An excitation signal for CA and b) a chronoamperometric response.⁶⁶

In this study, the Q value that passes through the cell is calculated by integrating current (i) vs. the time (t) following a Faraday's law⁷⁶:

$$Q = it = nF$$

where F is a Faraday's constant (96500 C·mol⁻¹) and n is the number of moles of electrons. Therefore, n can be calculated from the Q obtained and the known F. Moreover, the FE can be calculated by using the n value obtained, according to a following equation:^{77, 78}

$$\% \text{ FE} = \frac{e_{\text{input}}}{e_{\text{output}}} \times 100$$

where e_{input} is the total number of moles of electrons passing through the cell and e_{output} is the numbers of moles of electrons required for the electrochemical reaction.

2.5. Gas Chromatography (GC)^{79, 80}

The GC is a separation technique for identifying gas. An instrument for this technique consists of a column, an injection port, carrier gas, an oven, a detector and a computer as shown in **Figure 2-9**. The principle of this technique is to use a chromatographic technique under controlled temperature for separating analyte gas based on partition of the analyte between a stationary phase of column and mobile phase of the carrier gas. Since different compounds have different strength of interaction with the stationary phase (“like-dissolves-like” rule), each compound spends different time to move to the detector. The stronger the compounds interact with the stationary phase, the more time it spends to travel through the stationary phase, resulting in longer retention time.

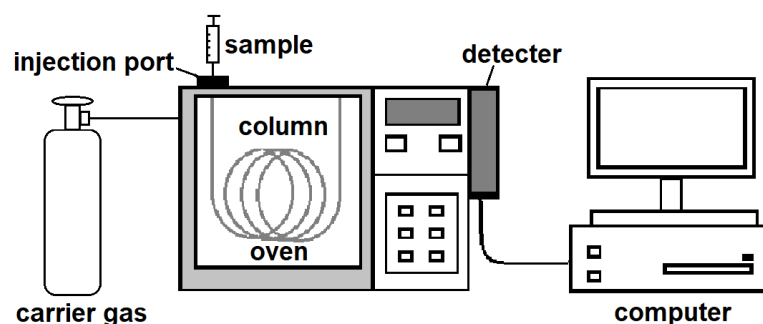


Figure 2-9. A schematic diagram of a GC setup.

2.6. Ion Chromatography (IC)⁸¹

The IC is a technique for analyzing ions and polar molecules based on chromatographic theory and ion equilibrium.⁸² In this study, it was used to measure the product(s) in a liquid phase obtained from the electrochemical reduction of CO_2 , such as formate, carbonate, oxalate and acetate. A typical instrument setup is shown in **Figure 2-10**.⁸³ Initially, an eluent solution, which is conductive, such as aqueous solution of KOH or $\text{NaHCO}_3/\text{Na}_2\text{CO}_3$, is loaded into the system by using a high-pressure pump. After that, the sample is injected and carried by the eluent solution through a guard column that prevent impurities in the sample from entering a main ion exchange column. In the ion exchange column, ion-exchange separation occurs,

depending on difference in the charge and size of the ions. The small and high-charge ion can move faster than the big and low-charge one. After separation, the solution of the analyte ions moves to a suppressor part to reduce the conductivity of the eluent and enhance the conductivity of the analyte ions. After that, the analyte ions are detected by a conductivity detector to monitor the separated ions. All processes are controlled by a computer.

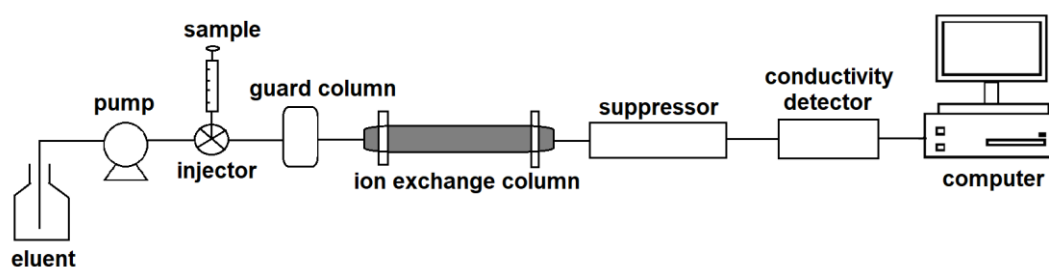


Figure 2-10. Schematic diagram of an ion chromatography setup.⁸³

2.7 Raman spectroscopy^{84, 85}

The Raman spectroscopy is a technique for identifying a compound having polarizability in a molecule, normally in a symmetrical one. This technique is complementary with an infrared spectroscopy. The principle of the Raman spectroscopy is based on interaction between high intensity of laser light and chemical bonds in the molecule, corresponding to specific molecular bond vibration. Typically, there are two types of Raman scattering, non-resonance and resonance one.⁸⁶ The non-resonance Raman scattering occurs when the molecule absorbed photon energy from light that does not match with energy band of electronic transition. This photon energy excites the molecule from its ground state to an unstable virtual state that cause immediately emission of scattered photon afterwards, as shown **Figure 2-11**.⁸⁷ The energy-band transition of electrons can be measured by the UV-visible spectrophotometry. In case of the resonance Raman scattering, the molecule absorbs photon energy from light and gets excited to an electronic state which is quite stable. After that, there are two possibilities to release the energy to come back to the ground state. One is scattering photon and the other

is giving fluorescence. The former is related to vibrational vibration, while the latter is related to electronic energy band. The fluorescence occurs when the excited molecule releases the energy to the lowest vibrational level of the excited electronic state via vibrational relaxation, and this fluorescence emission can interfere the Raman feature by giving a huge band in a Raman spectrum.⁸⁸ Therefore, the non-resonant Raman scattering has a better defined feature than the resonance one. However, both Raman scatterings are useful because they can give information about localization of electrons in molecule at the ground or the excited state. The non-resonance Raman scattering can be used to investigate the localization of the electrons at the ground state or at highest occupied molecular orbital (HOMO) because electrons do not get excited to the higher electronic states. On the other hand, the resonance Raman scattering is involved with both HOMO and LUMO because electrons are excited from the ground state to the higher electronic excited state. Hence, the different laser excitation wavelengths can give distinct information about the vibrational feature of electrons at the ground state and/or the excited state.

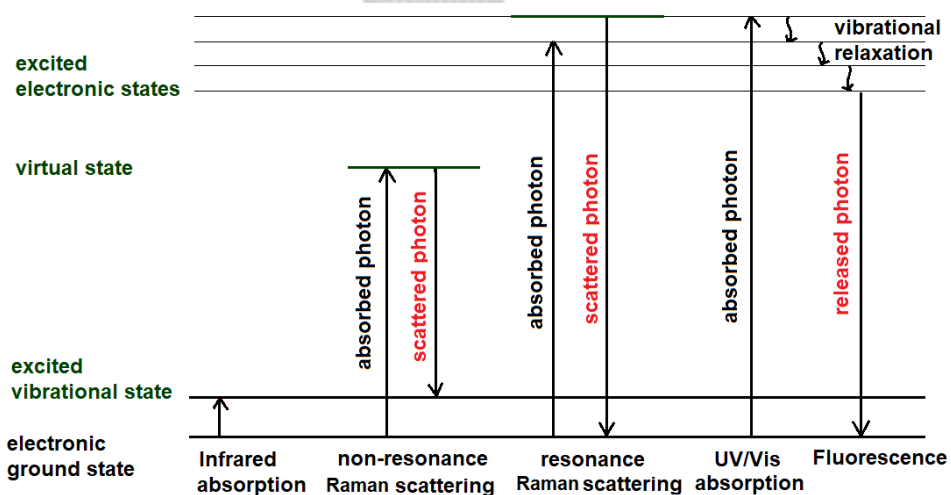


Figure 2–11. Energy diagrams of resonance Raman scattering and non-resonance Raman scattering spectroscopies, comparing with other spectroscopic techniques.⁸⁷

2.8 X-ray photoelectron spectroscopy (XPS)⁸⁹

The XPS is another powerful tool to determine chemical composition on the surface of the samples, types of the chemical bonds in the molecule, and oxidation states of some metal compounds. However, since practical depth of this measurement is around 10 nm from the surface, this technique may not be suitable for analyzing bulk composition of the materials. The principle of this technique is based on photoelectron effect described by Albert Einstein. As shown in **Figure 2–12**, the electron at a core shell is hit by an incident X-ray beam under an ultra-high vacuum condition, resulting in ionization and emission of an inner shell electron(s) (photoelectron). The elements of the surface composition are characterized by investigating binding energy (B.E.), corresponding with kinetic energy (K.E.) of the emitted photoelectron. The binding energy is specific for each element and can be calculated by a following equation described by Ernest Rutherford.⁹⁰

$$\text{B.E.} = h\nu \text{ (known)} - \text{K.E. (measured)} - \Phi_{\text{spec}} \text{ (calibrated)}$$

Where $h\nu$ is energy of an incident X-ray and Φ_{spec} is the work function which depends on both the spectrometer and the material.

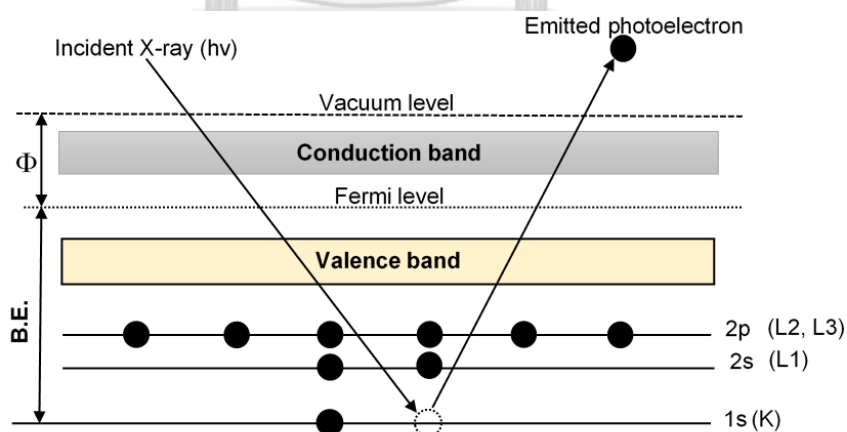


Figure 2–12. A schematic diagram of a photoelectron emission process.⁸⁹

CHAPTER 3

EXPERIMENTS

3.1 Chemicals

All chemicals were purchased from commercial sources and used without further purification unless noted otherwise. Carbon papers (AvCarb MGL190) and nafion membrane (117) were purchased from Fuel Cell Store (USA). The ITO/glass was brought from Semiconductor wafer, Inc.

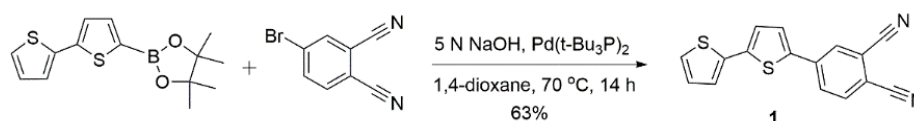
3.2 Analytical Instruments

$^1\text{H-NMR}$ and $^{13}\text{C-NMR}$ spectra were recorded from Bruker Avance 400, operated at 400 MHz and 100 MHz, respectively, in CDCl_3 or $(\text{CD}_3)_2\text{SO}$. Chemical shifts (δ) are reported in parts per million (ppm) relative to a residual CHCl_3 peaks ($\delta = 7.26$ ppm for $^1\text{H-NMR}$ spectroscopy and $\delta = 77.16$ ppm for $^{13}\text{C-NMR}$ spectroscopy) and $(\text{CH}_3)_2\text{SO}$ peaks as reference ($\delta = 2.50$ ppm for $^1\text{H-NMR}$ spectroscopy and $\delta = 39.5$ ppm for $^{13}\text{C-NMR}$ spectroscopy). Mass spectra were obtained from a high-resolution electrospray ionization MS (HR-ESI-MS), a matrix-assisted laser desorption ionization time-of-flight MS (MALDI-TOF-MS) or a high-resolution matrix-assisted laser desorption ionization spiral time-of-flight MS (HR-MALDI-spiralTOF-MS). Absorption spectra were measured in a THF solution at room temperature by using a Cary 60 UV-vis spectrophotometer and extinction coefficients (ϵ) were reported in $\text{M}^{-1}\cdot\text{cm}^{-1}$. Fluorescence spectra were measured in THF using a Perkin-Elmer LS45 luminescence spectrometer at room temperature. The XPS measurements were performed using an ESCALAB 250Xi XPS Microprobe (Thermo Scientific). ATR-FTIR spectra were recorded on a Bruker Vertex 80-ATR. The electrochemical experiments were performed by using a potentiostat (Vertex.One). The Raman measurements were operated at room temperature using a Horiba LabRAM HR800 micro-Raman spectrometer with a 514.7 nm line of a DPSS Cobolt laser and a 633 nm line of a He-Ne laser. All Raman spectra were calibrated with a signal of a silicon wafer in the Raman spectrum which typically showed a peak at 520 nm. For a single crystal X-ray diffraction (SC-XRD) measurement, a suitable crystal was selected and measured on a

Bruker APEX-II CCD diffractometer. The crystal was kept at 296.15 K during data collection. Using Olex2⁹¹, the structure was solved with a ShelXS⁹² structure solution program using Direct Methods and refined with a ShelXL⁹³ refinement package using Least Squares minimization.

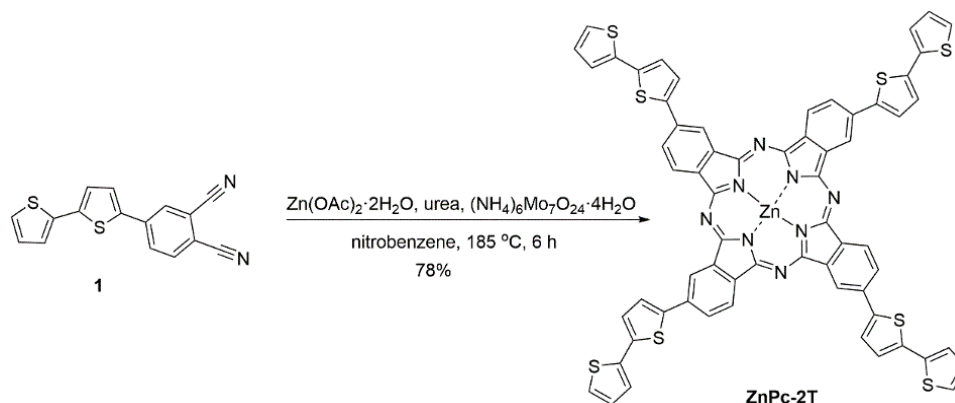
3.3 Synthesis Procedures

3.3.1 4-([2,2'-bithiophen]-5-yl)phthalonitrile (1)



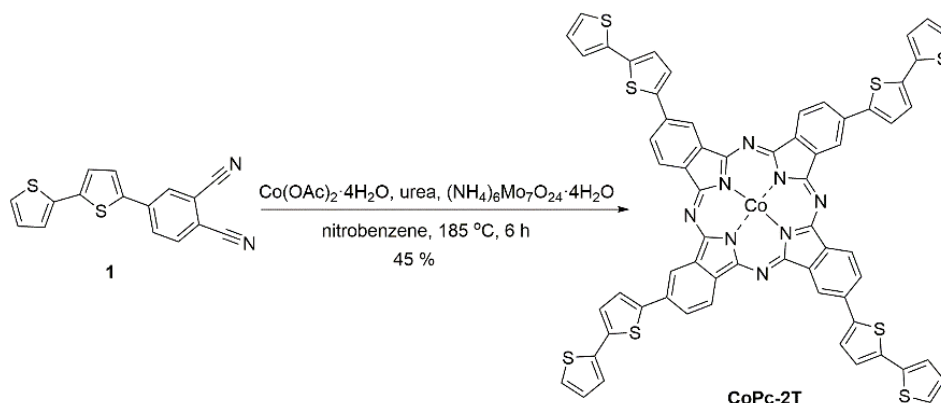
Following a reported procedure⁹⁴ with slight modification in a type of the starting materials and in purification steps, 4-bromophthalonitrile (0.209 g, 1.01 mmol), 2,2'-bithiophene-5-boronic acid pinacol ester (0.293 g, 1.05 mmol) and Pd(t-Bu₃P)₂ (0.004 g, 0.007 mmol) were dissolved in dry dioxane (2.0 mL) at room temperature under nitrogen atmosphere. After stirring for 10 min, a 5 N NaOH aqueous solution (0.12 mL) was added. Then, reaction mixture was stirred at 70 °C for 14 h. Afterwards, the resulting mixture was diluted with dichloromethane (250 mL) and filtered to remove the catalyst and salt. The filtrate was concentrated under reduced pressure to remove solvents. The resulting yellow solid was then dissolved in dichloromethane (250 mL) and precipitated by using hexanes. After filtration and washing with hexanes, a yellow solid was dried under reduce pressure to give the title compound (0.184 g, 63%). ¹H NMR (CDCl₃) (δ): 7.05–7.10 (m, 1H), 7.22 (d, *J* = 3.6 Hz, 1H), 7.27 (d, *J* = 3.6 Hz, 1H), 7.31 (d, *J* = 5.2 Hz, 1H), 7.41 (d, *J* = 4.0 Hz, 1H), 7.78 (d, *J* = 8.4 Hz, 1H), 7.86 (dd, *J* = 8.4, 2.0 Hz, 1H), 7.94–7.99 (m, 1H); ¹³C NMR (CDCl₃) (δ): 113.2, 115.3, 115.6, 117.0, 125.1, 125.3, 126.1, 127.5, 128.4, 129.0, 129.8, 134.2, 136.3, 137.8, 139.3, 141.2. HR-ESI-MS *m/z*: [(M⁺Na)⁺] calcd for C₁₆H₈N₂S₂Na⁺, 315.0021; found, 315.0047.

3.3.2 2,9,16,23-tetra([2,2'-bithiophen]-5-yl)phthalocyaninato-zinc(II)
(ZnPc-2T)



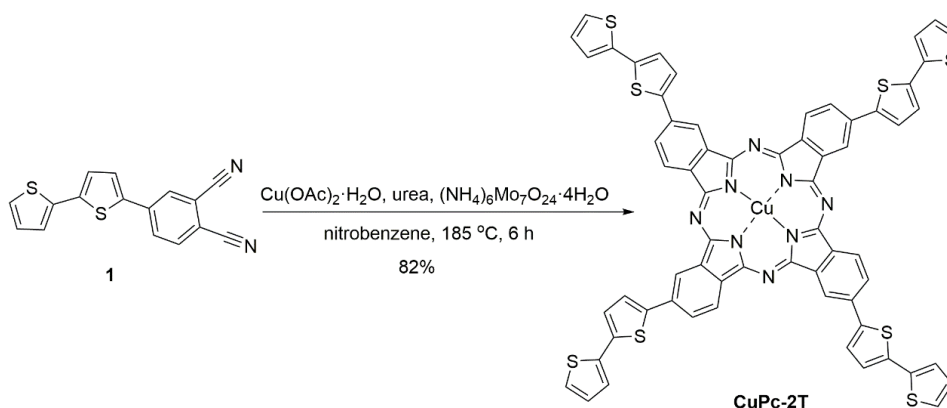
Following a reported procedure⁹⁴ with slight modification in a type of the starting materials and in purification steps, 4-([2,2'-bithiophen]-5-yl)phthalonitrile (**1**, 0.090 g, 0.31 mmol), zinc acetate dihydrate (0.022 mg, 0.10 mmol), urea (0.055 g, 0.85 mmol) and ammonium molybdate tetrahydrate (0.014 g, 0.0097 mmol) were dissolved in distilled nitrobenzene (0.8 mL) and the solution was stirred at 185 °C for 6 h. After that, the reaction mixture was cooled to room temperature and poured into methanol (50 mL). The resulting dark precipitate was filtered and washed thoroughly with formic acid (50 mL) and then methanol (50 mL). This process was repeated twice to remove impurity and by products. The resulting dark green precipitate was dissolved in THF and purified by flash chromatography (silica, THF) to remove residue compounds. The combined fraction was concentrated to 50 mL and methanol was added. The dark green precipitate was separated by filtration, and washed with ethanol, dichloromethane and hexanes. The resulting dark green solid was dried under reduced pressure to give the title compound (0.075 g, 78%). ¹H NMR ((CD₃)₂SO) (δ): 7.16–7.26 (m, 4H), 7.41–7.55 (m, 8H), 7.64 (s, 4H), 7.82–8.02 (m, 4H), 8.08–8.28 (m, 4H), 8.63–8.93 (m, 6H), 9.02–9.17 (m, 2H); ¹³C NMR ((CD₃)₂SO) (δ): 124.2, 124.3, 125.26, 125.33, 125.6, 125.9, 128.4, 133.9, 135.9, 136.7, 136.8, 136.9, 138.1, 142.6, 142.7, 151.4. UV–visible: λ_{abs} (ϵ) 362 (9.3×10^4), 637 (3.9×10^4), 707 (1.8×10^5) nm. λ_{em} ($\lambda_{\text{ex}} = 430$ nm): 514, 717, 796 nm; λ_{em} ($\lambda_{\text{ex}} = 650$ nm): 717, 796 nm. HR-MALDI-spiralTOF-MS m/z : (M^+) calcd for C₆₄H₃₂N₈S₈Zn 1231.9807; found, 1231.9826.

3.3.3 2,9,16,23-tetra([2,2'-bithiophen]-5-yl)phthalocyaninato-cobalt(II) (CoPc-2T)



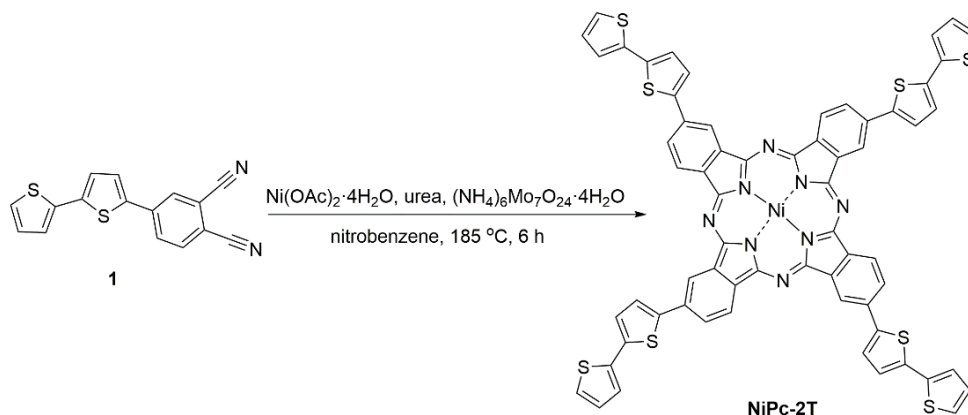
CoPc-2T was synthesized following the same procedure as for ZnPc-2T by using 4-([2,2'-bithiophen]-5-yl)phthalonitrile (**1**, 0.176 g, 0.603 mmol), cobalt acetate tetrahydrate (0.050 g, 0.20 mmol), urea (0.105 g, 1.75 mmol) and ammonium molybdate tetrahydrate (0.026 g, 0.021 mmol) in distilled nitrobenzene (1.6 mL) and the solution was stirred at 185 °C for 6 h. After that, the reaction mixture was cooled to room temperature and poured into methanol (50 mL). The resulting dark precipitate was filtered and washed thoroughly with formic acid (50 mL) and then methanol (50 mL). This process was repeated twice, and the resulting dark green precipitate was then dissolved with THF (250 mL) and filtered. The filtrate was concentrated to 50 mL and ethanol (50 mL) was added. The dark green precipitate was separated by filtration, and washed with hexanes (50 mL), dichloromethane (50 mL) and ethanol (50 mL). After drying under reduced pressure, **CoPc-2T** was obtained as a dark green solid (0.083 g, 45%). UV-visible: $\lambda_{\text{obs}}(\epsilon)$ 351 (9.3×10^4), 692 (8.8×10^4) nm. HR-MALDI-spiralTOF-MS m/z : found, 1226.9849 [M^+]; calcd, 1226.9848 (M^+ , $M = \text{C}_{64}\text{H}_{32}\text{N}_8\text{S}_8\text{Co}$).

3.3.4 2,9,16,23-tetra([2,2'-bithiophen]-5-yl)phthalocyaninato-copper(II)
(CuPc-2T)



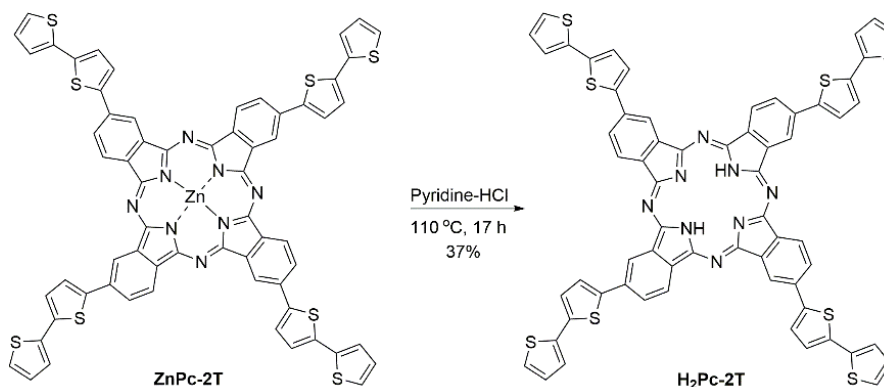
CuPc-2T was synthesized following the same procedure as that described for **ZnPc-2T** by using 4-([2,2'-bithiophen]-5-yl)phthalonitrile (**1**, 0.135 g, 0.462 mmol), copper acetate tetrahydrate (0.035 g, 0.18 mmol), urea (0.117 g, 1.94 mmol) and ammonium molybdate tetrahydrate (0.024 g, 0.019 mmol) in distilled nitrobenzene (1.8 mL). After the solution was stirred at 185 °C for 6 h, the reaction mixture was cooled to room temperature and poured into methanol (50 mL). The resulting dark precipitate was filtered and washed thoroughly with formic acid (50 mL), and then methanol (50 mL). This process was repeated twice, and the resulting dark green solid was washed with ethanol and then dichloromethane. After drying under reduced pressure, **CuPc-2T** was obtained as a dark green solid (0.116 g, 82%). UV-visible: λ_{abs} 370, 652, 707 nm. MALDI-TOF-MS m/z : found, 1230.981 [M^+]; calcd, 1231.304 (M^+ , $\text{M} = \text{C}_{64}\text{H}_{32}\text{N}_8\text{S}_8\text{Cu}$). ^1H and ^{13}C NMR spectroscopy and ϵ could not be determined due to low solubility and paramagnetic properties. Moreover, this compound did not show significant emission.

3.3.5 2,9,16,23-tetra([2,2'-bithiophen]-5-yl)phthalocyaninato-nickel(II)
(NiPc-2T)



NiPc-2T was synthesized following the same procedure as that described for ZnPc-2T by using 4-([2,2'-bithiophen]-5-yl)phthalonitrile (**1**, 0.088 g, 0.302 mmol), Nickel acetate tetrahydrate (0.025 g, 0.10 mmol), urea (0.051 g, 0.857 mmol) and ammonium molybdate tetrahydrate (0.013 g, 0.010 mmol) in distilled nitrobenzene (1.6 mL). After the solution was stirred at $185\text{ }^\circ\text{C}$ for 6 h, the reaction mixture was cooled to room temperature and poured into methanol (50 mL). The resulting dark precipitate was filtered and washed thoroughly with formic acid (50 mL), and then methanol (50 mL). This process was repeated twice, and the resulting dark green solid was washed with ethanol and then dichloromethane. After drying under reduced pressure, a dark green solid containing NiPc-2T (0.068 g) was obtained. MALDI-TOF-MS m/z : found, 1225.906 [M^+]; calcd, 1225.987 (M^+ , $\text{M} = \text{C}_{64}\text{H}_{32}\text{N}_8\text{S}_8\text{Ni}$). Due to low solubility of NiPc-2T, complete purification to get pure NiPc-2T was not possible.

3.3.6 2,9,16,23-tetra([2,2'-bithiophen]-5-yl)phthalocyanine (H_2Pc-2T)



Following a reported procedure,⁹⁵ a mixture of 2,9,16,23-tetra([2,2'-bithiophen]-5-yl)phthalocyaninato-zinc(II) (**ZnPc-2T**, 0.066 g, 0.054 mmol), pyridine-HCl (0.790 g, 6.80 mmol), and pyridine (1.6 mL) was stirred under N_2 atmosphere at 110 °C for 17 h. After cooling to room temperature, the reaction mixture was added H_2O (10 mL) and the resulting precipitate was filtered, and washed with H_2O , MeOH and then CH_2Cl_2 . After drying under vacuum, **H₂Pc-2T** was obtained as a dark green solid (0.023 g, 37%). UV-visible: λ_{abs} 339, 687 and 830 nm. λ_{em} (λ_{ex} = 370 nm): 491, 694, 741 nm; λ_{em} (λ_{ex} = 650 nm): 694 nm. MALDI-TOF-MS m/z : found, 1170.875 [M^+]; calcd, 1171.512 (M^+ , $M = C_{64}H_{34}N_8S_8$). 1H and ^{13}C NMR spectroscopic method and ϵ could not be determined due to low solubility of this compound.

3.4 Electrochemistry

3.4.1 Electropolymerization

The ITO/glasses and carbon papers were cut into 0.8 cm × 4.0 cm and 1.0 cm × 2.0 cm, respectively. A cleaning process and pretreatment of the ITO/glasses were performed by following procedures: the ITO glasses were wiped with KimWipe soaked with toluene, washed under sequential sonication for 15 min in acetone, isopropanol, de-ionized water, and then dried in oven at 100 °C. In case of the carbon papers, acetone was used in the washing process prior to the drying process in the oven at 100 °C. The electrochemical polymerization of **ZnPc-2T** and **CoPc-2T** was performed in a one-compartment three-electrode system by means of the CV as shown in **Figure 3–1**. The electrochemical cell consisted of the ITO/glass or the carbon paper as the WE, a home-made AgCl-coated Ag wire (Ag/AgCl) as a quasi-reference electrode (QRE)^{96, 97} and a Pt plate as the CE. The potential of the Ag/AgCl QRE was calibrated by a ferrocene/ferrocenium (fc/fc⁺) redox couple by showing $E_{1/2}$ potential of 3.5 V. The polymerization was electrochemically performed in a solution of 1.0 mM **ZnPc-2T** or 0.5 M **CoPc-2T** containing 0.1 mM tetrabutylammonium tetrafluoroborate (TBABF₄) in THF under the N₂ atmosphere. The applied potential of the WEs consisting of ITO and carbon paper for **ZnPc-2T** was used in a range of 0.00 and 1.20 V vs. Ag/AgCl QRE ITO/glass and carbon paper with the number of scanning cycles of 10. In case of **CoPc-2T**, the applied potentials of the WEs were used in a range of 0.00 V and 1.20 V vs. Ag/AgCl QRE for the ITO/glass and 0.00 V and 1.40 V vs. Ag/AgCl QRE for the carbon paper with the number of scanning cycles of 20 and 40, respectively. A scan rate of 50 mV s⁻¹ was used for electropolymerization experiments. Each resulting polymer film was deposited on the area of 0.8 cm × 2.0 cm or 1.0 cm × 1.2 cm on the ITO/glass or carbon paper, respectively. After completion of the eletropolymerization, the resulting polymer films were immediately washed with THF to remove excessive monomer and electrolyte salt and then, left dry under ambient condition.

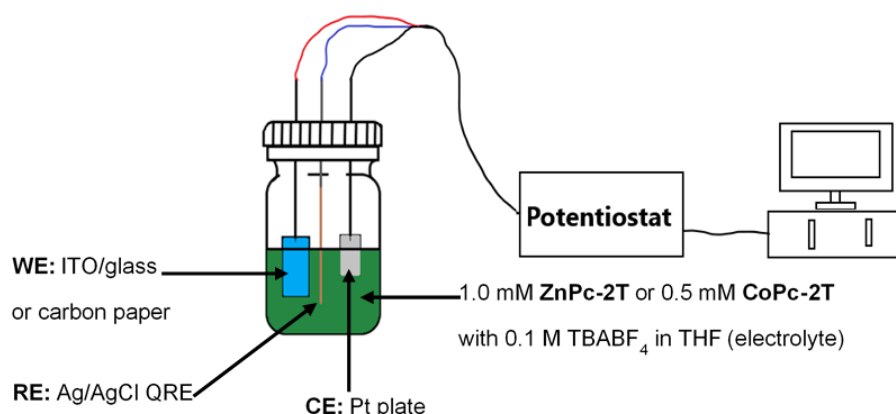


Figure 3–1. A one-compartment three-electrode electrochemical set up for electropolymerization.

3.4.2 CPE in a one-compartment electrochemical cell

CPE experiments were performed using the one-compartment three-electrode system in a 0.1 M tetrabutylammonium hexafluorophosphate (TBAPF₆) solution in acetonitrile (ACN) as shown in **Figure 3–2**. The electrochemical cell contained the polymer-coated ITO/glass or carbon paper as the WE, Pt plate as the CE, and the Ag/AgCl QRE and Ag/AgCl QRE. Prior to all CPE experiments, the CV of each WE was performed under N₂- or CO₂-saturated conditions using the same electrochemical setup in a potential range of 0.0 V to –1.7 V or to –1.8 V vs. Ag/AgCl QRE at the scan rate of 50 mV·s⁻¹ in order to estimate potential used for the CPE. According to the investigation, the potential of –1.7 V vs. Ag/AgCl QRE was applied for the CPE under the CO₂-saturated condition for 2 h or 12 h. At the end of each experiment, a portion of headspace gas (4.0 mL from total volume of 10.0 mL) was taken by a gas-tight syringe and analyzed with a Thermo Scientific Trace GC Ultra equipped with a thermal conductivity detector (TCD) for sequentially detecting CO and H₂ by using He and N₂ as carrier gases, respectively. For the liquid phase analysis, samples of the electrolysis solution (20 μL) were diluted with mill-Q water (1980 μL), filtrated by a syringe filter and determined by a Thermo Scientific Dionex-5000 ion chromatography system equipped with a suppressor-conductivity detector. The gradient KOH was used as an eluent periodically programed by 10 mM KOH (0 to 7

min), 100 mM KOH (7 to 14) and 10 mM KOH (14 to 27 min) at constant temperature of 30 °C with a flow rate of 0.25 mL·min⁻¹.

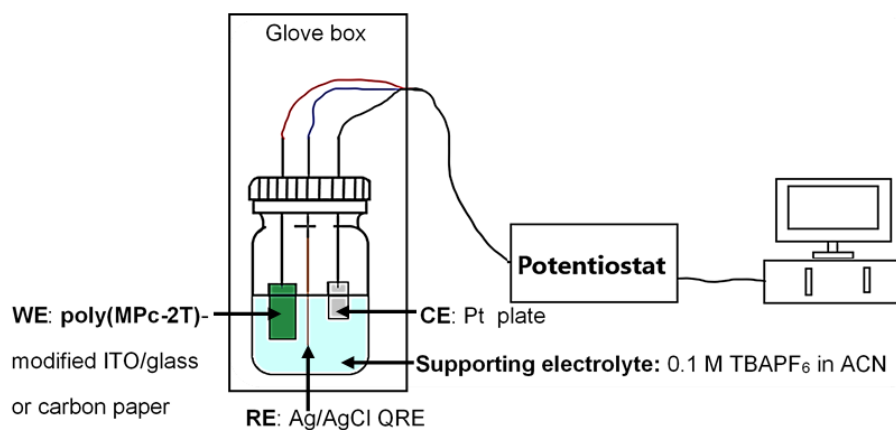


Figure 3–2. A one-compartment three-electrode electrochemical set up for CPE experiments.

3.4.3 CPE in a two-compartment electrochemical cell

This method was carried out using a home-made two-compartment electrochemical cell (H-cell) consisting of a cathodic and an anodic chambers as shown in **Figure 3–3**. The cathodic chamber contained the 1.0 cm × 1.0 cm polymer-coated carbon paper as the WE and an Ag/AgCl (3 M KCl) as the RE, while the anodic chamber contained the Pt plate as the CE. Both chambers were connected via a nafion membrane (117) which was previously activated with concentrated nitric acid at 80 °C for 1 h and washed with milli-Q water until the eluent become neutral.⁹⁸ Each chamber contained a 0.5 M KHCO₃ aqueous solution (35.0 mL, pH 8.4 and 7.3 for the experiments under the N₂- and CO₂-saturated conditions, respectively) or a 0.1 M KH₂PO₄/K₂HPO₄ aqueous solution (35.0 mL, pH 7.3 and 6.4 for the experiments under the N₂- and CO₂-saturated conditions, respectively). Each chamber was equipped with a silicon/PTFE septum and a SCHOTT screw cap with an aperture (GL 32) to keep the system tightly closed. N₂ or CO₂ was purged into each solution for 20 min before each measurement. Before performing the CPE, the CV of each polymer-coated carbon paper was performed at the potential ranging from 0.0 to -1.2 V or to -1.3 V vs. Ag/AgCl (3 M KCl) with the scan

rate of $50 \text{ mV}\cdot\text{s}^{-1}$. During the CPE experiments, the solutions was stirred at 400 rpm and the potential of -1.2 V or -1.3 V vs. Ag/AgCl (3 M KCl) was applied to the WE. After 2 h, a portion of the headspace gas (4.0 mL from total volume of 38.0 mL) was taken by the gas-tight syringe and analyzed with the GC and, the liquid sample was investigated by IC in the same manner as that described in section 3.4.2. The calculation of %FE, TON and TOF were showed in appendix.

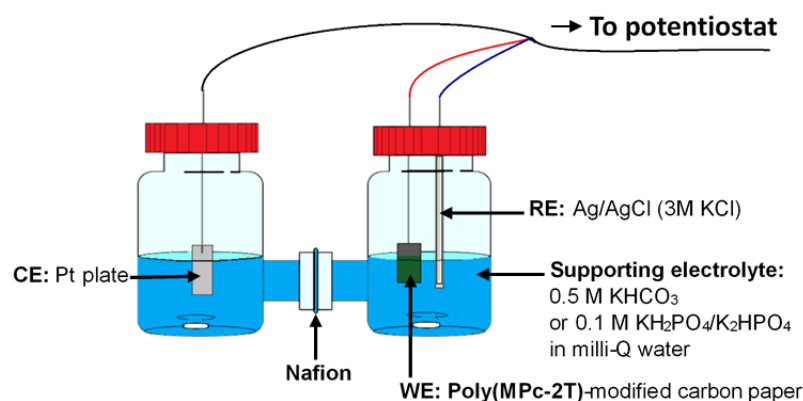


Figure 3–3. A two-compartment three-electrode electrochemical cell.

For accurate analysis of the formation of the reduction product(s) during the CPE, online GC was performed by using the same electrochemical setup with additional connection between the headspace of the cathodic chamber and a gas-sampling loop of the GC instrument via a gas tube as shown in **Figure 3–4**. CO₂ was continuously bubbled into the 0.5 M KHCO₃ cathodic electrolyte at the flow rate of $10 \text{ mL}\cdot\text{min}^{-1}$. During the CPE experiments, the solutions in both chamber were stirred at 400 rpm and the potentials of -1.2 V , -1.3 V and -1.4 V vs. Ag/AgCl (3 M KCl) were applied for 20 h. Quantitative analysis of the product formation was carried out every 30 min for 20 h.

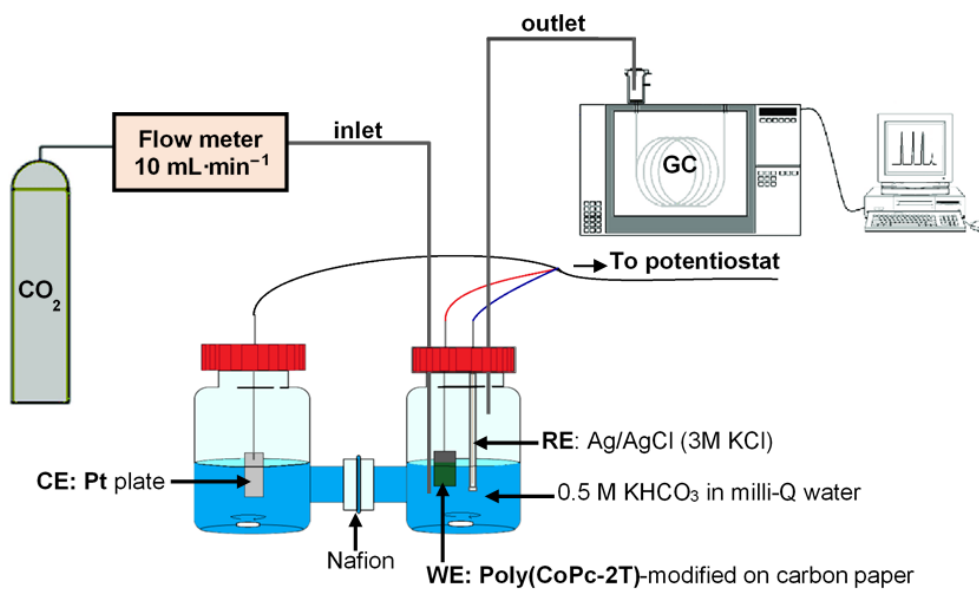


Figure 3–4. A two-compartment three-electrode electrochemical setup connected with online GC.

CHAPTER 4

RESULTS AND DISCUSSION

The main idea of this work is to improve catalytic activity and stability of **MPc** derivatives for the ECR of CO₂ by introducing polymerizable groups on the **H₂Pc** and **MPc** using the electropolymerization technique for preparing the **H₂Pc** or **MPc**-based polymer film on the ITO/glass and carbon paper substrates. The electropolymerization can extend the polymer network in two dimension (2D) and give controllable film thickness with well-defined morphologies.^{30, 64} The 2D structure of the resulting polymeric network are also expected to have high stability and high active surface area.

In this chapter, the target **MPc** monomers were characterized by means of spectroscopic methods consisting ¹H- and ¹³C-NMR spectroscopy, MS, UV-visible spectrophotometry, photoluminescence spectrophotometry, ATR-FTIR spectroscopy, and XPS analysis. After that, the corresponding polymers were prepared by CV technique and characterized by spectroscopic methods including UV-visible spectrophotometry, ATR-FTIR spectroscopy, XPS analysis, SEM and EDX. And then, their electrochemical features and catalytic performance for electrochemical reduction of CO₂ were investigated by mean of CV and controlled potential electrolysis (CPE). The reduction products after CPE were detected by the GC and the IC to estimate the catalytic performance in terms of FE, TON and TOF of the formation of the reduction product(s).

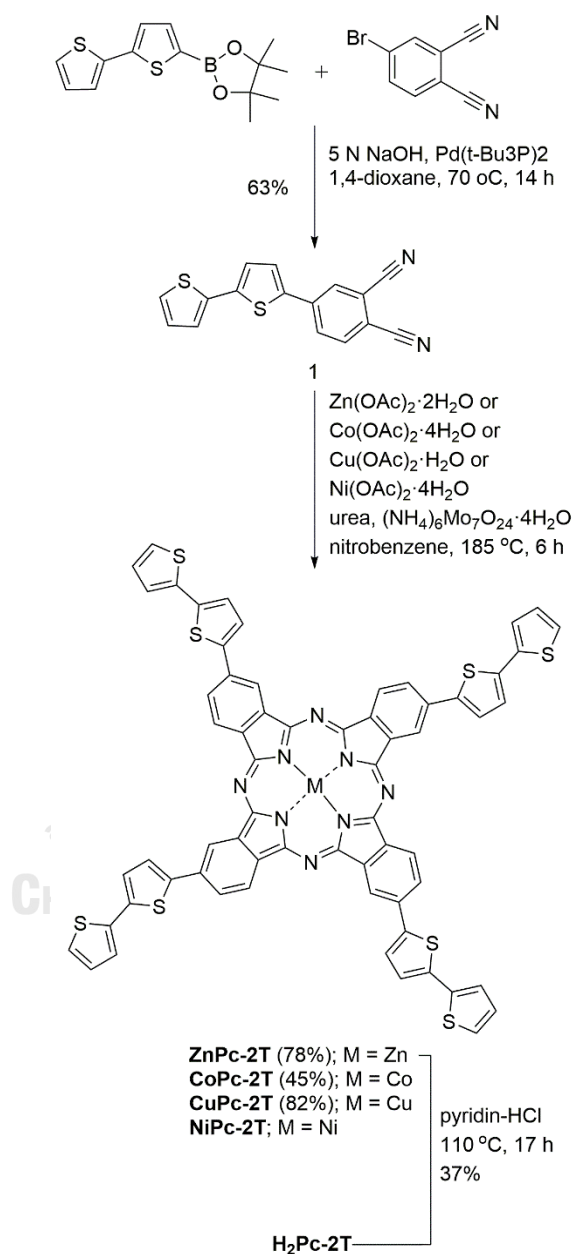
4.1 Synthesis and characterization of the target compounds

4.1.1 Synthesis and characterization of MPc-2Th

ZnPc-2T, **CoPc-2T**, **CuPc-2T** and **NiPc-2T** were synthesized via a two-step reaction as shown in **Scheme 4-1**. Suzuki cross-coupling reaction between 4-bromophthalonitrile and 2,2'-bithiophene-5-boronic acid pinacol ester gave 4-([2,2'-bithiophen]-5-yl) phthalonitrile (**1**), which underwent cyclization in the presence of appropriate metal acetate hydrates, urea and ammonium molybdate tetrahydrate to afford **ZnPc-2T**, **CoPc-2T** and **CuPc-2T** in 49%, 28%, 52% overall yield, respectively.

In case of **NiPc-2T**, the yield could not be determined due to difficulty in purification. To achieve **H₂Pc-2T**, **ZnPc-2T** was demetallated by using pyridine-HCl at 110 °C for 17 h, affording **H₂Pc-2T** in 37 % yield. The relatively low yield resulted from difficulty in column chromatography due to low solubility of this compound. Therefore, additional precipitation was required to remove further undesired byproducts. The formation of **ZnPc-2T**, **CoPc-2T**, **CuPc-2T**, **NiPc-2T** and **H₂Pc-2T** were confirmed by HR-MALDI-spiralTOF-MS or MALDI-TOF-MS showing their molecular ion peaks at m/z 1231.9826, 1226.9849, 1230.981, 1225.906 and 1170.875, respectively, with consistent isotopic patterns (Figure A-7, A-13, A-19, A-21 and A-17). A ¹H-NMR spectrum of **ZnPc-2T** exhibited signals of aromatic protons at δ 9.17–8.08 ppm and 8.02–7.21 ppm, corresponding to 12 phenyl and 20 bithiophenyl protons, respectively (Figure A-5). Moreover, a ¹³C-NMR spectrum of **ZnPc-2T** showed aromatic carbon peaks at 124.2–151.4 ppm (Figure A-6). Due to paramagnetic nature of metal centers in **CoPc-2T**, **CuPc-2T** and **NiPc-2T** as well as the low solubility of **CuPc-2T** and **H₂Pc-2T** in organic solvents, their NMR spectra could not be obtained. **ZnPc-2T** and **CoPc-2T** exhibited moderate solubilities in polar aprotic solvents, such as THF, DMF and DMSO, owing to available axial coordination at their metal centers, whereas **H₂Pc-2T** did not have such a coordination site and therefore had to confront molecular aggregation. **CuPc-2T** showed extremely low solubility even in coordinating solvents possibly due to significant coordination between copper central metals inside the phthalocyanine rings that led to high aggregation effect.⁹⁹ In case of **NiPc-2T**, attempts to purify the crude solid failed to give pure **NiPc-2T** due to extremely low solubility probably resulting from dimerization of Ni(II)-phthalocyanine rings via μ -oxo and μ -peroxo bridges,¹⁰⁰ as evidenced by the mass spectrum showing an additional $[M+O]^+$ peak at m/z 1239.951 (Figure A-21). **H₂Pc-2T**, **CuPc-2T** and **NiPc-2T** could be dissolved in strong acid, such as concentrated sulfuric acid and trifluoroacetic acid, leading to protonation of inner and outer nitrogens of **H₂Pc-2T**, as well as of the outer nitrogens of **NiPc-2T** and **CuPc-2T**. However, since the electropolymerization and the ECR of CO₂ required use of the common organic solvents, **H₂Pc-2T**, **CuPc-2T** and **NiPc-2T**

were not taken into account in these studies. **H₂Pc-2T** was used only in the investigation on the photophysical properties in comparison with that of **ZnPc-2T** and **CoPc-2T** as described in the next section, while **CuPc-2T** and **NiPc-2T** were not be further studied.



Scheme 4-1. Synthesis of **ZnPc-2T**, **CoPc-2T**, **CuPc-2T**, **NiPc-2T** and **H₂Pc-2T**.

4.1.2 Investigation of photophysical properties of the target compounds

To investigate the photophysical properties of the target compounds, the absorption and emission spectra were recorded in THF solution by using UV-visible and fluorescence spectrophotometry. The absorption and emission patterns of the target compounds were compared with **H₂Pc** or **MPc** (M = Zn or Co) as shown in the **Figures 4-1** and **4-2** and summarized in **Table 4-1**. The results showed that the typical absorption B- and Q-bands of the target compounds were observed in the range of 300–500 nm and 500–800 nm, respectively, with high extinction coefficient values of 10^4 – 10^5 L·mol⁻¹·cm⁻¹. These results are consistent with previously reported data for **H₂Pc** and **MPc** derivatives and the Gouterman's four-orbital LCAO model of an 18- π electron in aromatic system^{26, 43} Compared with the absorption pattern of **ZnPc** and **CoPc**, the introduction of the bithiophenyl groups at the β -positions of the **Pc** rings caused **ZnPc-2T** and **CoPc-2T** red shift of the Q-bands by 42 and 37 nm, as well as the presence of the additional absorption shoulders at 405 and 410 nm, respectively. The former observation could be explained by extended π -conjugation due to the bithiophenyl β -substituents, leading to destabilization of the HOMO level and consequently, reduction of the energy gap.²⁶ The latter could be due to absorption of conjugated bithiophenyl moieties.¹⁰⁵ In case of **H₂Pc**, where the molecular aggregation effect was quite strong, the absorption spectrum showed extraordinary splitting of the Q band due to D_{2h} symmetry and degeneracy of the LUMO energy level.²⁶ The splitting of Q band, however, is generally suppressed when the conjugation of the macrocycle was extended, as in **H₂Pc-2T**.²⁶

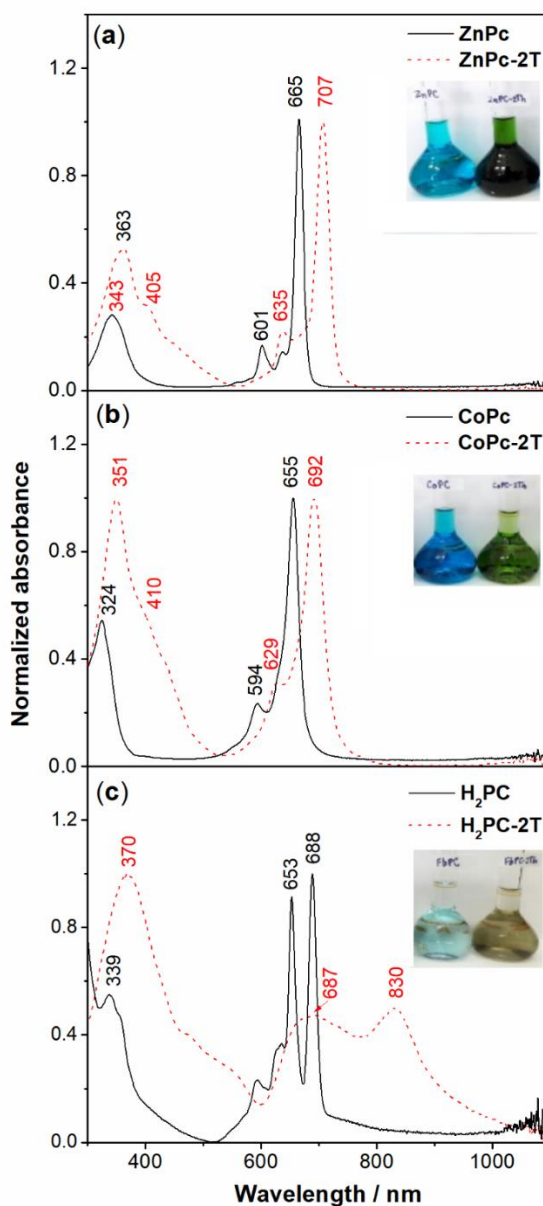


Figure 4-1. Absorption spectra and solution of (a) **ZnPc**, (b) **CoPc** and (c) **H₂Pc** derivatives having no substituent (black solid line and left flasks) and bearing bithiophenyl β -groups (red dashed lines and right flasks).

Upon excitation at the B- and Q-band regions, emission spectra of **ZnPc** and **ZnPc-2T** exhibited similar patterns with an additional peak at 514 nm and red-shift of the emission peak of 26 nm due to the addition of the bithiophenyl moieties (**Figure 4-2**). In case of **CoPc** and **CoPc-2Th** no emission peak was observed because of quenching effect by the central cobalt ion.^{26, 101} Interestingly, the emission patterns

of **H₂Pc** and **H₂Pc-2T** were found to be different from each other when these compounds were excited at their B-bands. The intense emission peak at 491 nm of **H₂Pc-2T** is attributed to the bithiophenyl groups. This observation also suggested that the photoexcitation at the B-band region could cause dominant electron distribution at the bithiophenyl groups of **H₂Pc-2T**. On the other hand, the emission spectra of **H₂Pc-2T** and **H₂Pc** upon the excitation at the Q band region gave the same similarity of both peak patterns and positions. This result could indicate that the photoexcitation at the Q band of **H₂Pc-2T** led to the major electron distribution at the macrocycle without electronic interference of the bithiophenyl β -substituents.

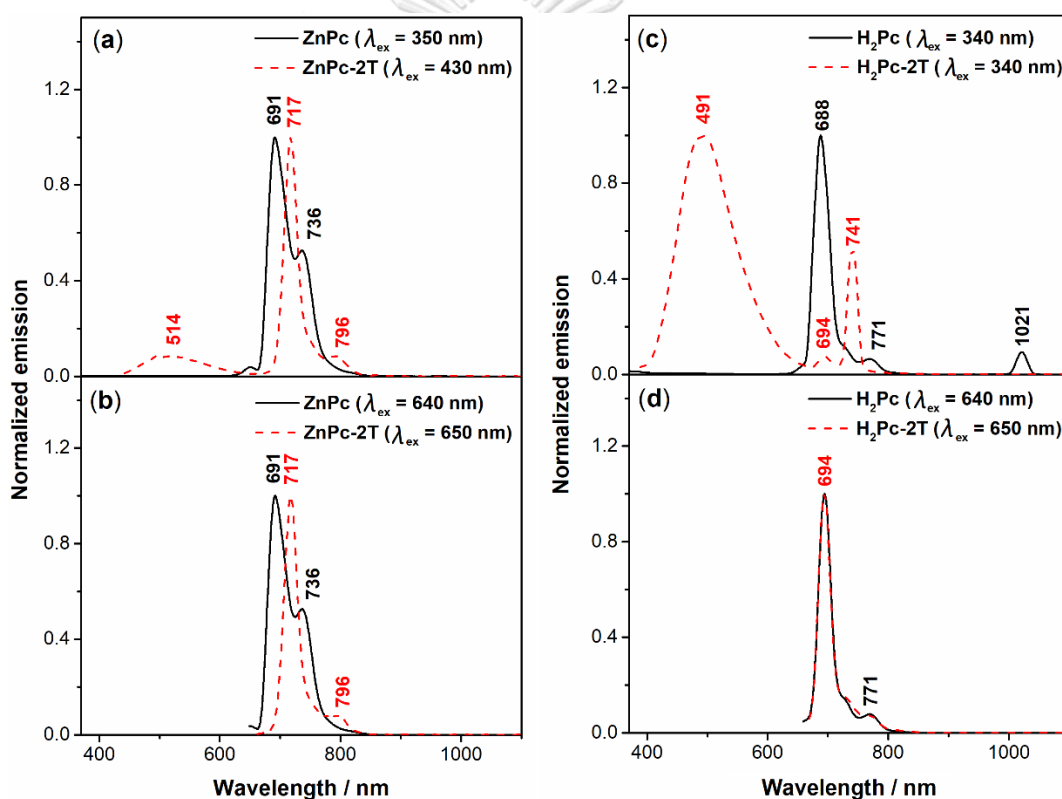


Figure 4–2. Emission spectra of **ZnPc** (black solid line) and **ZnPc-2T** (red dashed line) solutions upon excitation at their (a) B and (b) Q bands, and **H₂Pc** (black solid line) and **H₂Pc-2T** (red dashed line) solutions upon excitation at their (c) B and (d) Q bands.

Table 4-1. Photophysical properties of the target phthalocyanines compared with their unsubstituted analogs.

Compounds	$\lambda_{\text{abs}} / \text{nm} (\epsilon / \text{L}\cdot\text{mol}^{-1}\cdot\text{cm}^{-1})^{\text{a}}$		$\lambda_{\text{em}} / \text{nm}$	
	B-band	Q-band	Excitation at B band	Excitation at Q band
ZnPc	343	601, 665	691, 736	691, 736
ZnPc-2T	363 (9.3×10^4), 405	637 (3.9×10^4), 707 (1.8×10^5)	514, 717, 796	717, 796
CoPc	324	594, 655	$_{-}^{\text{b}}$	$_{-}^{\text{b}}$
CoPc-2T	351 (9.3×10^4), 410	629, 692 (8.8×10^4)	$_{-}^{\text{b}}$	$_{-}^{\text{b}}$
H ₂ Pc	339	653, 688	688, 771, 1021	694, 771
H ₂ Pc-2T	339	687, 830	491, 694, 741	694, 771

^a The ϵ values were determined for some absorption peaks having high absorptivity.

^b No emission spectra was observed.

4.2 Preparation and characterization of the target polymers

4.2.1 Electrochemical polymerization of ZnPc-2T

The polymerization of **ZnPc-2T** was performed by means of the CV on the ITO/glasses and carbon papers in the 0.1 M TBABF₄ solution in THF containing 1.0 mM **ZnPc-2T**. The reaction was conducted under N₂ atmosphere in a one-compartment three-electrode system consisting of the ITO/glass or carbon paper as the WE, the Pt plate as the CE and the Ag/AgCl QRE. The potential between 0.00 V and 1.20 V vs. Ag/AgCl QRE was applied at the scan rate of 50 mV·s⁻¹ with the number of the scanning cycles of 10.

As shown in **Figure 4-3a**, the first scanning oxidation cycle, represented the oxidative feature of the **ZnPc-2T** monomer, exhibited two peaks at 0.62 V and 0.82V vs. Ag/AgCl QRE, corresponding to the oxidation of the macrocyclic phthalocyanine and bithiophenyl moieties, respectively.^{48, 102} Upon increasing the number of the cycles to 10 cycles, the current density was increased, indicating the possible formation of the electroactive species or the polymer film on the ITO/glass. In addition, the second oxidation peak gradually shifted to higher potential and potential onset was significantly decreased from 0.42 V to 0.28 V vs. Ag/AgCl QRE, indicating the formation of the polymeric species that was easier to oxidize than the monomeric one.^{63, 64} When the carbon paper was used, the similar pattern of the cyclic voltammogram as that observed in the case of the ITO/glass were detected (**Figure 4-3b**). The current densities were found to be slightly higher than those observed when the ITO/glass was used due to higher geometric surface area of the carbon paper. The resulting greenish polymer films were quite homogeneous and stable under ambient condition.

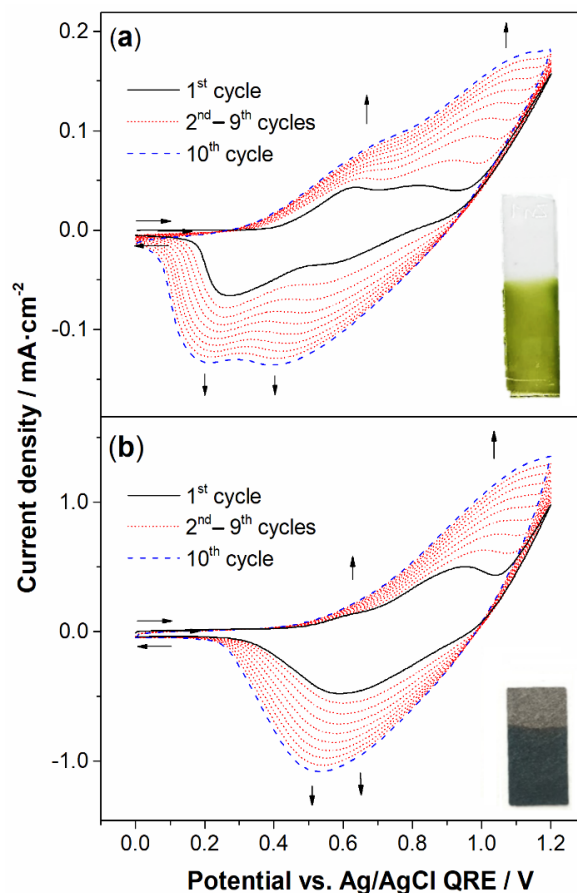


Figure 4–3. Cyclic voltammograms and films obtained from electrochemical polymerization of **ZnPc-2T** at the first cycle (black solid line), the 2nd–9th cycles (red dotted lines) and the 10th cycle (blue dashed line) on (a) an ITO/glass and (b) a carbon paper.

4.2.2 Electrochemical polymerization of CoPc-2T

In a similar manner as the procedure described for **ZnPc-2T**, the polymer films of **CoPc-2T** were prepared by using in the 0.1 M TBABF₄ solution in THF containing 0.5 mM **CoPc-2T** monomer. The potential range of 0.00–1.20 V and 0.00–1.40 V vs. Ag/AgCl QRE, and the number of scanning cycles of 20 and 40 were applied at the scan rate of 50 mV·s⁻¹ when the ITO/glass and carbon paper were used as the substrates, respectively. The cyclic voltammogram of the **CoPc-2T** on the ITO/glass showed two oxidation peaks at the potential of 0.75 V and 1.00 V vs. Ag/AgCl QRE in the first sweeping cycle, corresponding to oxidation of the Co(II) to Co(I)^{32, 48, 63, 102} and bithiophenyl moieties,^{103, 104} respectively (**Figure 4–4a**). Upon

increase in the number of the cycles, the current density was increased with the two oxidation peaks observed at 0.50 V and 0.75 V vs. Ag/AgCl QRE, which gradually shifted into the higher positive potential, indicating the possible formation of the electroactive species or polymer film on the electrode surface. The cyclic voltammograms of **CoPc-2T** on the carbon paper exhibited a similar features as those observed for the polymerization on the ITO/glass (**Figure 4-4b**). In this case, the wider potential range, *i.e.* from 0.00 to 1.40 V vs. Ag/AgCl QRE, and the higher number of the scanning cycles, *i.e.* 40, were required in order to obtain good coverage of the polymer on the carbon paper surface.

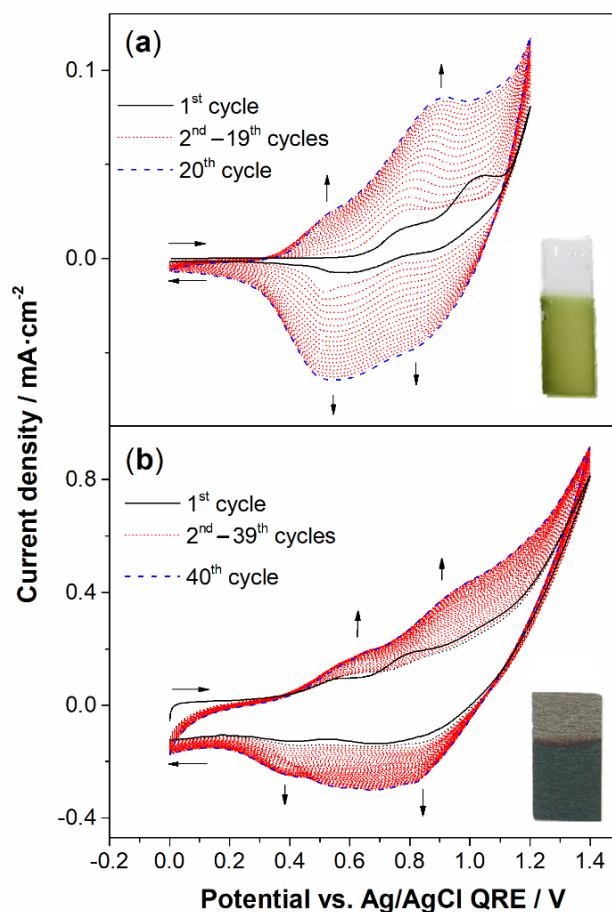


Figure 4-4. Cyclic voltammograms and films obtained from electrochemical polymerization of **CoPc-2T** at the first cycle (black solid line), (a) the 2nd–19th cycles (red dotted lines) and 20th (blue dashed line) on an ITO/glass and (b) 2nd–39th (red dotted lines) and the 40th cycles (blue dashed line) on a carbon paper.

4.2.3 Investigation of the photophysical properties of the polymer films

To confirm the formation of the polymer films of **ZnPc-2T poly(ZnPc-2T)** and **CoPc-2T poly(CoPc-2T)** from the above-mentioned electrochemical polymerization, the resulting films were investigated by the UV-visible spectrophotometry, the ATR FT-IR spectroscopy, the Raman spectroscopy, the SEM equipped with the EDX, and the XPS analysis. For the UV-Visible spectrophotometry, the intense absorption patterns of the **poly(ZnPc-2T)** were observed at 362 nm and 743 nm, while the **poly(CoPc-2T)** showed intense absorption bands at 359 nm and 723 nm, corresponding to those of their monomer solutions (**Figure 4-5**). However, in case of dropcasted films of their monomers, the broadening, spitting and the low intensity of the Q-bands were detected at 678 and 738 nm for **ZnPc-2T**, and at 650 and 725 nm for **CoPc-2T**, which were attributed to strong H-type aggregation effect of the **MPC** macrocycles (Davidov spitting effect).^{105, 106} Therefore, the intense Q-bands observed from the polymer films supported the hypothesis that the electropolymerization technique could expand the polymer network to suppress the aggregation effect of the macrocyclic compounds. Furthermore, the additional shoulder observed around 451 nm for **poly(ZnPc-2T)** and 440 for **poly(CoPc-2T)** could correspond to newly formed quarterthiophenyl units¹⁰⁷ in the polymer network or be metal-ligand charge transfer band.²⁶ The blue-shifted peaks of the Q-band found in the monomer solutions, compared with that of the dropcasted monomer and polymer films could result from enhanced electron density at the metal centers of the **Pc** ligands due to the coordination with solvent.^{26, 108}

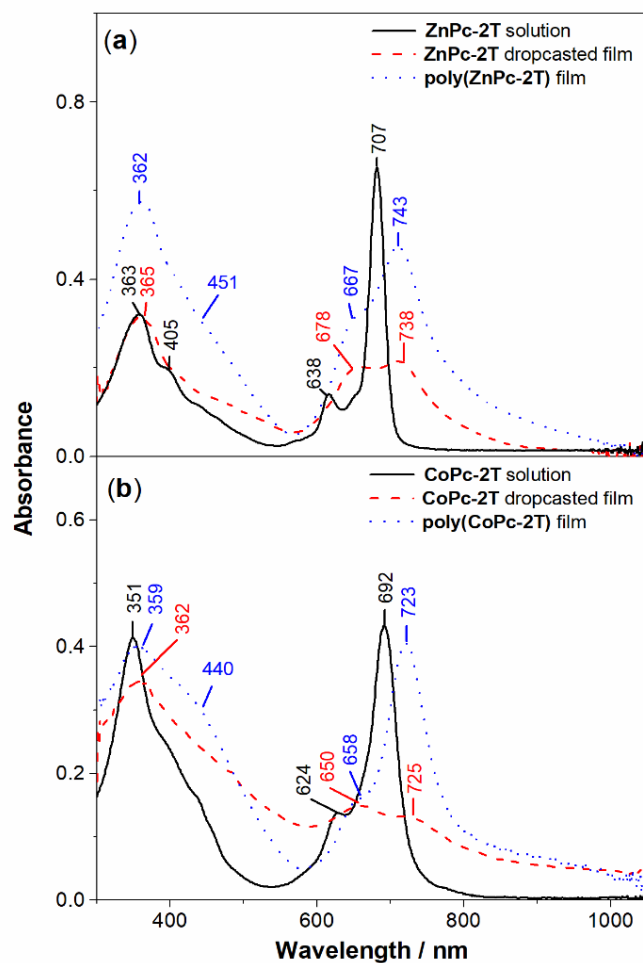


Figure 4–5. Absorption spectra of (a) a **ZnPc-2T** solution in THF (black solid line), a drop-casted film of **ZnPc-2T** (red dashed line) and a **poly(ZnPc-2T)** film on an ITO/glass (blue dotted line), and (b) a **CoPc-2T** solution in THF (black solid line), a drop-casted film of **CoPc-2T** (red dashed line) and a **poly(CoPc-2T)** film on the ITO/glass (blue dotted line).

In the Raman spectroscopy study, the Raman spectra of **poly(ZnPc-2T)** and **poly(CoPc-2T)** were collected in the region of 600 cm^{-1} to 1700 cm^{-1} and compared with the Raman features of the basic vibrational structures of their fundamental components, which are bithiophene (**2T**), unsubstituted **MPc** ($M=\text{Zn(II)}$ or Co(II)), and their monomers as shown in **Figures 4–6**. By using different laser excitation wavelengths corresponding to the UV-visible absorption patterns of each material, *i.e.* 514.7 nm or 633 nm, selective detection of the **MPc** macrocycle and the

bithiophenyl moieties could be achieved due to the different localization of the electron density at the HOMO and LUMO levels as mentioned in chapter 2. When the laser excitation at 514.7 nm was used, the Raman spectra of the target monomers showed the pronounced bithiophenyl feature at 1450 and 1551 cm^{-1} for **ZnPc-2T**, and at 1448 and 1545 cm^{-1} for **CoPc-2T**, which were consistent with Raman spectra of **2T** and their polymers. Upon the laser excitation at 633 nm, the macrocyclic vibration of the target monomers dominated and found at 681, 747 and 1505 cm^{-1} for **ZnPc-2T**, and at 688, 753 and 1542 cm^{-1} for **CoPc-2T**. Such bithiophenyl and macrocycle Raman features were also observed in the cases of **poly(ZnPc-2T)** and **poly(CoPc-2T)**. The Raman features of the target polymers upon laser excitation at 514.7 nm tended to be broader than those of the corresponding monomers possibly because of increase in the delocalization of the electrons and extended π -conjugated system in the polymer networks.¹⁰⁹ Besides, additional peaks at 1487 cm^{-1} and 1485 cm^{-1} were observed for **poly(ZnPc-2T)** and **poly(CoPc-2T)**, respectively, which are attribute to the vibration in the quarterthiophene bridges as described in a previous report.¹¹⁰ Therefore, these results could clearly confirm that the polymers obtained from the electropolymerization process are the polymer of **ZnPc-2T** and **CoPc-2T**.

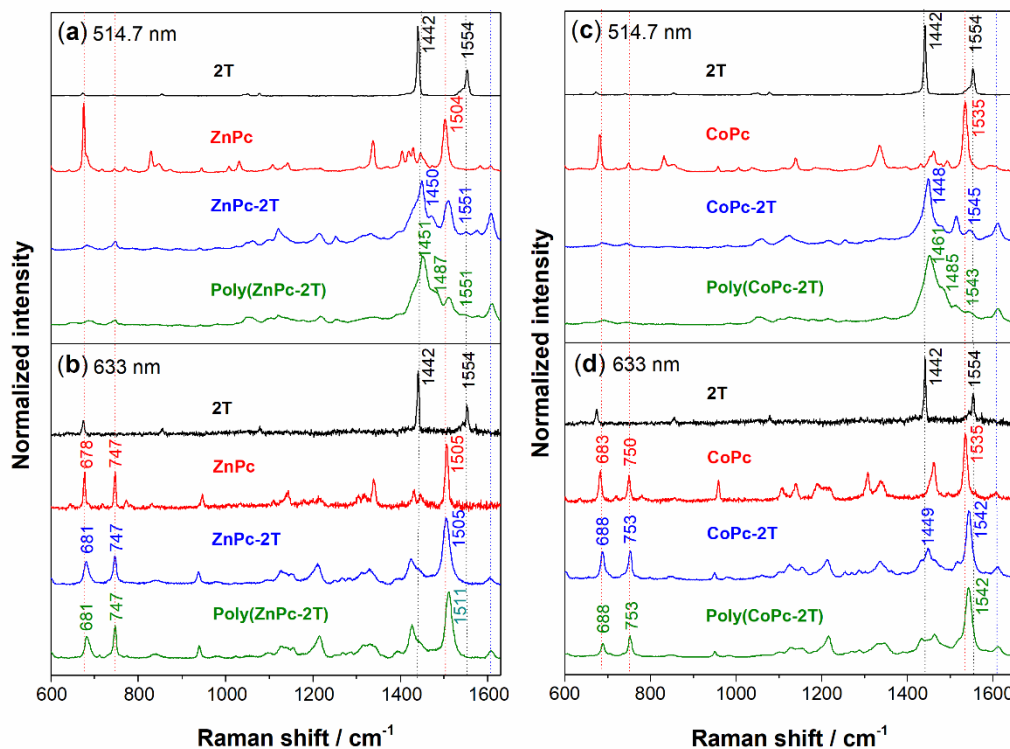


Figure 4–6. Raman spectra of **2T** (black line), **ZnPc** (red line), **ZnPc-2T** (blue line) and **poly(ZnPc-2T)** (green line) upon laser excitation at (a) 514.7 nm and (b) 633 nm, as well as Raman spectra of **2T** (black line), **CoPc** (red line), **CoPc-2T** (blue line) and **poly(CoPc-2T)** (green line) at laser excitation at (c) 514.7 nm and (d) 633 nm.

As complementary study to the Raman spectroscopy, the ATR FT-IR spectroscopy was also used to investigate the vibration features of **poly(ZnPc-2T)** and **poly(CoPc-2T)** in comparison with **2T**, **MPc** (M= Zn or Co) and their monomers as shown in **Figure 4–7**. The ATR FT-IR spectra of **poly(ZnPc-2T)** and **poly(CoPc-2T)** were recorded in the range of 600 cm^{-1} and 1650 cm^{-1} , which is a fingerprint region of the π - conjugated system.¹¹¹ As the results, the main features of the macrocyclic vibrations of **ZnPc-2T** and **CoPc-2T** were detected at 747 cm^{-1} , 1049 cm^{-1} , 1097 cm^{-1} and 1143 cm^{-1} , and at 747 cm^{-1} , 795 cm^{-1} and 1097 cm^{-1} , respectively, consistent with those observed in the cases of that unsubstituted **MPc** analogs. In addition, out-of-plane bending vibration modes at α -C-H bands of the bithiophene moieties of both monomers were observed at 685 cm^{-1} , 824 cm^{-1} and 836 cm^{-1} , which are consistent with those detected in **2T**.^{64, 112} In the case of the polymers, the presence

of the macrocyclic vibrational features and the absence of the α -C-H vibration bands, supported the conclusion that the desired **poly(MPc-2T)** films could be successfully formed through the α -C-H sites of the bithiophene substituents. In addition, several additional bands observed in range of 1200 cm^{-1} and 1600 cm^{-1} in the ATR FT-IR spectra of both polymer films are attributed to the increase in the numbers of atoms in the polymeric networks, according to the number of vibrational modes calculated from $3N_{\text{atom}}-6$.¹¹³

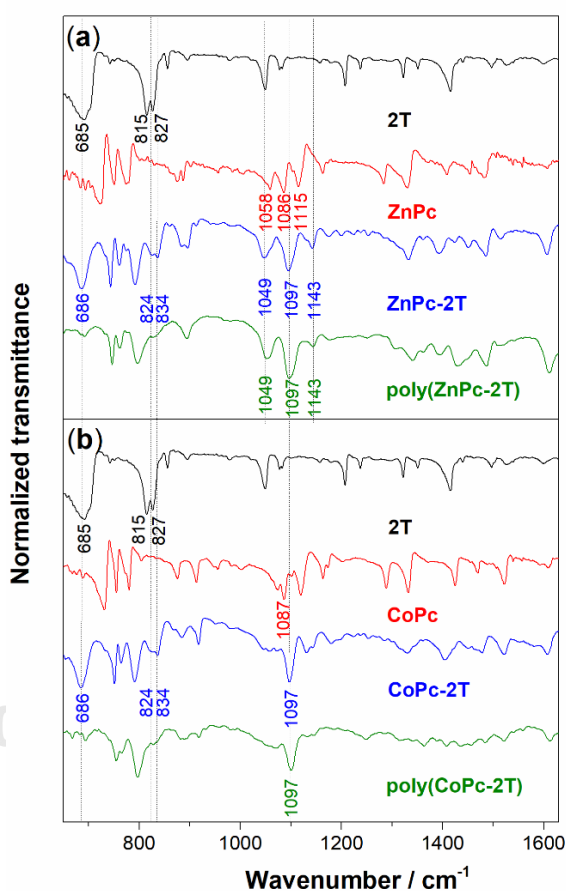


Figure 4–7. ATR FT-IR spectra of bithiophene (**2T**) (black line), unsubstituted **MPc** (red line), **MPc-2T** (blue line) and **poly(MPc-2T)** (green line) when M is (a) Zn and (b) Co.

To further confirm the formation of the desirable polymer films from the electropolymerization process, the XPS analysis was used to determine the elemental composition of **poly(CoPc-2T)** and **poly(ZnPc-2T)**, in comparison with those of their monomers in forms of pristine powder and drop-casted films. The results in **Table 4–2** showed that elemental compositions of all samples were in

good agreement and corresponded with the calculated theoretical values. Therefore, it could be concluded that the polymer films obtained from the electropolymerization of ZnPc-2T or CoPc-2T was the corresponding polymers, poly(ZnPc-2T) or poly(CoPc-2T), respectively.

Table 4-2. XPS analysis data of poly(ZnPc-2T), poly(CoPc-2T) and their monomers.

Samples	Co or Zn: N: S ratio
Calculated	1: 8: 8
ZnPc-2T powder	1: 9.3: 7.8
ZnPc-2T drop-casted film	1: 9.3: 7.8
poly(ZnPc-2T) film	1: 9.0: 7.7
CoPc-2T Powder	1: 9.9: 7.6
CoPc-2T drop-casted film	1: 10.3: 7.9
poly(CoPc-2T) film	1: 10.9: 8.8

According a microscopic study, poly(ZnPc-2T) and poly(CoPc-2T) were found to have good coverage on the fiber-like carbon papers as shown in Figures 4-8a and 4-9a with slight agglomeration of the polymer as observed by SEM (Figures 4-8b and 4-9b). Moreover, the EDX performed in the same area on the carbon paper substrate also confirmed the full coverage of poly(ZnPc-2T) and poly(CoPc-2T) by showing throughout distribution of S and Zn (Figure 8c, 8d), and of S and Co (Figure 9c, 9d) on the carbon papers, respectively. These results indicated that the poly(ZnPc-2T) and poly(CoPc-2T) films were well coated on the high surface area of the carbon papers and suitable for further studies on the catalytic activity for the ECR of CO₂.

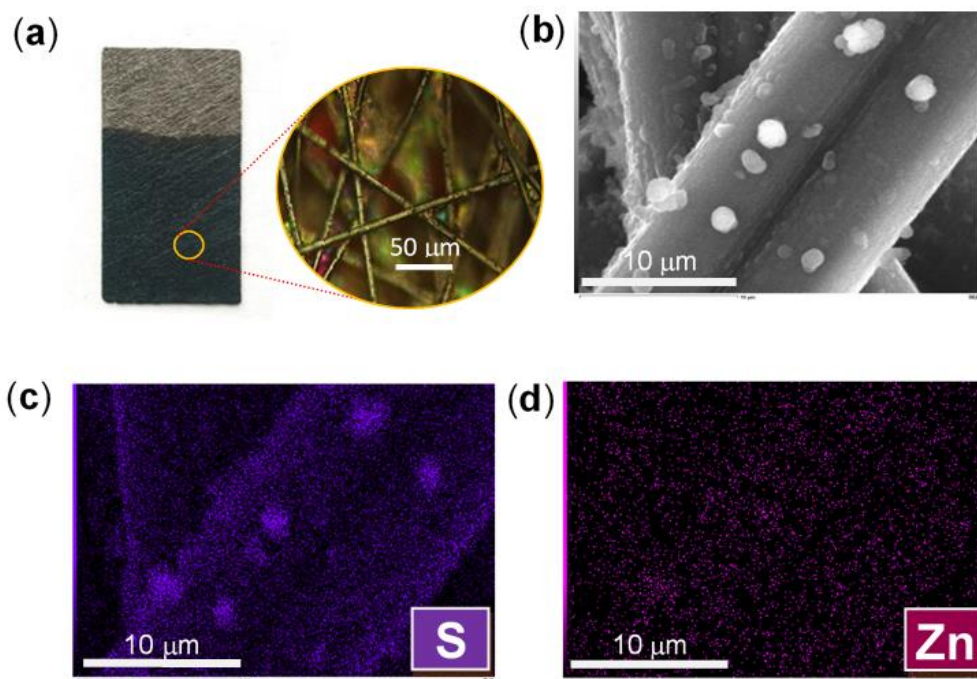


Figure 4–8. (a) a Microscopic image, (b) a SEM image, and EDX maps showing (c) sulfur (S) and (d) zinc (Zn) atoms of a **poly(ZnPc-2T)** film on a carbon paper.

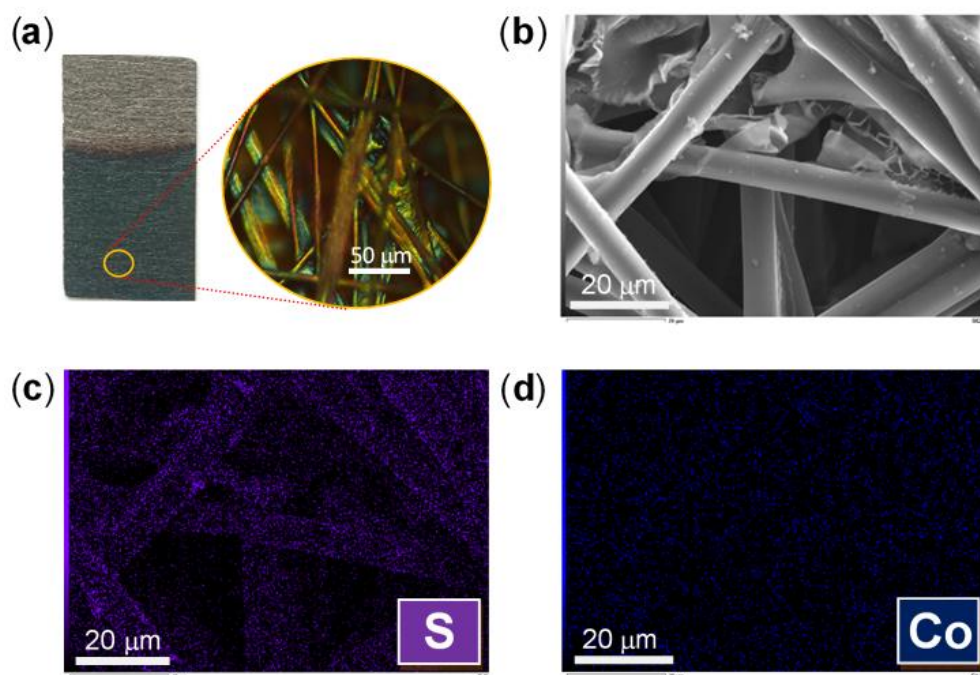


Figure 4–9. (a) a Microscopic image, (b) a SEM image, and EDX maps showing (c) sulfur (S) and (d) cobalt (Co) atoms of a **poly(CoPc-2T)** film on a carbon paper.

4.3 Investigation of the electrocatalytic performance of the target polymers towards the CO₂ reduction

4.3.1 Cyclic voltammetry (CV) studies and controlled potential electrolysis (CPE) measurements in a one-compartment cell and organic medium.

In this study, the CV was performed in a 0.1 M TBAPF₆ solution in ACN and the one-compartment three-electrode system consisting of the polymer-modified carbon paper as the WE, the Pt plate as the CE and Ag/AgCl QRE. The polymer-modified ITO/glass was not used in this study due to low stability of ITO/substrate which is not sufficiently stable for the CPE measurement. Therefore, the polymer-modified carbon paper was used as the WE due to the high surface area and stability properties. Before each experiment, the solution was purged with N₂ or CO₂ for 15 min. The applied potential range of 0.00 V to -1.70 V vs. Ag/AgCl QRE and the scan rate of 50 mV·s⁻¹ were used for all measurements. As a result, the cyclic voltammogram of the **poly(ZnPc-2T)**-modified carbon paper under N₂-saturated condition exhibited two reversible reduction peaks at peak potentials (E_{peak}) of -1.22 V and -1.57 V vs. Ag/AgCl QRE, corresponding to two reduction steps of the **ZnPc** macrocycle (**Figure 4-10**).^{48, 102} Under CO₂-saturated condition, the cyclic voltammogram of the **poly(ZnPc-2T)**-modified carbon paper showed increase of the current densities at the onset potential (E_{onset}) around -0.6 V vs. QRE Ag/AgCl, in comparison with those observed under the N₂-saturated condition. These results indicated that the presence of **poly(ZnPc-2T)** might involve in the ECR of CO₂. Since the ECR of CO₂ required at least two-electron to generate primary products, such as HCOO⁻ and CO,^{38, 39} this study suggested that the suitable applied potential for the CPE measurements of the polymer modified carbon paper described in the next section should be -1.70 V vs. Ag/AgCl QRE or higher.

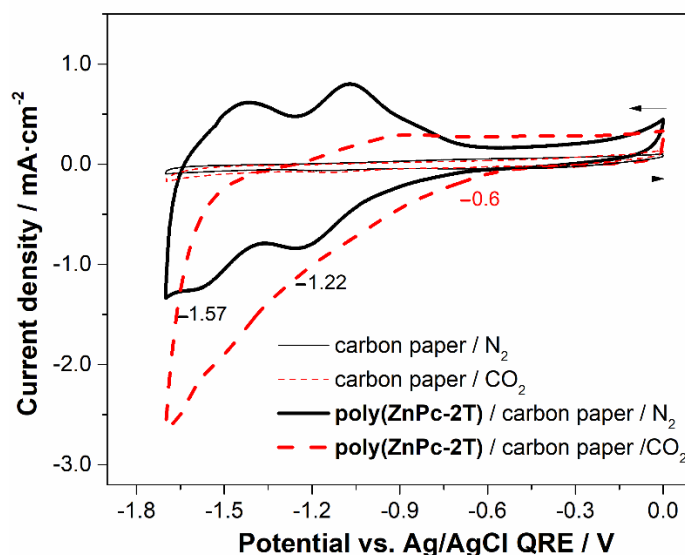


Figure 4–10. Cyclic voltammogram of a **poly(ZnPc-2T)**-modified carbon paper under N_2 - (thick black solid line) and CO_2 -saturated (thick red dashed line) conditions, compared with those of bare carbon papers under the N_2 - (thin black solid line) and CO_2 -saturated (thin red dashed line) conditions recorded in a 0.1 M TBAPF₆ in ACN solution in a one-compartment three-electrode cell.

As regards the CV of the **poly(CoPc-2T)**-modified carbon paper under the N_2 -saturated condition, the cyclic voltammogram exhibited two reduction peaks at the E_{peak} values of -0.67 V and -1.50 V vs. Ag/AgCl QRE (**Figure 4–11**), attributed to the reduction of Co(II) to Co(I) and macrocyclic phthalocyanine moieties, respectively.^{26, 48, 102} Under the CO_2 -saturated condition, the cyclic voltammogram of this modified carbon paper showed cathodic peak at the E_{peak} values of -0.75 V vs. Ag/AgCl QRE and -1.46 V vs. Ag/AgCl QRE, corresponding with slightly change of the first peak and enhanced current density of the second peak, respectively. This result indicated that the first reduction of the cobalt metal center was unlikely to involve the reduction of CO_2 , and the reduced species started to influence the reduction of CO_2 at E_{onset} of -1.13 V vs. Ag/AgCl QRE and higher. This study suggested that the suitable applied potential for the CPE measurements described in the next section should be -1.70 V vs. Ag/AgCl QRE or higher to ensure that at least two-electron reduction process of CO_2 could occur to achieve the reduction products, such as $HCOO^-$ and CO.

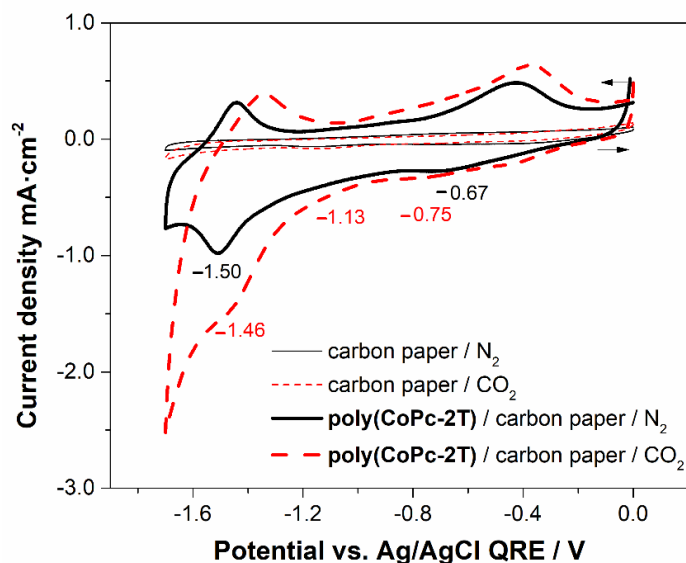


Figure 4-11. Cyclic voltammograms of a **poly(CoPc-2T)**-modified carbon paper under N_2 - (thick black solid line) and CO_2 -saturated (thick red dashed line) conditions compared with those of bare carbon papers under the N_2 - (thin black solid line) and CO_2 -saturated (thin red dashed line) conditions recorded in a 0.1 M TBAPF₆ in ACN solution in a one-compartment three-electrode cell.

The CPE experiments were performed in the same experimental setup as that explained for CV technique. The **poly(CoPc-2T)**-modified carbon paper was applied by the potential of -1.7 V vs Ag/AgCl QRE for 3 h in the CO_2 -saturated condition of a 0.1 M TBAPF₆ solution in ACN to determine the catalytic performance towards the ECR of CO_2 . After completion of each experiment, the gas and liquid samples from the cell were analyzed by the GC and the IC, respectively. As shown in **Figure 4-12a**, the current densities of chronoamperograms of the bare carbon paper and the **poly(ZnPc-2T)**-modified carbon paper were very low throughout the period of 3 h, while the **poly(CoPc-2T)**-modified carbon paper gave slight enhancement of the current density up to 0.1 mA·cm⁻². According to the GC analysis, CO was found as the only product with the FE of 1% for the bare carbon paper and the **poly(ZnPc-2T)**-modified carbon paper, and 16% for the **poly(CoPc-2T)**-modified one after 3 h (**Table 4-3**). To determine the stability of the polymer, the experiment was extended to 12 h under the same condition. The chronoamperograms in **Figure 4-12b** showed that the bare carbon paper exhibited the very low current density, < 0.1

$\text{mA}\cdot\text{cm}^{-2}$ throughout 12 h, while the **poly(ZnPc-2T)**- and **poly(CoPc-2T)**-modified carbon papers gave significantly enhanced current densities of up to $2.3 \text{ mA}\cdot\text{cm}^{-2}$ and $2.7 \text{ mA}\cdot\text{cm}^{-2}$, respectively. However, the FEs were found to be only 2 % for the CO formation without detection of any other products in both cases. The low FEs could come from many reasons, such as degradation of the polymer films on the electrodes, accumulating electric charge during the potential application,^{114, 115} lack of proton source to regenerate catalyst again^{95, 116} or reoxidation of the newly formed reduction products from CO_2 at the anode.¹¹⁷

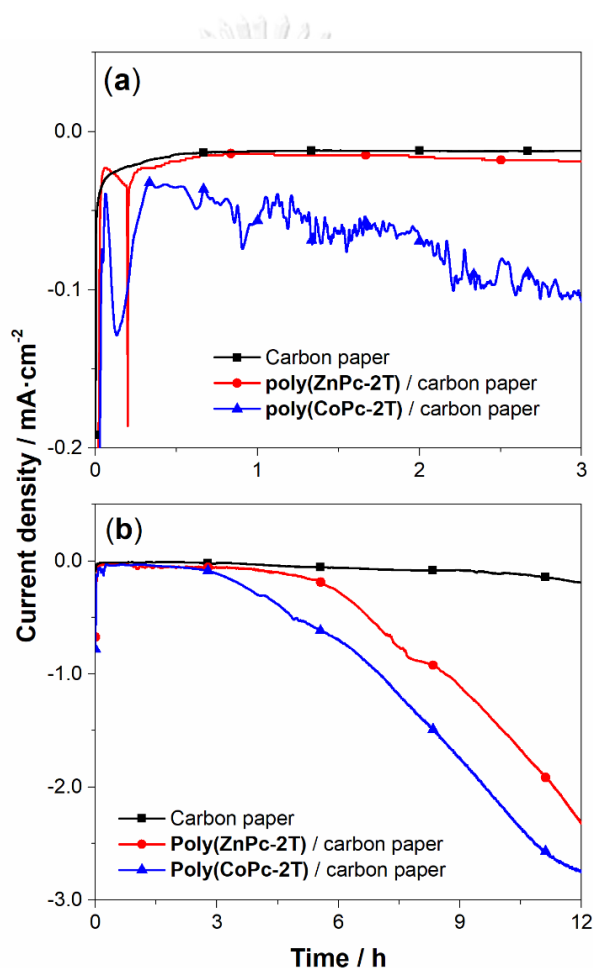


Figure 4-12. Chronoamperometric responses of the ECR of CO_2 in a 0.1 M TBAPF_6 solution in ACN at the potential of -1.70 V vs. Ag/AgCl QRE for (a) 3 h and (b) 12 h of a bare carbon paper (square symbol with black line), a **poly(ZnPc-2T)**-modified carbon paper (circle symbol with red line) and a **poly(CoPc-2T)**-modified carbon paper (triangle symbol with blue line) in a one-compartment three-electrode cell.

Table 4–3 Catalysis performance of **poly(ZnPc-2T)** and **poly(CoPc-2T)**-modified carbon papers for ECR of CO₂ performed in a 0.1 M TBAPF₆/ACN solution at the applied potential of –1.70 V vs. Ag/AgCl QRE with one-compartment three-electrode cell.

Catalysts	Time / h	Maximum Current density / mA·cm ⁻²	% FE of CO formation
carbon paper	3	<0.1	1
	12	<0.1	2
poly(ZnPc-2T)/ carbon paper	3	<0.1	1
	12	2.3	2
poly(CoPc-2T)	3	0.1	16
	12	2.7	2

4.3.2 Cyclic voltammetry (CV) studies and controlled potential electrolysis (CPE) measurements in a two-compartment cell and aqueous medium.

In order to improve the efficiency of the ECR of CO₂, the two-compartment three-electrode cell consisting of cathodic and anodic chambers was used. Each chamber was separated by a nafion membrane to prevent the reduced products produced from the cathode side passing through the anode side. The cathodic chamber contained the polymer-coated carbon paper as the WE and the Ag/AgCl (3 M KCl) as the RE, while the anodic chamber contained the Pt plate as the CE. A 0.5 M KHCO₃ aqueous solution saturated with N₂ (pH 8.4) or CO₂ (pH 7.3) was used as the electrolyte to obtain buffering capacity of bicarbonate, to increase capability of CO₂ on the catalyst sites and to provide the proton source for the ECR of CO₂.¹¹⁸⁻¹²¹

Under the CO₂- and N₂-saturated conditions, the cyclic voltammograms of the bare carbon paper did not show any peak in range of 0.00 V to –1.20 V vs. Ag/AgCl (3M KCl), indicating no interference of the substrate in the ECR of CO₂ (**Figures 4–13a** and **13b**). Also, the cyclic voltammogram of the **poly(ZnPc-2T)**-modified carbon paper under the N₂-saturated condition, which was recorded in the same potential range, did not give any redox peak unlike what observed for the above-mentioned

experiments in the one-compartment cell and the organic medium. This observation possibly resulted from the hydrophobicity of the polymer-modified electrode that led to weak interaction between the aqueous electrolyte and the WE. Under the CO₂-saturated condition at the same potential range, this WE showed the increase in the background current density and the slight enhancement of cathodic current density starting from -0.80 V vs. Ag/AgCl (3M KCl) (Figure 4-13a) possibly due to catalytic activity with CO₂. In case of the poly(CoPc-2T)-modified carbon paper, the

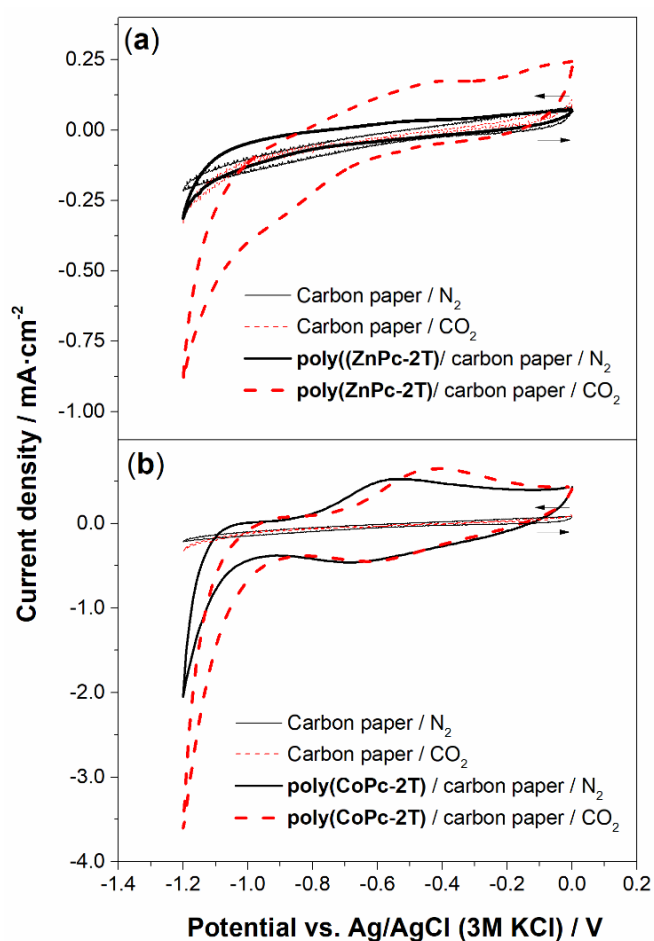


Figure 4-13. Cyclic voltammograms of (a) poly(ZnPc-2T)- and (b) poly(CoPc-2T)-modified carbon papers under N₂- (thick black solid line) and CO₂-saturated (thick red dashed line) condition, compared with those of bare carbon papers under the N₂- (thin black solid line) and CO₂-saturated (thin red dashed line) conditions recorded in a 0.5 M KHCO₃ solution in a two-compartment three-electrode cell.

cyclic voltammogram was recorded under the same condition in the same potential range. The cyclic voltammogram obtained under the N₂-saturated condition showed a broad cathodic peak at the E_{peak} of -0.64 V vs. Ag/AgCl (3M KCl), typically identified as the reduction of Co(II) to Co(I)^{28, 122, 123} as presented in **Figure 4-13b**. The enhancement of the current density was observed starting from -1.10 V vs. Ag/AgCl (3M KCl) might correspond to the H₂ evolution in the aqueous media that was promoted by **poly(CoPc-2T)**.²⁵ Under the CO₂-saturated condition, this WE gave the cyclic voltammogram having the similar pattern with higher current density and lower E_{onset}, *i.e.* -0.90 V vs. Ag/AgCl (3M KCl), compared with that observed under the N₂-saturated condition, suggesting that the WE might catalyze the ECR of CO₂ and/or the hydrogen evolution at this range of potential.^{28, 124}

To determine the type(s) of the reduction products(s) from the ECR of CO₂ under catalysis with the **poly(ZnPc-2T)**- or **poly(CoPc-2T)**-modified carbon paper, the CPE measurements were performed by using the same two-compartment three-electrochemical cell setup in a 0.5 M KHCO₃ aqueous solution at -1.20 vs. Ag/AgCl (3M KCl) for 2 h under the CO₂-saturated condition. As a result, the chronoamperograms showed the constant current densities of 0.07 mA·cm⁻² and 0.9 mA·cm⁻² when the **poly(ZnPc-2T)**- and **poly(CoPc-2T)**-modified carbon papers were used, respectively (**Figure 4-14a**). However, the bare carbon paper exhibited the enhancement of current density after 50 min to 0.4 mA·cm⁻². This observation suggested that, without the polymer films, the bare carbon paper may deteriorate under this condition. In case of the **poly(CoPc-2T)**-modified carbon paper, the great enhancement of the current density was observed since the beginning of the experiment, suggesting that the significant catalytic activity for the ECR of CO₂ could be expected. According to the GC analysis, no carbon-based reduction product was detected when the bare carbon paper and the **poly(ZnPc-2T)**-modified one were used (**Figure 4-14b**), but, instead, H₂ was found as a single product with the FE of 25% and 11%, respectively. When the **poly(CoPc-2T)**-modified carbon paper served as the WE, CO was found as a major product and H₂ as a minor one with the FE of 83% and 16%, respectively. The results suggested that **poly(CoPc-2T)** could serve as

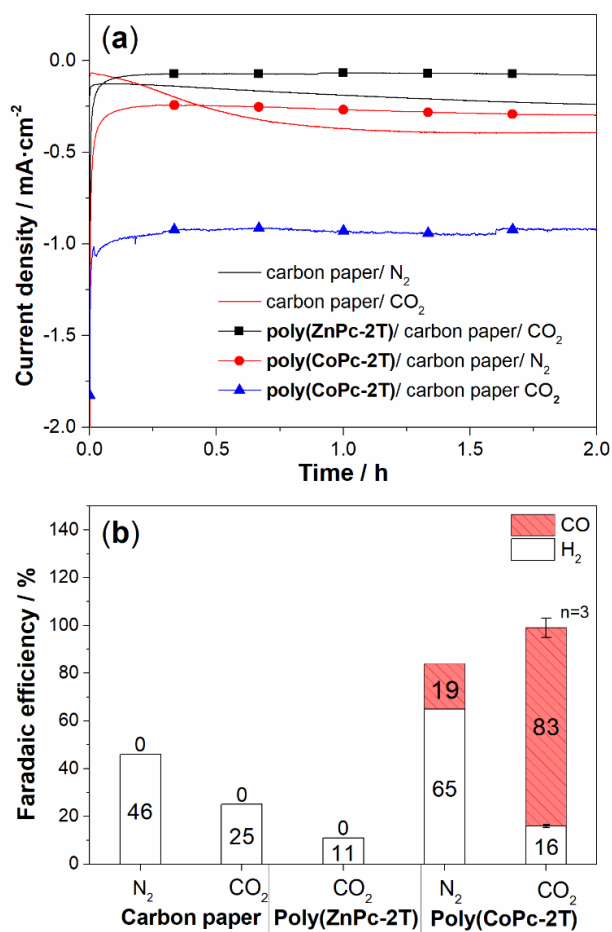


Figure 4-14. (a) Chronoamperometric responses of a CPE experiment at the potential of -1.20 V vs. Ag/AgCl (3M KCl) for 2 h of a bare carbon paper under N₂- (black line) or CO₂- (red line) saturated conditions, a poly(ZnPc-2T)-modified carbon paper under CO₂-saturated condition (square symbol with black line) and a poly(CoPc-2T)-modified carbon paper under N₂- (circle symbol with red line) or CO₂- (triangle symbol with blue line) saturated condition in a 0.5 M KHCO₃ electrolyte b) % Faradaic efficiencies of CO and H₂ production from the CPE at the potential of -1.20 V vs. Ag/AgCl (3M KCl) for 2 h in presence of a bare carbon paper, and a poly(ZnPc-2T)- and a poly(CoPc-2T)-modified carbon papers in a N₂- or CO₂-saturated 0.5 M KHCO₃ electrolyte solution and a two-compartment three-electrode cell.

the catalyst for the ECR of CO_2 under this condition. Interestingly, the CPE using the **poly(CoPc-2T)**-modified carbon paper as the WE gave CO and H_2 with the FE of 19% and 65%, respectively, under the N_2 -saturated condition. While the bare carbon paper serves as the WE under the N_2 -saturated condition, only H_2 was detected with the FE of 46%. However, the chronoamperograms of both cases shown in **Figure 4-14a** exhibited lower current densities than those observed under the CO_2 -saturated condition, suggesting that product amount might be low. This observation indicated that $\text{HCO}_3^-/\text{CO}_2$ equilibrium might play a role as the source of a small amount of CO_2 for the ECR of the **poly(CoPc-2T)**-modified electrode even without the external input of CO_2 . Moreover, it is also possible to further develop the electrochemical setup studied herein to convert the conventional bicarbonate aqueous solution into CO. In case of the **poly(ZnPc-2T)**-modified carbon paper, no reduction product was detected by the GC and IC for both gas and liquid phases even at the potential as high as -1.30 V vs. Ag/AgCl (3M KCl). In addition, the current density under the CO_2 -saturated conditions was relatively low. These observations might come from the redox property of the inactive **ZnPc** macrocycle, leading to the reduction of only macrocyclic phthalocyanine without participation of the metal ion as described in chapter 2.2.2. However, the **poly(ZnPc-2T)**-modified electrode seemed to be stable under the condition studied herein and, hence, might be interesting for further studies for other electrochemical applications.

To find the optimized catalytic performance towards CO_2 conversion of **poly(CoPc-2T)**-modified carbon paper, the potential was increased from -1.2 V to -1.30 V vs. Ag/AgCl (3M KCl). The results showed that the higher constant current densities were observed throughout the CPE using the **poly(CoPc-2T)**-modified electrode both under the N_2 - and CO_2 -saturated conditions, indicating more catalytic activity and the same stability of the **poly(CoPc-2T)** film on the carbon paper (**Figure 4-15**).

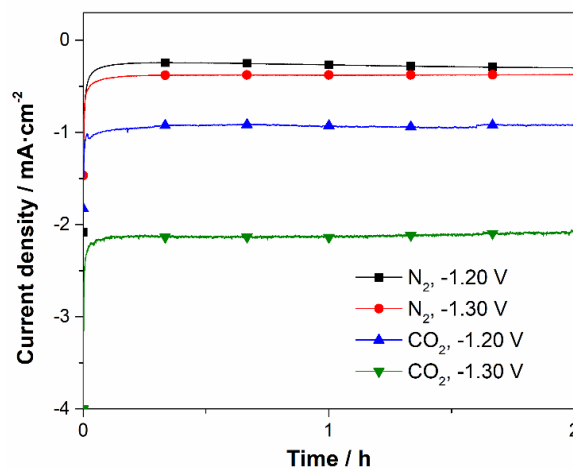


Figure 4–15. a) Chronoamperometric responses of 2-h CPE using a **poly(CoPc-2T)**-modified carbon paper as a WE in a N_2 -saturated 0.5 M $KHCO_3$ solution at the applied potential of -1.20 V (square symbol with black line) and at -1.30 V vs. Ag/AgCl (3M KCl) (circle symbol with red line) and in a CO_2 -saturated one under applied potential at -1.20 V (up-pointing triangle symbol with blue line) and at -1.30 V vs. Ag/AgCl (3M KCl) (down-pointing triangle symbol with green line) in a two-compartment three-electrode electrochemical cell.

According to the GC quantitative analysis, the CPE for 2 h using the bare carbon paper electrodes under the N_2 - and CO_2 -saturated conditions gave H_2 as the major product with the increase in the FEs from 46% and 26% to 94% and 80%, respectively, when the potential was increased from -1.20 V to -1.30 V vs. Ag/AgCl (3M KCl), without any carbon-based product detected (**Figure 4–16a**). Under the CO_2 -saturated condition in the presence of the **poly(CoPc-2T)** film, significant suppression of the H_2 evolution from the FEs of 16% to 7% and the enhanced CO formation from 83% FE to 94% FE were observed upon the potential increase from -1.20 V to -1.30 V vs. Ag/AgCl (3M KCl), respectively. The quantitative analysis for the accumulated amounts of CO obtained from the 2-h ECR of CO_2 at -1.20 V and -1.30 V vs. Ag/AgCl (3M KCl) were found to be 0.83 mL and 1.94 mL, respectively (**Figure 4–16b**). Under the N_2 -saturated condition in the presence of the **poly(CoPc-2T)** film, the formation of CO was slightly enhanced from 19% FE to 42% FE, while the H_2 production were suppressed from 65% FE to 21% FE, when the potential was raised

from -1.20 V to -1.30 V vs. Ag/AgCl (3M KCl), equivalent to 0.05 mL and 0.14 mL CO, respectively.

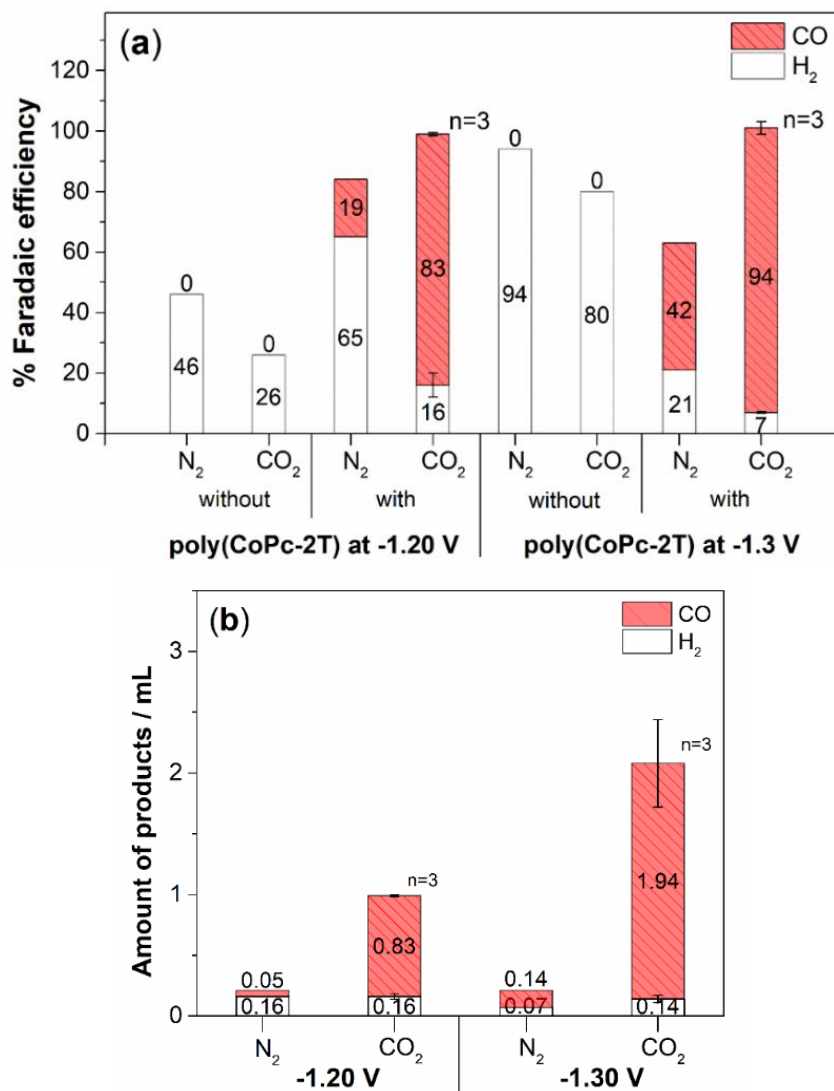


Figure 4-16. a) % FE of CO and H₂ formation from 2-h CPE at applied potentials of -1.20 V and -1.30 V vs. Ag/AgCl (3M KCl) in the absence and presence of a **poly(CoPc-2T)** film on carbon paper and in a N₂- or CO₂-saturated 0.5 M KHCO₃ solution. b) Quantitative analysis of gas products from 2-h CPE using the **poly(CoPc-2T)**-modified carbon paper as a WE at the potentials of -1.20 V and -1.30 V vs. Ag/AgCl (3M KCl) a in N₂- or CO₂- saturated 0.5 M KHCO₃ solution and a two-compartment three-electrode electrochemical cell.

To study the ECR of CO₂ without the in-situ generation of CO₂ from the bicarbonate buffer, the similar experiments were achieved in a 0.1 M KH₂PO₄/K₂HPO₄ solution. In **Figure 4-17**, the cyclic voltammograms of the bare carbon paper under the N₂- and CO₂-saturated solutions did not show any peak in range of 0.00 V to -1.30 V vs. Ag/AgCl (3M KCl), indicating no reduction occurred in these region. In case where the **poly(CoPc-2T)**-modified carbon paper was used, the cyclic voltammogram under the N₂-saturated condition showed a small peak at around E_{peak} of -0.48 V vs. Ag/AgCl (3M KCl), which could be characterized as the reduction of Co(II) to Co(I),^{28, 122, 123} while the enhancement of the current density was observed at E_{onset} of -1.12 V vs. Ag/AgCl (3M KCl), possibly due to the H₂ evolution. Under the CO₂-saturated condition, the cyclic voltammogram showed a reduction peak of the metal center reduction at E_{peak} of -0.52 V vs. Ag/AgCl (3M KCl) with the enhancement of current density at E_{onset} of -1.05 V vs. Ag/AgCl (3M KCl), likely to be the catalytic activity with CO₂ as observed in the 0.5 M KHCO₃ solution. However, the reduction peak of the Co(II) metal center under this condition had lower current density than that observed in the 0.5 M KHCO₃ solution, which could result from the higher concentration of 0.5 M KHCO₃ solution comparing with 0.1 M KH₂PO₄/K₂HPO₄ one, leading to higher ion strength, conductivity and current density.^{125, 126} According to these observation, the suitable applied potential for the CPE measurement in this electrolyte solution should be higher than 1.05 V vs. Ag/AgCl (3M KCl) to gain the catalytic activity towards ECR of CO₂.

The CPE in the 0.1 M KH₂PO₄/K₂HPO₄ solution were performed for 2 h in the same two-compartment three-electrode system as described earlier. At the selected potential of -1.30 V vs. Ag/AgCl under the N₂- and CO₂-saturated conditions, the chronoamperograms of the **poly(CoPc-2T)**-modified carbon paper showed the steady current densities of 0.60 mA·cm⁻² and 3.1 mA·cm⁻², respectively, as shown in **Figure 4-18**. The higher of the current density observed under the CO₂-saturated condition, compared with the N₂-saturated one, indicated that the catalytic activity towards the ECR of CO₂ could be expected under this condition.

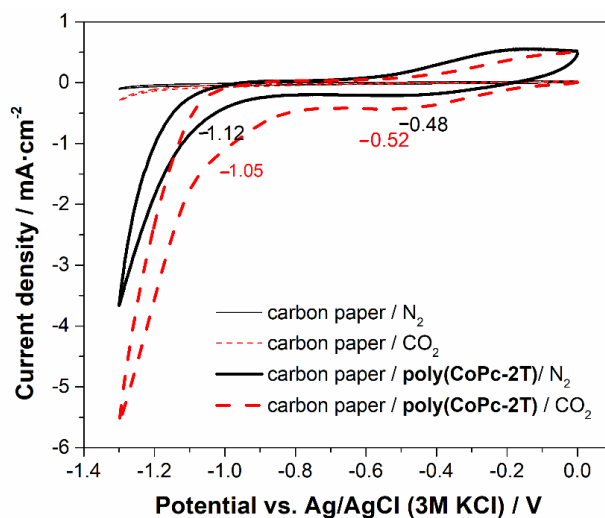


Figure 4-17. Cyclic voltammograms of a poly(CoPc-2T)-modified carbon paper under N_2 - (thin black line) and CO_2 -saturated conditions (thin red dashed line), compared with those of a bare carbon paper under the N_2 - (thick solid black line) and CO_2 -saturated conditions (thick red dashed line) recorded in a 0.1 M KH_2PO_4/K_2HPO_4 electrolyte solution.

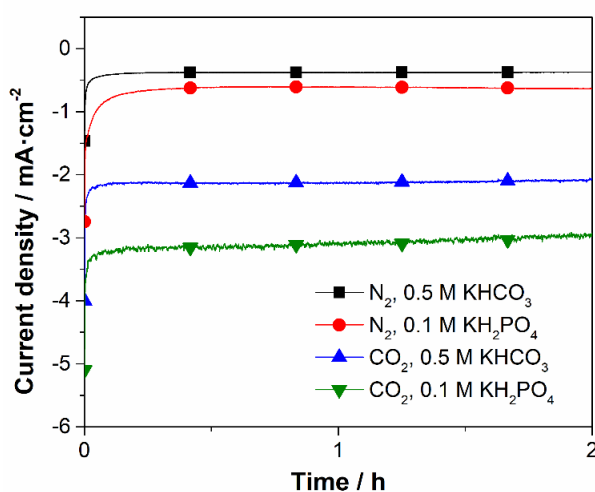


Figure 4-18. a) Chronoamperometric responses of 2-h using a poly(CoPc-2T)-modified carbon paper as a WE at potential of -1.30 V vs. Ag/AgCl (3M KCl) under N_2 -saturated condition in a 0.5 M $KHCO_3$ (square symbol with black line) and in a 0.1 M KH_2PO_4/K_2HPO_4 (circle symbol with red line) and under CO_2 -saturated condition in a 0.5 M $KHCO_3$ (up-pointing triangle symbol with blue line) and in a 0.1 M KH_2PO_4/K_2HPO_4 (down-pointing triangle symbol with blue green) in a two-compartment three-electrode electrochemical cell.

According to the GC analysis of the CPE in the CO₂-saturated 0.1 M KH₂PO₄/K₂HPO₄ solution by using the **poly(CoPc-2T)**-modified carbon paper as the WE at applied potential of -1.30 V vs. Ag/AgCl for 2 h, CO and H₂ were detected with the FE of 85% and 16%, equivalent to the accumulated CO and H₂ of 2.05 mL and 0.38 mL, respectively, as shown in **Figures 4-19a** and **19b**. In the case where the bare carbon paper served as the WE, only H₂ was detected with the FE of 88%. The results showed that the %FE of the CO production under the CO₂-saturated condition observed in the 0.1 M KH₂PO₄/K₂HPO₄ solution was lower than that observed in the 0.5 M KHCO₃ solution (94% vs. 85%), likely due to the equilibrium of CO₂ and HCO₃⁻ that could increase the CO₂ concentration at surrounding catalyst site.¹¹⁸⁻¹²¹ On the other hand, under the N₂-saturated condition in the presence and absence of the **poly(CoPc-2T)** film on carbon paper, a formation of CO was detected at lower than 1% FE for both cases, while the FE of the H₂ evolution was observed at 88% and 87%, respectively. This observation supported the condition concerning the in-situ generation of CO₂ in bicarbonate media. Moreover, the higher current density and the higher accumulated CO product were observed in the presence of the **poly(CoPc-2T)** film under the CO₂-saturated 0.1 M KH₂PO₄/K₂HPO₄ solution, compared with the CO₂-saturated 0.5 M KHCO₃ one. This result could come from the pH change from 7.3 to 6.4 after the CO₂ was purged into the 0.1 M KH₂PO₄/K₂HPO₄ solution causing the potential shift in a reversible hydrogen electrode (RHE) scale.⁷⁸ Therefore, the applied potential under the CO₂-saturated 0.1 M KH₂PO₄/K₂HPO₄ solution is higher than 0.5 M KHCO₃ solution in a potential of -0.05 V in the RHE scale and led to the higher current density and the higher accumulated CO product. In terms of selectivity, the 0.5 M KHCO₃ solution gave higher selectivity to the CO production and the same stability of current density for both conditions throughout the 2-h process. Therefore, the 0.5 M KHCO₃ solution is still suitable electrolyte for the ECR of CO₂ and for further study on the stability of the **poly(CoPc-2T)** film on carbon paper below.

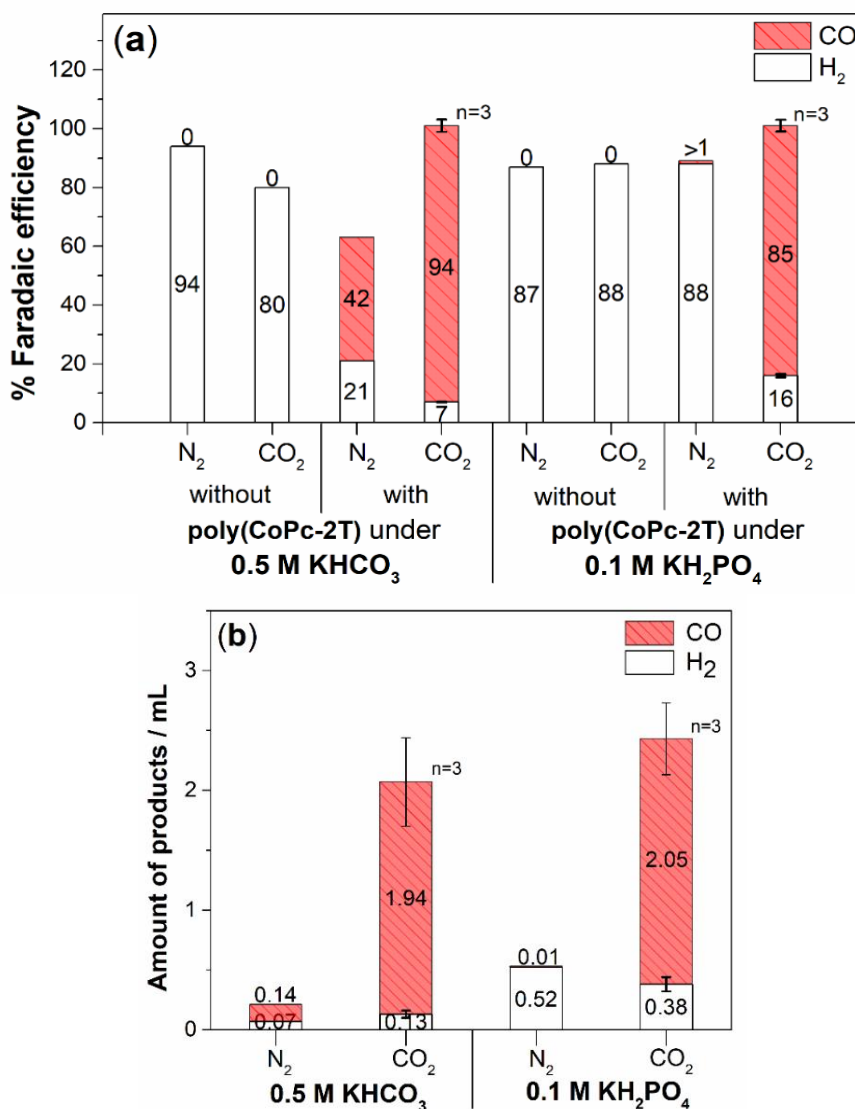


Figure 4-19. a) % FE of CO and H₂ formations from 2-h CPE at applied potential of -1.30 V vs. Ag/AgCl (3M KCl) in the absence and presence of a **poly(CoPc-2T)** film on carbon paper electrode under a N₂- or CO₂- saturated condition of 0.5 M KHCO₃ or 0.1 M KH₂PO₄/K₂HPO₄ solution. b) Quantitative analysis of gas products from 2-h CPE using the **poly(CoPc-2T)**-modified carbon paper as a WE at the potentials of -1.30 V vs. Ag/AgCl (3M KCl) in a N₂- or CO₂- saturated conditions of 0.5 M KHCO₃ or 0.1 M KH₂PO₄/K₂HPO₄ solution in a two-compartment three-electrochemical cell.

The stability of the **poly(CoPc-2T)** film on carbon paper was investigated by extending the CPE experiments to 20 h and monitoring the amount of CO every 30 min by the online GC with continuous CO₂ purging into the 0.5 M KHCO₃ solution in

the cathodic side of the two-compartment three-electrode cell with the flow rate of 10 mL·min⁻¹. The applied potential was kept constant at -1.20 V, -1.30 V or -1.40 V vs. Ag/AgCl (3M KCl). The current density, %FE and the amount of CO detected during the period of the CPE were shown in **Figure 4-20**. At -1.20 V vs. Ag/AgCl (3M KCl), the average current density was found to be 0.7 mA·cm⁻² with the average FE for the CO formation of 61% and the accumulated amount of CO of 4 mL, corresponding to accumulated TON of 4,518 and average TOF of 0.06 s⁻¹ as shown in **Table 4-4**. When the potential was increased to -1.30 V vs. Ag/AgCl (3M KCl), the average current density and FE of CO formation were enhanced to 1.7 mA·cm⁻² and 72%, respectively, corresponding accumulated TON and average TOF of 12,358 and 0.17 s⁻¹, respectively. The result also showed that the accumulated amount of CO obtained from the ECR of CO₂ at -1.30 V vs. Ag/AgCl (3M KCl) was 2.5 times higher than that obtained at -1.20 V vs. Ag/AgCl (3M KCl), *i.e.* 10.7 mL vs. 4.2 mL. However, when the applied potential was increased to -1.4 V vs. Ag/AgCl (3M KCl), the current density was found to decrease from 2.7 mA·cm⁻² to 1.2 mA·cm⁻² over time, while the average FE and the accumulated amount of the CO were not significantly improved, compared with those obtained at -1.30 vs. Ag/AgCl (3M KCl), *i.e.* 75% and 11 mL, respectively. The current density decay observed in this case was attributed to over-limited potential for the **poly(CoPc-2T)** film under this condition. Consequently, the TON and TOF became slightly lower (11,485 and 0.16 s⁻¹, respectively) than the case where the potential of -1.30 V vs. Ag/AgCl (3M KCl) was applied. These results suggested that the optimum potential for the ECR of CO₂ under the catalysis of the **poly(CoPc-2T)**-modified carbon paper was -1.30 V vs. Ag/AgCl (3M KCl), corresponding to -0.67 V vs. RHE. Compared with the FE of CO production obtained from the batch experiments, the lower value gained from the online experiments was attributed to the difference in the experimental setup. The online experiment was carried out in a flow system, while the batch one was performed in a closed system allowing the accumulating of the products in the cathodic chamber.

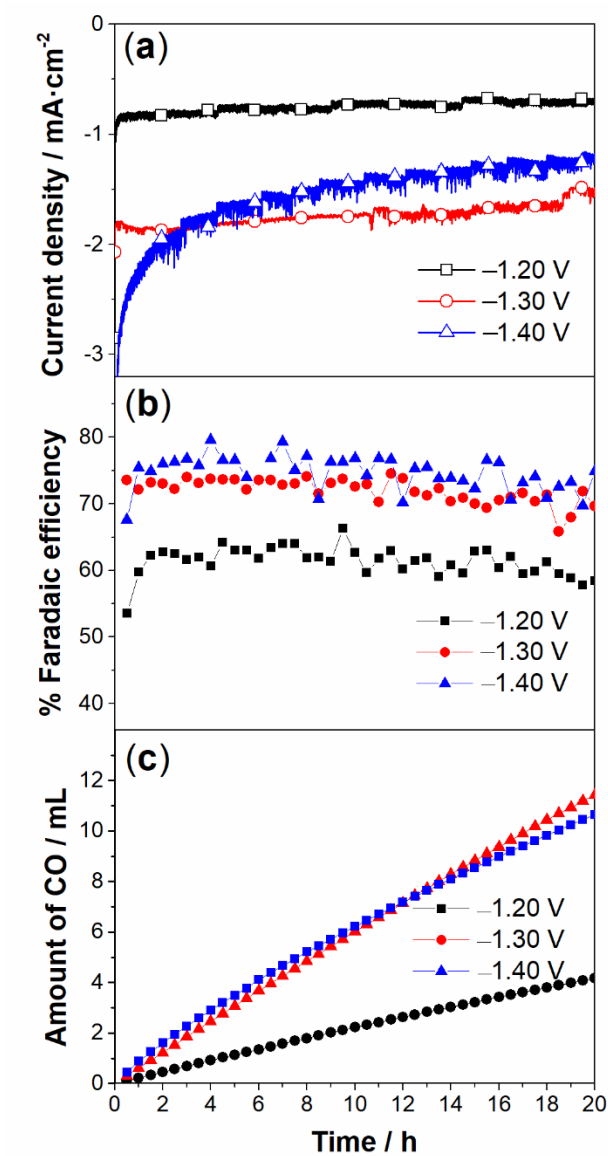


Figure 4-20. Catalysis performance of a poly(CoPc-2T)-modified carbon papers for ECR of CO₂ studied by an online GC technique over 20 h at potential of -1.20 V, -1.30 V and -1.40 V vs. Ag/AgCl (3M KCl) in a CO₂-saturated 0.5 M KHCO₃ solution in terms of a) current density, b) % FE of CO formation and c) an accumulated amount of CO product.

Table 4-4. Catalytic activity of the **Poly(CoP-2T)** films for the 20-hour ECR of CO₂

Applied potential / V vs. Ag/AgCl (3M KCl)	Average current density / mA·cm ⁻²	% FE (CO formation)			TON	TOF / s ⁻¹	Accumulated amount of CO / mL
		Mean	Min.	Max.			
-1.20	0.7	61	53	66	4,518	0.06	4.2
-1.30	1.7	72	66	75	12,359	0.17	10.7
-1.40	1.2 – 2.7	75	68	80	11,420	0.16	11.4

4.4 Comparison to other literatures

Table 4-5 summarized the catalytic performance the **poly(CoPc-2T)**-modified carbon paper for the ECR of CO₂ in comparison with previously reported high performance catalysts that were studied in a comparable scale and in the aqueous media. The typical preparation of the modified-electrodes used in these selected works were based-on a drop-casting technique or chemical polymerization. In this work, the electropolymerization technique was employed for preparing the well covered and stable polymer films on the carbon papers, comparably or more remarkable catalytic performance, compared with others. Our optimum condition for the ECR of CO₂ was the use of the **poly(CoPc-2T)**-modified carbon paper as the WE at -0.67 V vs. RHE in a 0.5 M KHCO₃ electrolyte solution to give current density at 2.5 mA·cm⁻² and the %FE for the CO production of 94%. Although the calculated TOF value of 0.29 s⁻¹ was still to be improved, this value is still in the range required for industrial related applications, *i.e.* from 10⁻² to 10² s⁻¹.¹²⁷ Therefore, it should be convincing **poly(CoPc-2T)**-modified carbon paper developed in this work can be a very promising catalyst candidate for the ECR of CO₂.

Table 4–5 Comparison of the catalytic performance of the **poly(CoPc-2T)**-modified carbon paper develop from this work with other reported high-performance catalysts for the ECR of CO₂ to CO in aqueous media.

Catalyst/substrate	Applied potential vs. RHE ^a /V (Time/h)	Current density, J /mA·cm ⁻²	Electrolyte (pH)	Avg. %FE		TOF ^c /s ⁻¹	Ref.
				CO	H ₂		
poly(CoPc-2T) / carbon paper	-0.67 (2)	2.5	0.5 M KHCO ₃ (7.3)	94	7	0.29	This work
poly(CoPc-2T) / carbon paper	-0.71 (2)	3.2	0.1 M KH ₂ PO ₄ (6.4)	85	16	0.31	This work
poly(CoPc-2T) / carbon paper	-0.67 (20)	2.5	0.5 M KHCO ₃ (7.3)	72	- ^b	0.17	This work
CoPc/CNT carbon paper	-0.63 (1)	10	0.1 M KHCO ₃ (6.8)	92	6	2.7	28
COF-367-Co / carbon fabric	-0.67 (24)	3.3	0.5 M KHCO ₃ (7.3)	91	20	0.53	128
CoFPc / carbon cloth	-0.80 (2)	4.4	0.5 M NaHCO ₃ (7.3)	93	6	1.6	129
CoPc-P4VP/ graphite disc	-0.73 (2)	2	0.1 M NaH ₂ PO ₄ pH (4.7)	89	5	4.8	130

^a $E_{RHE} = E_{Ag/AgCl} + (0.059 \times pH) + E^{\circ}_{Ag/AgCl}$ where E_{RHE} is the converted potential vs. RHE, $E^{\circ}_{Ag/AgCl} = 0.1976$ at 25 °C.⁷⁸

^b the product was not measured.

^c the value was reported for the CO formation.

CHAPTER 5

CONCLUSION

A series of novel phthalocyanine derivatives bearing bithiophene units, **ZnPc-2T**, **CoPc-2T**, **NiPc-2T**, **CuPc-2T** and **H₂Pc-2T**, were synthesized and characterized by the ¹H-NMR and ¹³C-NMR spectroscopy, MS and UV-Visible and fluorescence spectrophotometry. The polymer films of **ZnPc-2T** and **CoPc-2T** were successfully prepared on the ITO/glass and carbon paper, and characterization by the spectroscopic methods including UV-visible spectrophotometry, Raman and ATR-FTIR spectroscopy, XPS analysis, SEM and EDX. Moreover, the suppressed aggregation of the macrocyclic phthalocyanine in the resulting polymers was proved by the UV-visible spectrophotometry. The electrochemical features and heterogeneous catalytic performance of these polymers-modified carbon papers towards the ECR of CO₂ in the ACN and aqueous media were investigated by means of the CV and CPE measurements. The **poly(ZnPc-2T)**-modified carbon paper gave the low significant catalytic activity for the ECR of CO₂ in both the ACN and aqueous media, possibly resulting from the inactivated macrocyclic phthalocyanine after reduction of CO₂. In case of the **poly(CoPc-2T)**-modified carbon paper, the result showed the moderated catalytic performance in the ECR of CO₂ in the ACN media, while the possible decomposition of this electrode was observed in the 12-h experiments, likely due to the lack of the proton source and the reoxidation of the newly formed reduced product(s) at the anode in one-compartment setup. These problems were overcome by using the aqueous media as the electrolyte and the two-compartment three-electrode electrochemical cell. In this step, the **poly(CoPc-2T)**-modified carbon paper showed the remarkable catalytic activity and stability towards the ECR of CO₂ at applied potential of -1.3 V vs. (3M Ag/AgCl). For the CPE, the average FE, TON and TOF for the CO production were found to be 94%, 2,099 and 0.29, respectively, in the 2-h batch experiments, and 72 %, 12,359 and 0.17 s⁻¹, respectively, in the 20-h experiment with the online GC analysis. Moreover, our electrochemical set up based on the **poly(CoPc-2T)**-modified carbon paper gave

relatively high catalytic performance for the electrochemical conversion of CO₂ to CO in the aqueous media, when compared with other reported catalytic system.



REFERENCES

1. Lüthi, D.; Le Floch, M.; Bereiter, B.; Blunier, T.; Barnola, J.-M.; Siegenthaler, U.; Raynaud, D.; Jouzel, J.; Fischer, H.; Kawamura, K., High-resolution carbon dioxide concentration record 650,000–800,000 years before present. *Nature* **2008**, *453* (7193), 379.
2. Lambert, F.; Delmonte, B.; Petit, J.-R.; Bigler, M.; Kaufmann, P. R.; Hutterli, M. A.; Stocker, T. F.; Ruth, U.; Steffensen, J. P.; Maggi, V., Dust-climate couplings over the past 800,000 years from the EPICA Dome C ice core. *Nature* **2008**, *452* (7187), 616.
3. Den Elzen, M.; Meinshausen, M., Multi-gas emission pathways for meeting the EU 2 C climate target. *Avoiding dangerous climate change* **2006**, 299–309.
4. Edenhofer, O.; Pichs-Madruga, R.; Sokona, Y.; Agrawala, S.; Bashmakov, I.; Blanco, G.; Broome, J.; Bruckner, T.; Brunner, S.; Bustamante, M., Summary for policymakers. **2014**.
5. Jenkinson, D. S.; Adams, D.; Wild, A., Model estimates of CO₂ emissions from soil in response to global warming. *Nature* **1991**, *351* (6324), 304.
6. Joos, F.; Plattner, G.-K.; Stocker, T. F.; Marchal, O.; Schmittner, A., Global warming and marine carbon cycle feedbacks on future atmospheric CO₂. *Science* **1999**, *284* (5413), 464–467.
7. Collin, J. P.; Sauvage, J. P., Electrochemical reduction of carbon dioxide mediated by molecular catalysts. *Coordination Chemistry Reviews* **1989**, *93* (2), 245–268.
8. Sakakura, T.; Choi, J.-C.; Yasuda, H., Transformation of Carbon Dioxide. *Chemical Reviews* **2007**, *107* (6), 2365–2387.
9. Whipple, D. T.; Kenis, P. J., Prospects of CO₂ utilization via direct heterogeneous electrochemical reduction. *The Journal of Physical Chemistry Letters* **2010**, *1* (24), 3451–3458.
10. Ganesh, I., Electrochemical conversion of carbon dioxide into renewable fuel chemicals–The role of nanomaterials and the commercialization. *Renewable and Sustainable Energy Reviews* **2016**, *59*, 1269–1297.

11. Kuhl, K. P.; Hatsukade, T.; Cave, E. R.; Abram, D. N.; Kibsgaard, J.; Jaramillo, T. F., Electrocatalytic Conversion of Carbon Dioxide to Methane and Methanol on Transition Metal Surfaces. *Journal of the American Chemical Society* **2014**, *136* (40), 14107–14113.
12. Al-Rowaili, F. N.; Jamal, A.; Ba Shammakh, M. S.; Rana, A., A Review on Recent Advances for Electrochemical Reduction of Carbon Dioxide to Methanol Using Metal–Organic Framework (MOF) and Non-MOF Catalysts: Challenges and Future Prospects. *ACS Sustainable Chemistry & Engineering* **2018**, *6* (12), 15895–15914.
13. Costentin, C.; Robert, M.; Saveant, J. M., Catalysis of the electrochemical reduction of carbon dioxide. *Chem Soc Rev* **2013**, *42* (6), 2423–2436.
14. Zhang, Y.-J.; Sethuraman, V.; Michalsky, R.; Peterson, A. A., Competition between CO₂ reduction and H₂ evolution on transition-metal electrocatalysts. *ACS Catalysis* **2014**, *4* (10), 3742–3748.
15. Meshitsuka, S.; Ichikawa, M.; Tamaru, K., Electrocatalysis by metal phthalocyanines in the reduction of carbon dioxide. *Journal of the Chemical Society, Chemical Communications* **1974**, (5), 158–159.
16. Kapusta, S.; Hackerman, N., Carbon dioxide reduction at a metal phthalocyanine catalyzed carbon electrode. *Journal of The Electrochemical Society* **1984**, *131* (7), 1511–1514.
17. Abe, T.; Taguchi, F.; Yoshida, T.; Tokita, S.; Schnurpfeil, G.; Wöhrle, D.; Kaneko, M., Electrocatalytic CO₂ reduction by cobalt octabutoxyphthalocyanine coated on graphite electrode. *Journal of Molecular Catalysis A: Chemical* **1996**, *112* (1), 55–61.
18. Zhang, X.; Wu, Z.; Zhang, X.; Li, L.; Li, Y.; Xu, H.; Li, X.; Yu, X.; Zhang, Z.; Liang, Y.; Wang, H., Highly selective and active CO₂ reduction electrocatalysts based on cobalt phthalocyanine/carbon nanotube hybrid structures. *Nature Communications* **2017**, *8*, 14675.
19. Zhao, Z.-H.; Fan, J.-M.; Wang, Z.-Z., Photo-catalytic CO₂ reduction using sol–gel derived titania-supported zinc-phthalocyanine. *Journal of Cleaner Production* **2007**, *15* (18), 1894–1897.
20. Marais, E.; Klein, R.; Antunes, E.; Nyokong, T., Photocatalysis of 4-nitrophenol using zinc phthalocyanine complexes. *Journal of Molecular Catalysis A: Chemical*

2007, 261 (1), 36–42.

21. Meshitsuka, S.; Tamaru, K., Photoelectrocatalysis by metal phthalocyanine evaporated films in the oxidation of oxalate ion. *Journal of the Chemical Society, Faraday Transactions 1: Physical Chemistry in Condensed Phases* **1977**, 73 (0), 236–242.
22. Minami, N.; Watanabe, T.; Fujishima, A.; Honda, K.-I., Photoelectrochemical study on copper phthalocyanine films. *Berichte der Bunsengesellschaft für physikalische Chemie* **1979**, 83 (5), 476–481.
23. Schutte, W.; Sluyters-Rehbach, M.; Sluyters, J., Aggregation of an octasubstituted phthalocyanine in dodecane solution. *The Journal of Physical Chemistry* **1993**, 97 (22), 6069–6073.
24. Choi, M. T.; Li, P. P.; Ng, D. K., A direct comparison of the aggregation behavior of phthalocyanines and 2, 3-naphthalocyanines. *Tetrahedron* **2000**, 56 (24), 3881–3887.
25. Snow, A. W., Phthalocyanine Aggregation 109. *The Porphyrin Handbook: Phthalocyanines: Properties and Materials* **2000**, 17, 129.
26. Jiang, J., *Functional phthalocyanine molecular materials*. Springer: 2010; Vol. 135.
27. Prakash, G. K. S.; Viva, F. A.; Olah, G. A., Electrochemical reduction of CO₂ over Sn-Nafion® coated electrode for a fuel-cell-like device. *Journal of Power Sources* **2013**, 223, 68–73.
28. Zhang, X.; Wu, Z.; Zhang, X.; Li, L.; Li, Y.; Xu, H.; Li, X.; Yu, X.; Zhang, Z.; Liang, Y.; Wang, H., Highly selective and active CO₂ reduction electrocatalysts based on cobalt phthalocyanine/carbon nanotube hybrid structures. *Nature Communications* **2017**, 8 (1), 14675.
29. Ma, S.; Odgaard, M.; Skou, E., Carbon dioxide permeability of proton exchange membranes for fuel cells. *Solid State Ionics* **2005**, 176 (39), 2923–2927.
30. Zhang, Q.; Dong, H.; Hu, W., Electrochemical polymerization for two-dimensional conjugated polymers. *Journal of Materials Chemistry C* **2018**, 6 (40), 10672–10686.
31. Muto, T.; Temma, T.; Kimura, M.; Hanabusa, K.; Shirai, H., A new phthalocyanine derivative having peripheral 2-thienyl substituents. *Chemical Communications* **2000**, (17), 1649–1650.

32. Obirai, J.; Rodrigues, N. P.; Bedioui, F.; Nyokong, T., Synthesis, spectral and electrochemical properties of a new family of pyrrole substituted cobalt, iron, manganese, nickel and zinc phthalocyanine complexes. *Journal of Porphyrins and Phthalocyanines* **2003**, 7 (7), 508–520.
33. Solis, C.; Baigorria, E.; Milanesio, M. E.; Morales, G.; Durantini, E. N.; Otero, L.; Gervaldo, M., Electrochemical polymerization of EDOT modified Phthalocyanines and their applications as electrochromic materials with green coloration, and strong absorption in the Near-IR. *Electrochimica Acta* **2016**, 213, 594–605.
34. Isaacs, M.; Armijo, F.; Ramírez, G.; Trollund, E.; Biaggio, S. R.; Costamagna, J.; Aguirre, M. J., Electrochemical reduction of CO₂ mediated by poly-M-aminophthalocyanines (M=Co, Ni, Fe): poly-Co-tetraaminophthalocyanine, a selective catalyst. *Journal of Molecular Catalysis A: Chemical* **2005**, 229 (1–2), 249–257.
35. Lamy, E.; Nadjó, L.; Saveant, J. M., Standard potential and kinetic parameters of the electrochemical reduction of carbon dioxide in dimethylformamide. *Journal of Electroanalytical Chemistry and Interfacial Electrochemistry* **1977**, 78 (2), 403–407.
36. Schwarz, H. A.; Dodson, R. W., Reduction potentials of CO₂ and the alcohol radicals. *The Journal of Physical Chemistry* **1989**, 93 (1), 409–414.
37. Schröder, D.; Schalley, C. A.; Harvey, J. N.; Schwarz, H., On the formation of the carbon dioxide anion radical CO₂^{•-} in the gas phase. *International journal of mass spectrometry* **1999**, 185, 25–35.
38. Dean, J. A., *Lange's handbook of chemistry*. New York; London: McGraw-Hill, Inc.: 1999.
39. Hong, J.; Zhang, W.; Ren, J.; Xu, R., Photocatalytic reduction of CO₂: a brief review on product analysis and systematic methods. *Analytical Methods* **2013**, 5 (5), 1086.
40. Scibioh, M. A.; Viswanathan, B. In *Electrochemical reduction of carbon dioxide: a status report*, Proc Indian Natn Sci Acad, 2004; 1–56.
41. Tanabe, H.; Ohno, K., Electrocatalysis of metal phthalocyanine thin film prepared by the plasma-assisted deposition on a glassy carbon in the reduction of carbon dioxide. *Electrochimica Acta* **1987**, 32 (7), 1121–1124.
42. Furuya, N.; Matsui, K., Electroreduction of carbon dioxide on gas-diffusion

electrodes modified by metal phthalocyanines. *Journal of Electroanalytical Chemistry and Interfacial Electrochemistry* **1989**, 271 (1), 181–191.

43. Mack, J.; Stillman, M. J., 103 - Electronic Structures of Metal Phthalocyanine and Porphyrin Complexes from Analysis of the UV–Visible Absorption and Magnetic Circular Dichroism Spectra and Molecular Orbital Calculations A2 - Kadish, Karl M. In *The Porphyrin Handbook*, Smith, K. M.; Guillard, R., Eds. Academic Press: Amsterdam, 2003; 43–116.

44. Lever, A. B. P.; Licoccia, S.; Magnell, K.; Minor, P. C.; Ramaswamy, B. S., Mapping of the Energy Levels of Metallophthalocyanines via Electronic Spectroscopy, Electrochemistry, and Photochemistry. In *Electrochemical and Spectrochemical Studies of Biological Redox Components*, AMERICAN CHEMICAL SOCIETY: 1982; Vol. 201, 237–252.

45. Walter, M. G.; Rudine, A. B.; Wamser, C. C., Porphyrins and phthalocyanines in solar photovoltaic cells. *Journal of Porphyrins and Phthalocyanines* **2010**, 14 (9), 759–792.

46. Wöhrle, D.; Bannehr, R.; Schumann, B.; Meyer, G.; Jaeger, N., Synthesis and electrochemical and photoelectrochemical properties of polyphthalocyanine-coated electrodes. *Journal of Molecular Catalysis* **1983**, 21 (1), 255–263.

47. Abraham, K. M.; Alamgir, M.; Willstaedt, E. B.; Kilroy, W. P., Metal phthalocyanine-catalysed Li/SOCl₂ cells. *Electrochimica Acta* **1992**, 37 (3), 531–543.

48. L'Her, M.; Pondaven, A., 104 - Electrochemistry of Phthalocyanines A2 - Kadish, Karl M. In *The Porphyrin Handbook*, Smith, K. M.; Guillard, R., Eds. Academic Press: Amsterdam, 2003; 117–169.

49. Büttner, E.; Holze, R., Hydroquinone oxidation electrocatalysis at polyaniline films. *Journal of Electroanalytical Chemistry* **2001**, 508 (1–2), 150–155.

50. Zucolotto, V.; Ferreira, M.; Cordeiro, M. R.; Constantino, C. J.; Moreira, W. C.; Oliveira Jr, O. N., Nanoscale processing of polyaniline and phthalocyanines for sensing applications. *Sensors and Actuators B: Chemical* **2006**, 113 (2), 809–815.

51. Yasuda, T.; Tsutsui, T., Organic field-effect transistors based on high electron and ambipolar carrier transport properties of copper–phthalocyanine. *Chemical physics letters* **2005**, 402 (4–6), 395–398.

52. Wróbel, D.; Dudkowiak, A., Porphyrins and phthalocyanines–functional molecular materials for optoelectronics and medicine. *Molecular Crystals and Liquid Crystals* **2006**, *448* (1), 15–167.
53. Yoon, S. M.; Lou, S. J.; Loser, S.; Smith, J.; Chen, L. X.; Facchetti, A.; Marks, T., Fluorinated copper phthalocyanine nanowires for enhancing interfacial electron transport in organic solar cells. *Nano letters* **2012**, *12* (12), 6315–6321.
54. Liao, M.-S.; Scheiner, S., Electronic structure and bonding in metal phthalocyanines, Metal=Fe, Co, Ni, Cu, Zn, Mg. *The Journal of Chemical Physics* **2001**, *114* (22), 9780–9791.
55. Jasinski, R., Cobalt phthalocyanine as a fuel cell cathode. *Journal of the Electrochemical Society* **1965**, *112* (5), 526–528.
56. Monama, G. R.; Mdluli, S. B.; Mashao, G.; Makhafola, M. D.; Ramohlola, K. E.; Molapo, K. M.; Hato, M. J.; Makgopa, K.; Iwuoha, E. I.; Modibane, K. D., Palladium deposition on copper (II) phthalocyanine/metal organic framework composite and electrocatalytic activity of the modified electrode towards the hydrogen evolution reaction. *Renewable energy* **2018**, *119*, 62–72.
57. Manbeck, G. F.; Fujita, E., A review of iron and cobalt porphyrins, phthalocyanines and related complexes for electrochemical and photochemical reduction of carbon dioxide. *Journal of Porphyrins and Phthalocyanines* **19** (1–3), 45–64.
58. Ke, W.; Zhao, D.; Grice, C. R.; Cimaroli, A. J.; Fang, G.; Yan, Y., Efficient fully-vacuum-processed perovskite solar cells using copper phthalocyanine as hole selective layers. *Journal of Materials Chemistry A* **2015**, *3* (47), 23888–23894.
59. Verma, D.; Dash, R.; Katti, K. S.; Schulz, D. L.; Caruso, A. N., Role of coordinated metal ions on the orientation of phthalocyanine based coatings. *Spectrochimica Acta Part A: Molecular and Biomolecular Spectroscopy* **2008**, *70* (5), 1180–1186.
60. Fietzek, C.; Bodenhöfer, K.; Haisch, P.; Hees, M.; Hanack, M.; Steinbrecher, S.; Zhou, F.; Plies, E.; Göpel, W., Soluble phthalocyanines as coatings for quartz-microbalances: specific and unspecific sorption of volatile organic compounds. *Sensors and Actuators B: Chemical* **1999**, *57* (1–3), 88–98.
61. Kajihara, K.; Tanaka, K.; Hirao, K.; Soga, N., Photovoltaic effect in titanium

- dioxide/zinc phthalocyanine cell. *Japanese journal of applied physics* **1996**, *35* (12A), 6110.
62. Griveau, S.; Albin, V.; Pauporté, T.; Zagal, J. H.; Bedioui, F., Comparative study of electropolymerized cobalt porphyrin and phthalocyanine based films for the electrochemical activation of thiols. *Journal of Materials Chemistry* **2002**, *12* (2), 225–232.
63. Trombach, N.; Hild, O.; Schlettwein, D.; Wöhrle, D., Synthesis and electropolymerisation of pyrrol-1-yl substituted phthalocyanines. *Journal of Materials Chemistry* **2002**, *12* (4), 879–885.
64. Yavuz, A.; Bezgin Çarbaş, B.; Aras, L.; Önal, A. M., Electropolymerization of a new 4-(2,5-Di-2-thiophen-2-yl-pyrrol-1-yl)-tetra substituted nickel phthalocyanine derivative. *Journal of Applied Polymer Science* **2011**, *122* (2), 1293–1299.
65. Özçeşmeci, İ.; Burat, A. K.; İpek, Y.; Koca, A.; Bayır, Z. A., Synthesis, electrochemical and spectroelectrochemical properties of phthalocyanines having extended π -electrons conjugation. *Electrochimica Acta* **2013**, *89*, 270–277.
66. Bard, A. J.; Faulkner, L. R.; Leddy, J.; Zoski, C. G., *Electrochemical methods: fundamentals and applications*. Wiley New York: 1980; Vol. 2.
67. Nicholson, R. S., Theory and application of cyclic voltammetry for measurement of electrode reaction kinetics. *Analytical chemistry* **1965**, *37* (11), 1351–1355.
68. Kissinger, P. T.; Heineman, W. R., Cyclic voltammetry. *Journal of Chemical Education* **1983**, *60* (9), 702.
69. Evans, D. H.; O'Connell, K. M.; Petersen, R. A.; Kelly, M. J., Cyclic voltammetry. ACS Publications: 1983.
70. Braungardt, C. B., Evaluation of Analytical Instrumentation. Part XXVI: Instrumentation for Voltammetry. *Analytical Methods* **2015**, *7* (4), 1249–1260.
71. Elgrishi, N.; Rountree, K. J.; McCarthy, B. D.; Rountree, E. S.; Eisenhart, T. T.; Dempsey, J. L., A practical beginner's guide to cyclic voltammetry. *Journal of Chemical Education* **2017**, *95* (2), 197–206.
72. Zoski, C. G., *Handbook of electrochemistry*. Elsevier: 2006.
73. Swesi, A. T.; Masud, J.; Nath, M., Nickel selenide as a high-efficiency catalyst for

oxygen evolution reaction. *Energy & Environmental Science* **2016**, *9* (5), 1771–1782.

74. Carlin, R. T.; Crawford, W.; Bersch, M., Nucleation and morphology studies of aluminum deposited from an ambient-temperature chloroaluminate molten salt. *Journal of The Electrochemical Society* **1992**, *139* (10), 2720–2727.

75. Silvester, D. S.; Ward, K. R.; Aldous, L.; Hardacre, C.; Compton, R. G., The electrochemical oxidation of hydrogen at activated platinum electrodes in room temperature ionic liquids as solvents. *Journal of Electroanalytical Chemistry* **2008**, *618* (1–2), 53–60.

76. Strong, F. C., Faraday's laws in one equation. *Journal of Chemical Education* **1961**, *38* (2), 98.

77. Chen, C. S.; Handoko, A. D.; Wan, J. H.; Ma, L.; Ren, D.; Yeo, B. S., Stable and selective electrochemical reduction of carbon dioxide to ethylene on copper mesocrystals. *Catalysis Science & Technology* **2015**, *5* (1), 161–168.

78. Choi, J.; Kim, J.; Wagner, P.; Gambhir, S.; Jalili, R.; Byun, S.; Sayyar, S.; Lee, Y. M.; MacFarlane, D. R.; Wallace, G. G.; Officer, D. L., Energy efficient electrochemical reduction of CO₂ to CO using a three-dimensional porphyrin/graphene hydrogel. *Energy & Environmental Science* **2019**, *12* (2), 747–755.

79. Linde, G., Adsorptive method for the separation of a gas mixture. Google Patents: 1984.

80. Harris, D. C., *Quantitative chemical analysis*. Macmillan: 2010.

81. Rieman, W.; Walton, H. F., *Ion exchange in analytical chemistry: international series of monographs in analytical chemistry*. Elsevier: 2013.

82. Bellot, J.; Condoret, J., Modelling of liquid chromatography equilibria. *Process Biochemistry* **1993**, *28* (6), 365–376.

83. Ng, B. K.; Tan, T. T. Y.; Shellie, R. A.; Dicoski, G. W.; Haddad, P. R., Computer-assisted simulation and optimisation of retention in ion chromatography. *TrAC Trends in Analytical Chemistry* **2016**, *80*, 625–635.

84. Long, D. A.; Long, D., *Raman spectroscopy*. McGraw-Hill New York: 1977; Vol. 276.

85. Ferraro, J. R., *Introductory raman spectroscopy*. Elsevier: 2003.

86. Zgierski, M., Interference between resonance and preresonance Raman scattering. *Journal of Raman Spectroscopy* **1977**, *6* (1), 53–56.
87. Baker, M. J.; Hughes, C. S.; Hollywood, K. A., Raman spectroscopy. In *Biophotonics: Vibrational Spectroscopic Diagnostics*, Morgan & Claypool Publishers: 2016.
88. Tackley, D. R.; Dent, G.; Ewen Smith, W., Phthalocyanines: structure and vibrations. *Physical Chemistry Chemical Physics* **2001**, *3* (8), 1419–1426.
89. Haasch, R. T., X-ray photoelectron spectroscopy (XPS) and auger electron spectroscopy (AES). In *Practical Materials Characterization*, Springer: 2014; 93–132.
90. Jenkin, J.; Leckey, R.; Liesegang, J., The development of x-ray photoelectron spectroscopy: 1900–1960. *Journal of electron spectroscopy and related phenomena* **1977**, *12* (1), 1–35.
91. Dolomanov, O. V.; Bourhis, L. J.; Gildea, R. J.; Howard, J. A.; Puschmann, H., OLEX2: a complete structure solution, refinement and analysis program. *Journal of Applied Crystallography* **2009**, *42* (2), 339–341.
92. Sheldrick, G. M., A short history of SHELX. *Acta Crystallographica Section C: Structural Chemistry* **2008**, *A64*, 112–122.
93. Sheldrick, G. M., Crystal structure refinement with SHELXL. *Acta Crystallographica Section C: Structural Chemistry* **2015**, *71* (1), 3–8.
94. Sundarraj, S.; Bruder, I.; Hwang, J. H.; Schoeneboom, J.; Koenemann, M.; Bahulayan, S.; Ojala, A.; Wui, A. L. Y.; Erk, P.; Sens, R. Use of phthalocyanine compounds with aryl or hetaryl substituents in organic solar cells. 2012.
95. Alzeer, J.; Roth, P. J. C.; Luedtke, N. W., An efficient two-step synthesis of metal-free phthalocyanines using a Zn(ii) template. *Chemical Communications* **2009**, (15), 1970–1971.
96. Inzelt, G., Pseudo-reference Electrodes. In *Handbook of Reference Electrodes*, Inzelt, G.; Lewenstam, A.; Scholz, F., Eds. Springer Berlin Heidelberg: Berlin, Heidelberg, 2013; 331–332.
97. Chloriding silver wire, Rev 9.1.99. [https://sites.chem.colostate.edu/diverdi/c431/experiments/simultaneous%20spectroscopy%20and%20electrochemistry/apparatus/silver-silver%20chloride%20reference%20electrodes/coating%20silver%20with%](https://sites.chem.colostate.edu/diverdi/c431/experiments/simultaneous%20spectroscopy%20and%20electrochemistry/apparatus/silver-silver%20chloride%20reference%20electrodes/coating%20silver%20with%20)

20silver%20chloride.pdf (accessed 30/10/2019).

98. Napoli, L.; Lavorante, M.; Franco, J.; Sanguinetti, A.; Fasoli, H., Effects on nafion® 117 membrane using different strong acids in various concentrations.
99. Ghani, F.; Kristen, J.; Riegler, H., Solubility Properties of Unsubstituted Metal Phthalocyanines in Different Types of Solvents. *Journal of Chemical & Engineering Data* **2012**, *57* (2), 439–449.
100. Perez, E. F.; Kubota, L. T.; Tanaka, A. A.; Neto, G. D. O., Anodic oxidation of cysteine catalysed by nickel tetrasulphonated phthalocyanine immobilized on silica gel modified with titanium (IV) oxide. *Electrochimica acta* **1998**, *43* (12–13), 1665–1673.
101. Han, J.; Zhang, F.; You, J.; Hiroaki, Y.; Yamada, S.; Morifuji, T.; Wang, S.; Li, X., The first transition metal phthalocyanines: sensitizing rubrene emission based on triplet–triplet annihilation. *Photochemical & Photobiological Sciences* **2017**, *16* (9), 1384–1390.
102. Zagal, J. H.; Bedioui, F., *Electrochemistry of N4 Macrocyclic Metal Complexes*. 2016.
103. Funt, B. L.; Lowen, S. V., Mechanistic studies of the electropolymerization of 2, 2'-bithiophene and of pyrrole to form conducting polymers. *Synthetic metals* **1985**, *11* (3), 129–137.
104. Krische, B.; Zagorska, M., Polythiophene synthesis by electropolymerization of thiophene and bithiophene. *Synthetic metals* **1989**, *33* (3), 257–267.
105. Karan, S.; Mallik, B., Effects of annealing on the morphology and optical property of copper (II) phthalocyanine nanostructured thin films. *Solid State Communications* **2007**, *143* (6–7), 289–294.
106. Zhai, D.; Xu, W.; Zhang, L.; Chang, Y.-T., The role of “disaggregation” in optical probe development. *Chemical Society Reviews* **2014**, *43* (8), 2402–2411.
107. Kolodziejczyk, B.; Mayevsky, D.; Winther-Jensen, B., Enhanced absorption spectra of conducting polymers co-polymerised from thiophene derivatives. *RSC Advances* **2013**, *3* (14), 4568–4573.
108. Isago, H., *Optical spectra of phthalocyanines and related compounds*. Springer: 2015.
109. Schlotter, N. E., 21 - Raman Spectroscopy. In *Comprehensive Polymer Science and Supplements*, Allen, G.; Bevington, J. C., Eds. Pergamon: Amsterdam, 1989; 469–

497.

110. Furukawa, Y.; Akimoto, M.; Harada, I., Vibrational key bands and electrical conductivity of polythiophene. *Synthetic Metals* **1987**, *18* (1), 151–156.

111. Larkin, P. J., Chapter 6 - IR and Raman Spectra–Structure Correlations: Characteristic Group Frequencies. In *Infrared and Raman Spectroscopy (Second Edition)*, Larkin, P. J., Ed. Elsevier: 2018; 85–134.

112. Furukawa, Y.; Akimoto, M.; Harada, I., Vibrational key bands and electrical conductivity of polythiophene. *Synthetic Metals* **1987**, *18* (1–3), 151–156.

113. Atkins, P. W.; De Paula, J.; Keeler, J., *Atkins' physical chemistry*. Oxford university press: 2018.

114. Plieth, W., *Electrochemistry for Materials Science*. 2008.

115. Makino, S.; Kitazumi, Y.; Nishi, N.; Kakiuchi, T., Charging current probing of the slow relaxation of the ionic liquid double layer at the Pt electrode. *Electrochemistry Communications* **2011**, *13* (12), 1365–1368.

116. Oh, Y.; Vrabel, H.; Guidoux, S.; Hu, X., Electrochemical reduction of CO₂ in organic solvents catalyzed by MoO₂. *Chemical Communications* **2014**, *50* (29), 3878–3881.

117. Wanninayake, N.; Ai, Q.; Zhou, R.; Hoque, M. A.; Herrell, S.; Guzman, M.; Risko, C.; Kim, D., Understanding the effect of host structure of nitrogen doped ultrananocrystalline diamond electrode on electrochemical carbon dioxide reduction. *Carbon* **2019**.

118. Hashiba, H.; Sato, H. K.; Yotsuhashi, S.; Fujii, K.; Sugiyama, M.; Nakano, Y., A broad parameter range for selective methane production with bicarbonate solution in electrochemical CO₂ reduction. *Sustainable Energy & Fuels* **2017**, *1* (8), 1734–1739.

119. Hashiba, H.; Weng, L.-C.; Chen, Y.; Sato, H. K.; Yotsuhashi, S.; Xiang, C.; Weber, A. Z., Effects of Electrolyte Buffer Capacity on Surface Reactant Species and the Reaction Rate of CO₂ in Electrochemical CO₂ Reduction. *The Journal of Physical Chemistry C* **2018**, *122* (7), 3719–3726.

120. Zhu, M.; Ye, R.; Jin, K.; Lazouski, N.; Manthiram, K., Elucidating the Reactivity and Mechanism of CO₂ Electroreduction at Highly Dispersed Cobalt Phthalocyanine. *ACS Energy Letters* **2018**, *3* (6), 1381–1386.

121. König, M.; Vaes, J.; Klemm, E.; Pant, D., Solvents and Supporting Electrolytes in the Electrocatalytic Reduction of CO₂. *iScience* **2019**, *19*, 135.
122. Han, N.; Wang, Y.; Ma, L.; Wen, J.; Li, J.; Zheng, H.; Nie, K.; Wang, X.; Zhao, F.; Li, Y.; Fan, J.; Zhong, J.; Wu, T.; Miller, D. J.; Lu, J.; Lee, S.-T.; Li, Y., Supported Cobalt Polyphthalocyanine for High-Performance Electrocatalytic CO₂ Reduction. *Chem* **2017**, *3* (4), 652–664.
123. Zhu, M.; Chen, J.; Guo, R.; Xu, J.; Fang, X.; Han, Y.-F., Cobalt phthalocyanine coordinated to pyridine-functionalized carbon nanotubes with enhanced CO₂ electroreduction. *Applied Catalysis B: Environmental* **2019**, *251*, 112–118.
124. Morlanés, N.; Takanabe, K.; Rodionov, V., Simultaneous reduction of CO₂ and splitting of H₂O by a single immobilized cobalt phthalocyanine electrocatalyst. *ACS Catalysis* **2016**, *6* (5), 3092–3095.
125. Wolf, A. V., Aqueous solutions and body fluids; their concentrative properties and conversion tables. **1966**.
126. Weast, R. C.; Astle, M. J.; Beyer, W. H., *CRC handbook of chemistry and physics*. CRC press Boca Raton, FL: 1988; Vol. 69.
127. Hagen, J., *Industrial catalysis: a practical approach*. John Wiley & Sons: 2015.
128. Lin, S.; Diercks, C. S.; Zhang, Y.-B.; Kornienko, N.; Nichols, E. M.; Zhao, Y.; Paris, A. R.; Kim, D.; Yang, P.; Yaghi, O. M.; Chang, C. J., Covalent organic frameworks comprising cobalt porphyrins for catalytic CO₂ reduction in water. *Science* **2015**, *349* (6253), 1208–1213.
129. Morlanés, N.; Takanabe, K.; Rodionov, V., Simultaneous Reduction of CO₂ and Splitting of H₂O by a Single Immobilized Cobalt Phthalocyanine Electrocatalyst. *ACS Catalysis* **2016**, *6* (5), 3092–3095.
130. Kramer, W. W.; McCrory, C. C. L., Polymer coordination promotes selective CO₂ reduction by cobalt phthalocyanine. *Chemical Science* **2016**, *7* (4), 2506–2515.
131. Short, G. D.; Bishop, E., Concentration Overpotentials on Antimony Electrodes in Differential Electrolytic Potentiometry. *Analytical Chemistry* **1965**, *37* (8), 962–967.
132. MH, C.; SOLUTIONS, H., 9. KINETIC THEORY OF GASES. **1950**.



จุฬาลงกรณ์มหาวิทยาลัย
CHULALONGKORN UNIVERSITY



APPENDIX

จุฬาลงกรณ์มหาวิทยาลัย
CHULALONGKORN UNIVERSITY

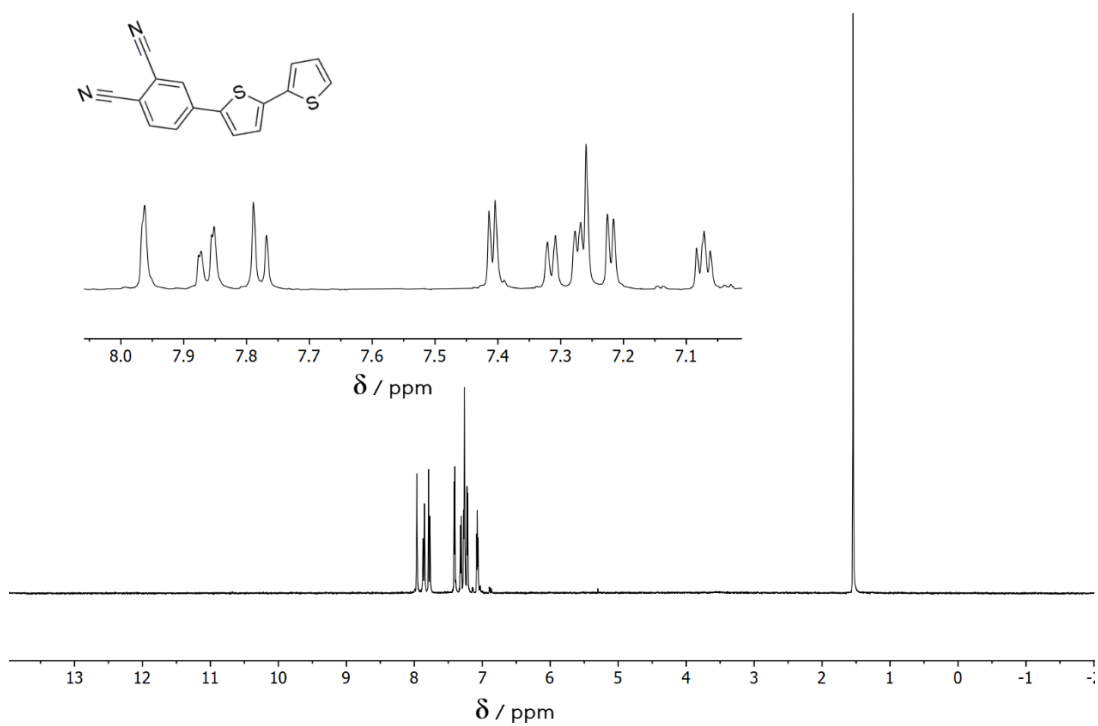


Figure A-1. A ¹H-NMR spectrum of compound 1 in CDCl₃

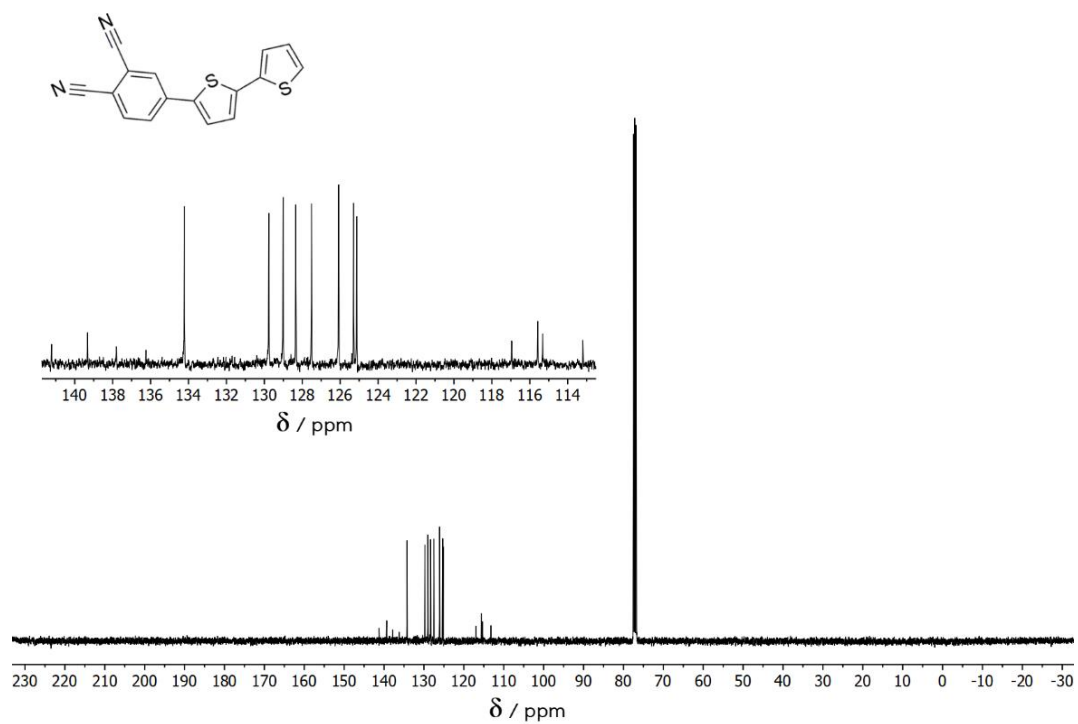


Figure A-2. A ¹³C-NMR spectrum of compound 1 in CDCl₃

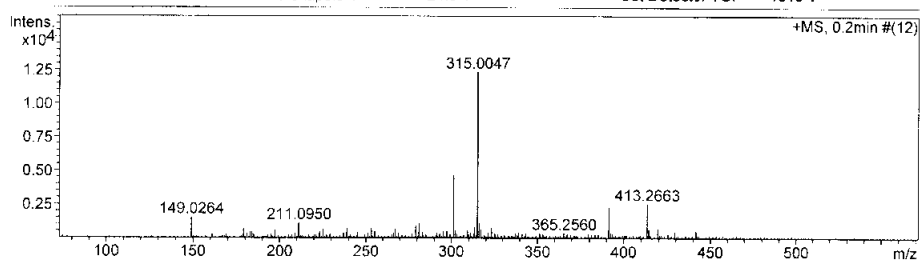
Mass Spectrum List Report

Analysis Info

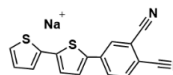
Analysis Name	OSCUHS5807270011.d	Acquisition Date	7/28/2015 1:51:19 PM
Method	Tune_low_POS_Natee20130403.m	Operator	Administrator
Sample Name	Thio-cyano	Instrument	micrOTOF 72
	Thio-cyano		

Acquisition Parameter

Source Type	ESI	Ion Polarity	Positive	Set Corrector Fill	79 V
Scan Range	n/a	Capillary Exit	120.0 V	Set Pulsar Pull	406 V
Scan Begin	50 m/z	Hexapole RF	130.0 V	Set Pulsar Push	388 V
Scan End	3000 m/z	Skimmer 1	45.0 V	Set Reflector	1300 V
		Hexapole 1	24.3 V	Set Flight Tube	9000 V
				Set Detector TOF	1910 V



#	m/z	I	I%	S/N	FWHM	Res.
1	149.0264	1549	12.5	169.2	0.0237	6300
2	179.0734	674	5.4	65.2	0.0272	6595
3	184.1120	463	3.7	43.8	0.0317	5810
4	197.0827	592	4.8	53.6	0.0344	5734
5	211.0950	1120	9.1	97.0	0.0371	5686
6	225.1070	674	5.4	55.7	0.0429	5251
7	239.1261	708	5.7	56.0	0.0851	2811
8	253.1296	687	5.6	52.1	0.0669	3785
9	255.1609	496	4.0	37.3	0.0393	6487
10	267.1444	676	5.5	49.2	0.0792	3372
11	279.1634	926	7.5	65.4	0.0542	5150
12	281.1695	1105	8.9	77.6	0.0569	4945
13	283.1422	442	3.6	30.7	0.0913	3100
14	295.1700	526	4.3	35.4	0.1033	2858
15	297.2164	432	3.5	28.9	0.1117	2661
16	301.1427	4678	37.8	313.0	0.0429	7023
17	302.1481	549	4.4	36.3	0.0480	6295
18	309.1929	594	4.8	38.6	0.0760	4069
19	313.1754	818	6.6	52.8	0.0586	5343
20	315.0047	12369	100.0	799.7	0.0418	7536
21	316.0078	1128	9.1	72.4	0.0448	7048
22	317.0015	627	5.1	40.0	0.0425	7457
23	321.2351	437	3.5	27.5	0.0612	5246
24	323.1588	740	6.0	46.6	0.0609	5304
25	391.2872	2266	18.3	147.5	0.0503	7776
26	413.2663	2565	20.7	172.6	0.0636	6498
27	414.2710	545	4.4	36.3	0.0734	5640
28	419.3144	740	6.0	49.9	0.0542	7735
29	429.2445	477	3.9	32.5	0.0721	5953
30	441.2957	565	4.6	39.3	0.0748	5897



Analysis	
<input checked="" type="checkbox"/> Formula:	C ₁₆ H ₈ N ₂ NaS ₂ ⁺
<input checked="" type="checkbox"/> Exact Mass:	315.0021
<input checked="" type="checkbox"/> Mol. Wt.:	315.3632
<input checked="" type="checkbox"/> m/z:	315.0021 (100.0%), 316.0055 (17.3%)
<input checked="" type="checkbox"/> Elem. Anal.:	C, 60.94; H, 2.56; N, 8.88; Na, 7.29; S, 20.33
Paste	

Figure A-3. HR-ESI mass spectrum of compound 1

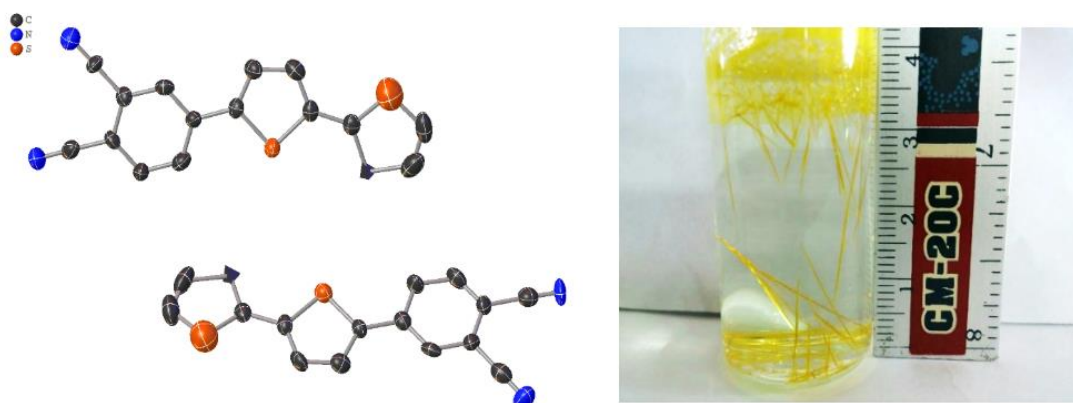


Figure A-4. Crystal Data for $C_{32}N_4S_4$ (**1**): triclinic, space group P-1 (no. 2), $a = 7.6076$ (14) Å, $b = 12.529(2)$ Å, $c = 15.757(3)$ Å, $\alpha = 105.655(5)^\circ$, $\beta = 100.619(5)^\circ$, $\gamma = 104.030(5)^\circ$, $V = 1352.0(4)$ Å³, $Z = 2$, $T = 296.15$ K, $\mu(\text{MoK}\alpha) = 0.381$ mm⁻¹, $D_{\text{calc}} = 1.397$ g/cm³, 16102 reflections measured ($2.786^\circ \leq 2\theta \leq 48.478^\circ$), 4322 unique ($R_{\text{int}} = 0.0520$, $R_{\text{sigma}} = 0.0669$) which were used in all calculations. The final R_1 was 0.1516 ($I > 2\sigma(I)$) and wR_2 was 0.4738 (all data).

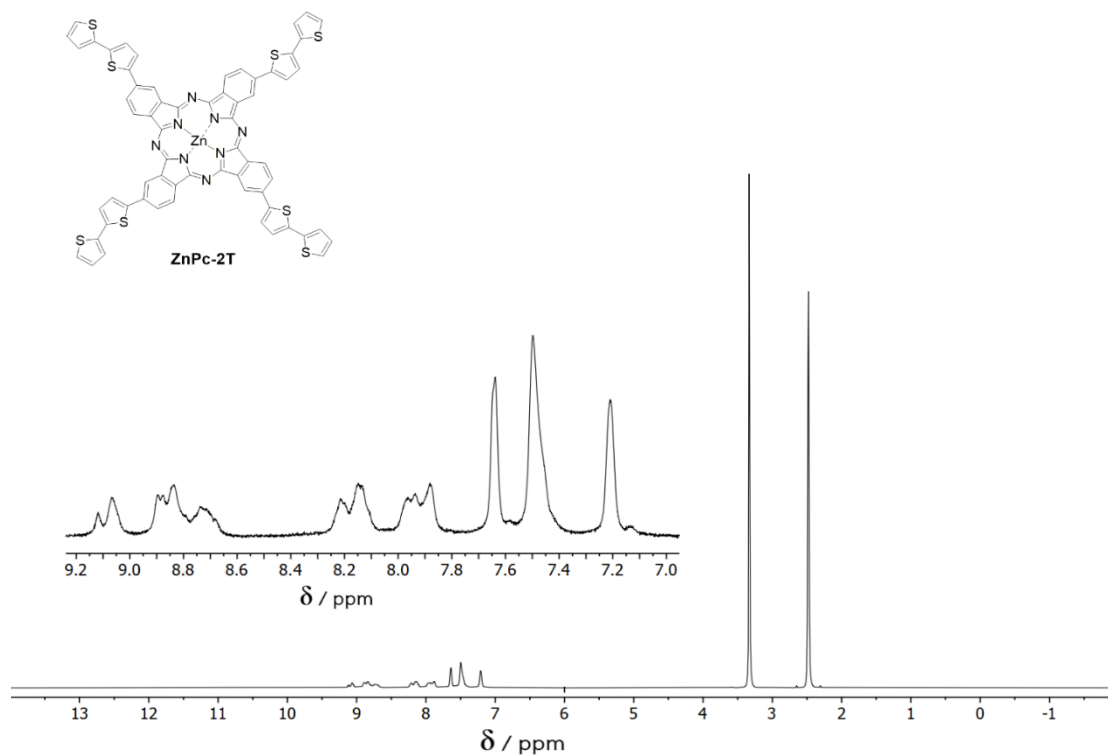


Figure A-5. A $^1\text{H-NMR}$ spectrum of ZnPc-2T in $(\text{CD}_3)_2\text{SO}$.

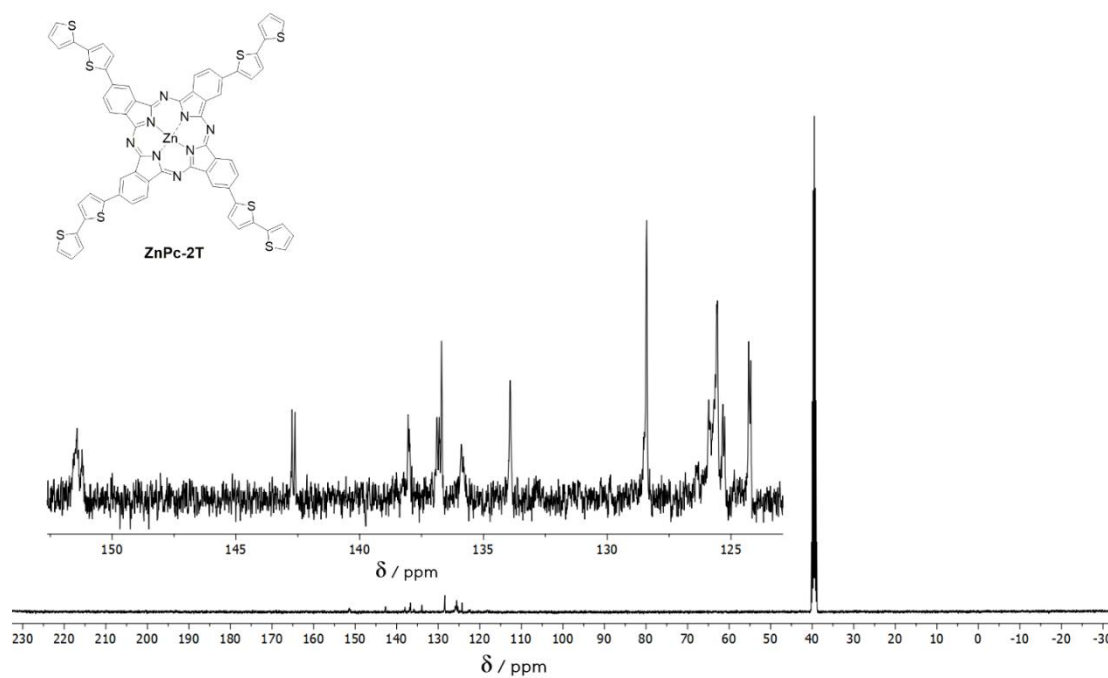


Figure A-6. A $^{13}\text{C-NMR}$ spectrum of ZnPc-2T in $(\text{CD}_3)_2\text{SO}$.

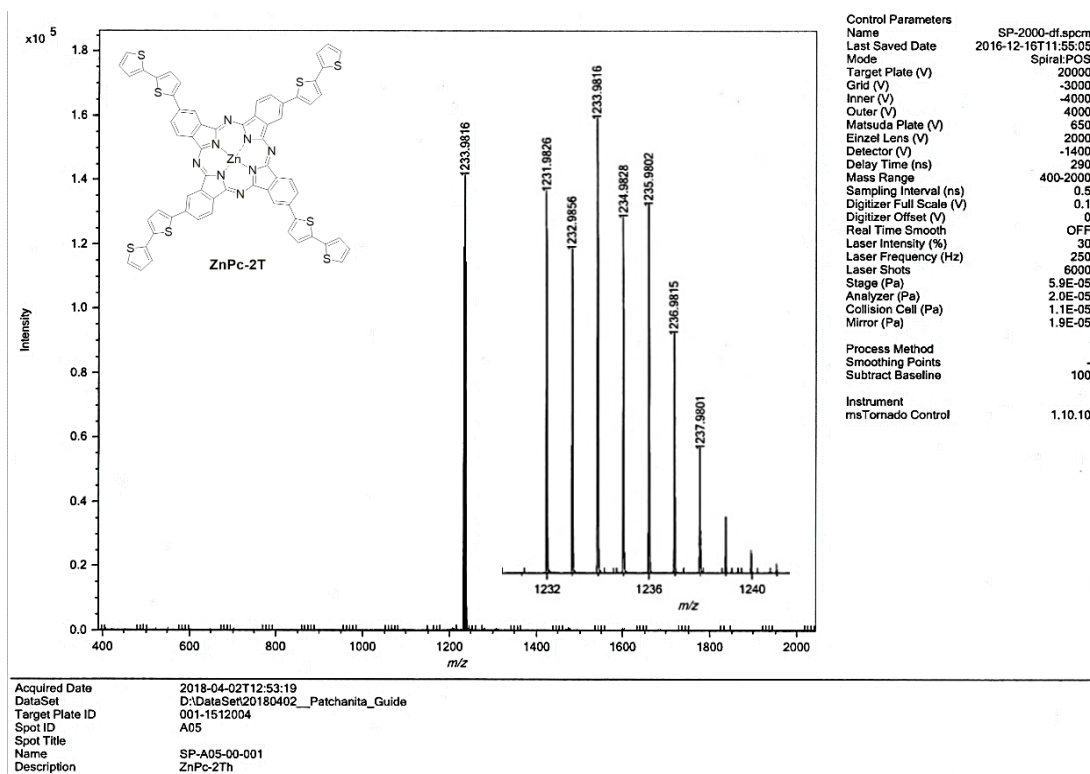


Figure A-7. A HR-MALDI-TOF mass spectrum and an isotopic pattern of a molecular ion peak of ZnPc-2T.

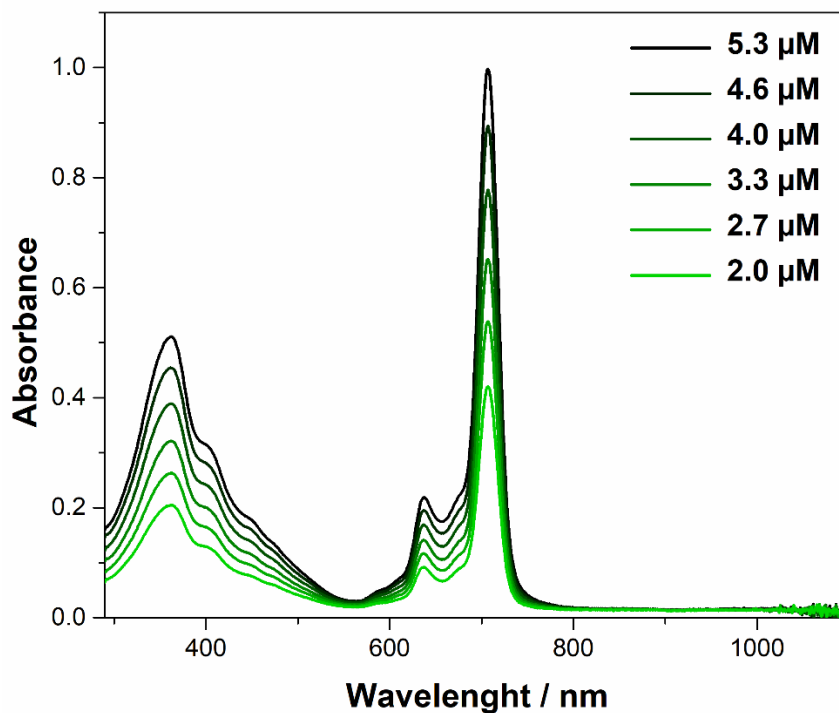


Figure A-8. Absorption spectra of ZnPc-2T in THF.

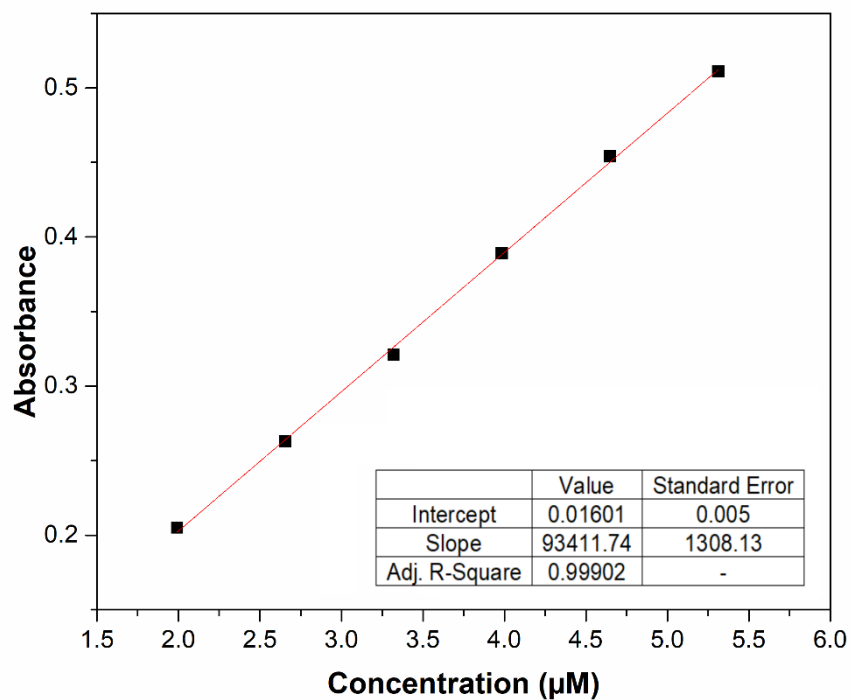


Figure A-9. A calibration curve for absorption at 362 nm of ZnPc-2T in THF.

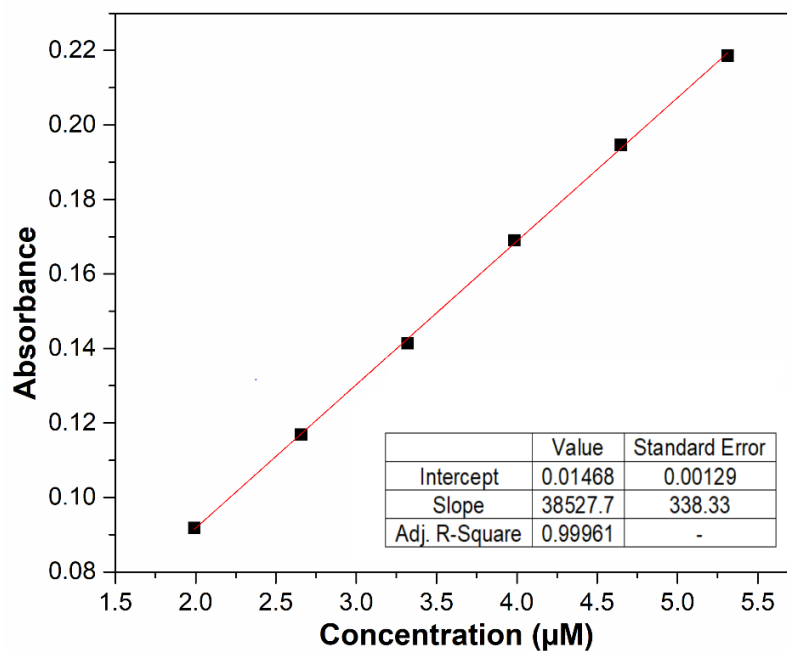


Figure A-10. A calibration curve for absorption at 637 nm of ZnPc-2T in THF.

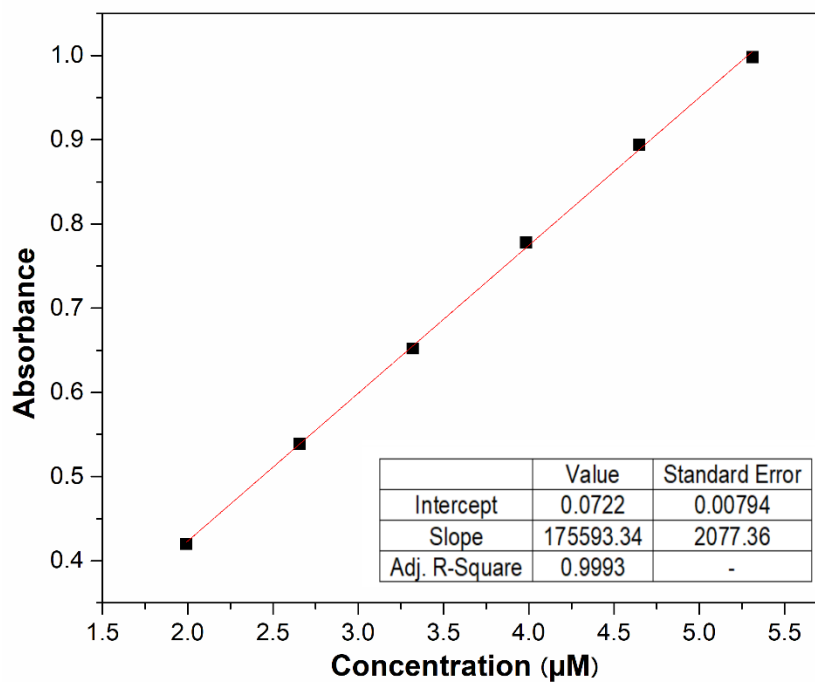


Figure A-11. A calibration curve for absorption at 707 nm of ZnPc-2T in THF.

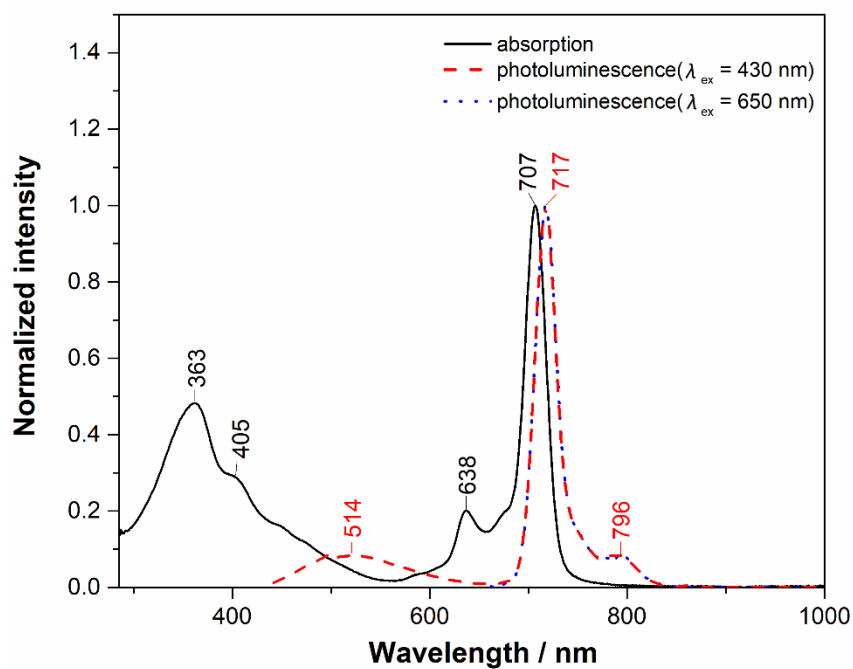


Figure A-12. Absorption and photoluminescence spectra of ZnPc-2T in THF.

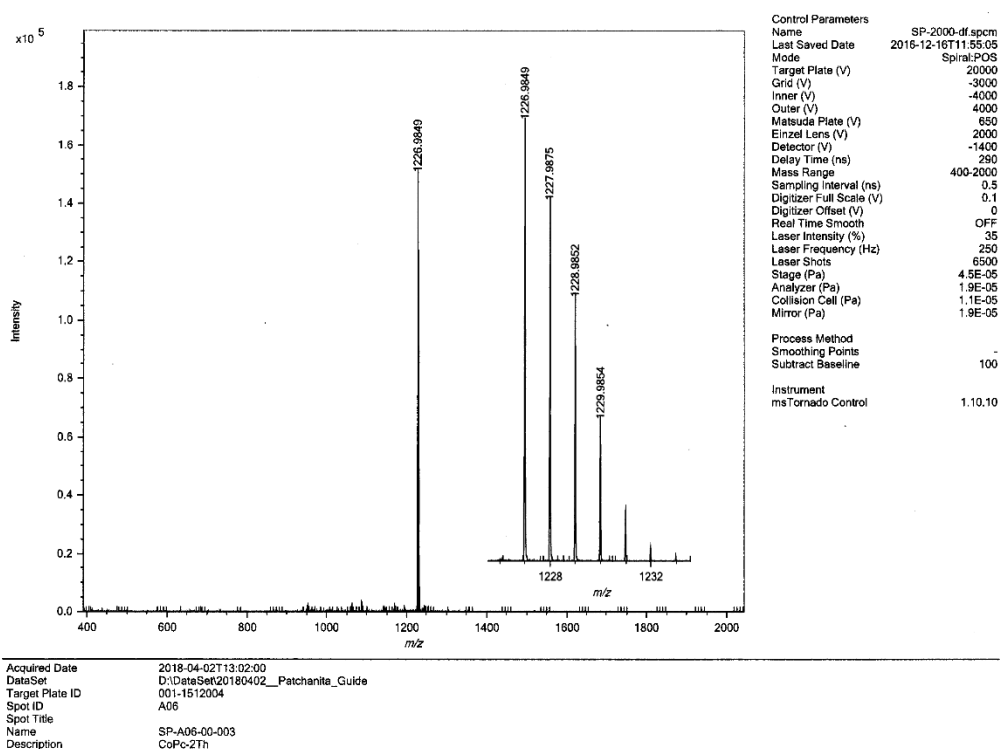


Figure A-13. A HR-MALDI-TOF mass spectrum and an isotopic pattern of a molecular ion peak of CoPc-2T

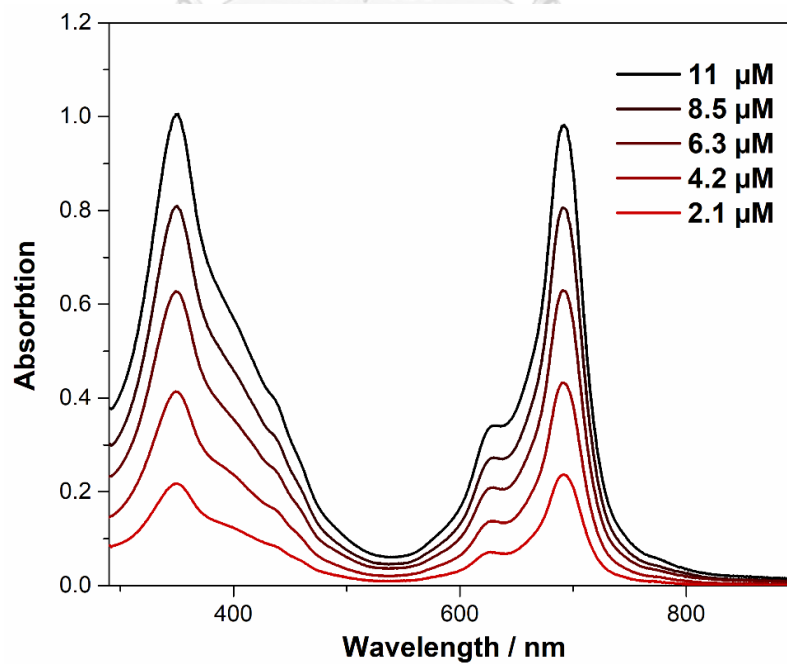


Figure A-14. Absorption spectra of CoPc-2T in THF.

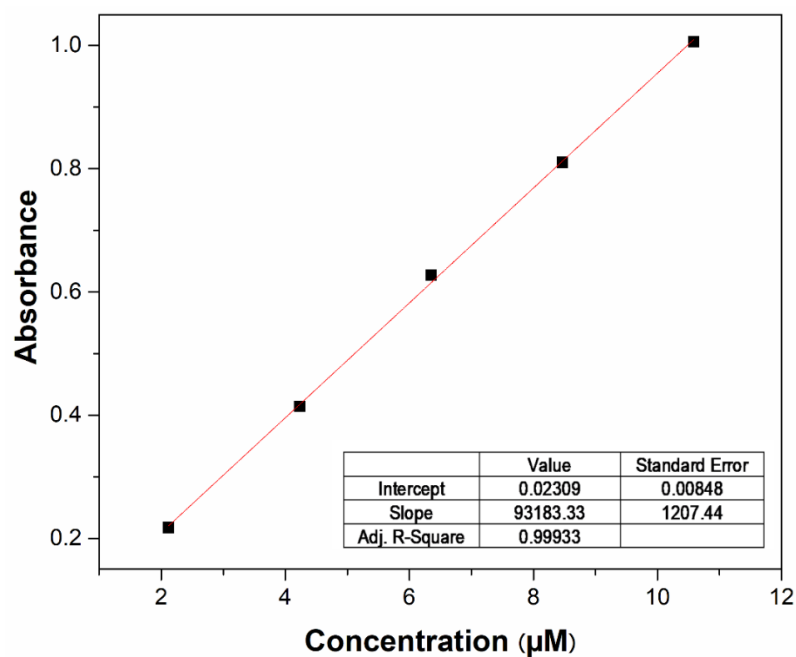


Figure A-15. A calibration curve for absorption at 351 nm of CoPc-2T in THF

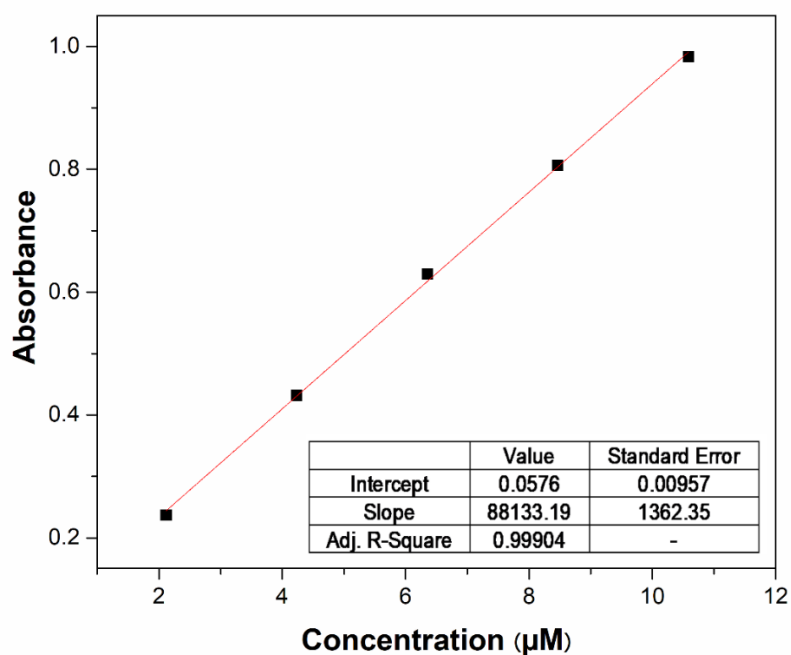


Figure A-16. A calibration curve for absorption at 692 nm of CoPc-2T in THF

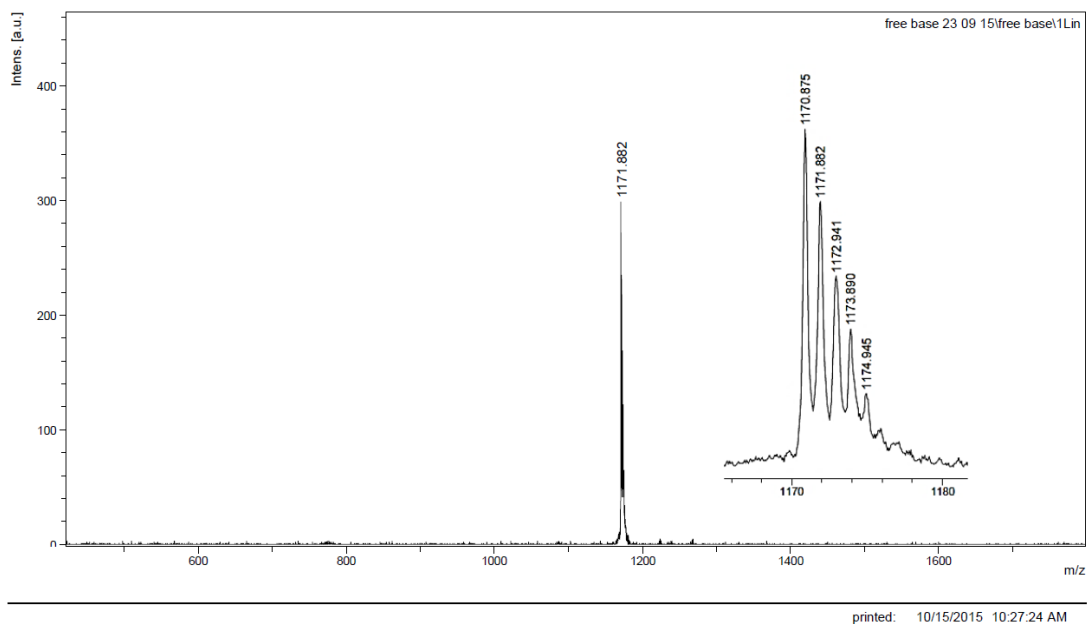


Figure A-17. A MALDI-TOF mass spectrum and an isotopic pattern of a molecular ion peak of H_2Pc-2T .

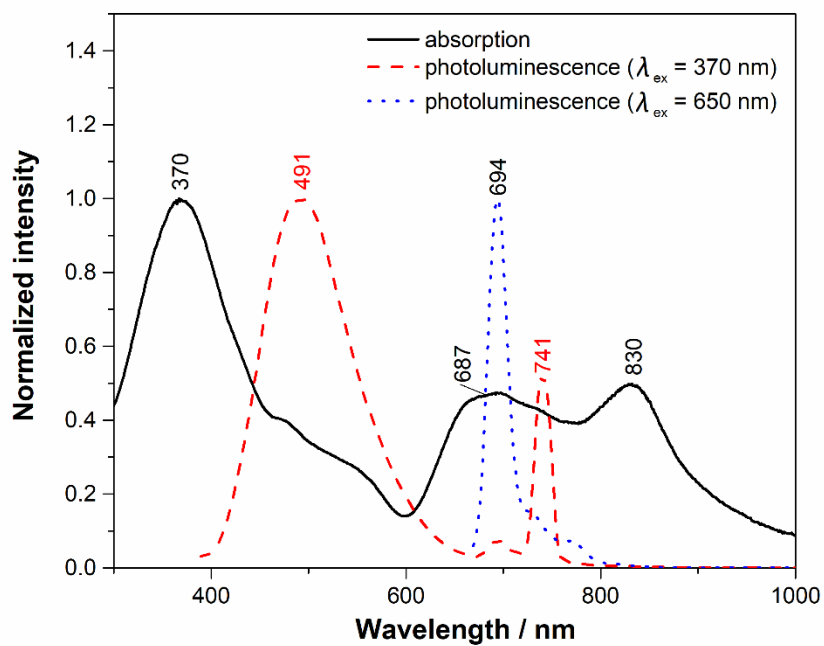


Figure A-18. Absorption and photoluminescence spectra of H_2Pc-2T in THF.

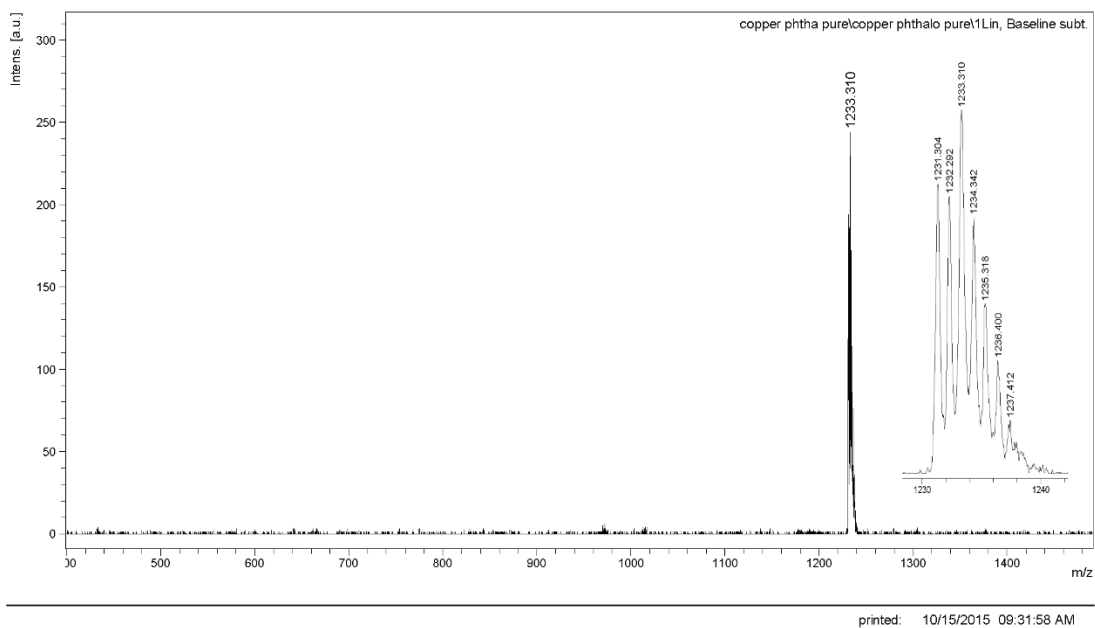


Figure A-19. A MALDI-TOF mass spectrum and an isotopic pattern of a molecular ion peak of CuPc-2T.

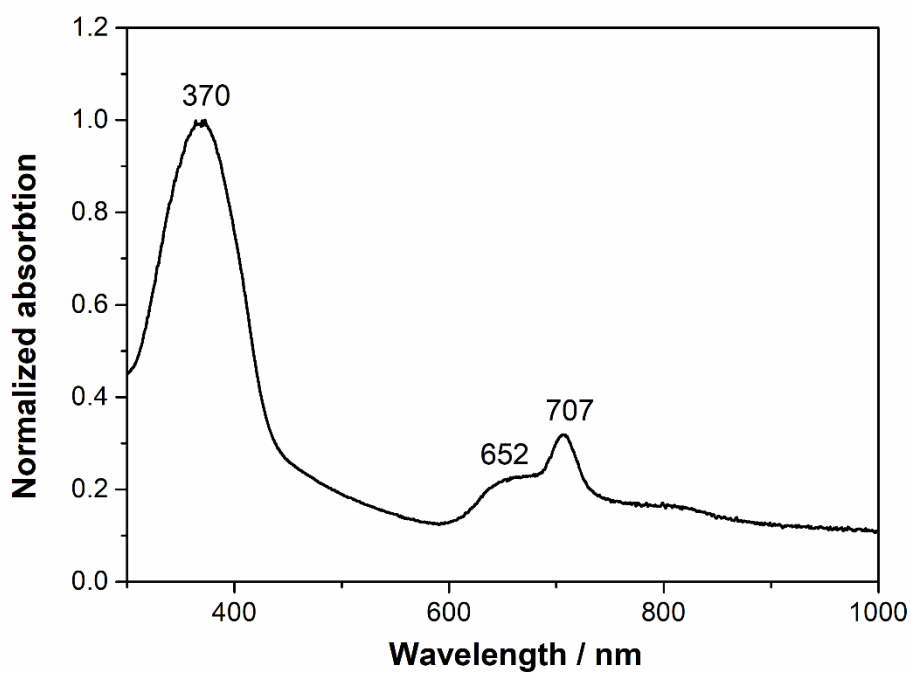


Figure A-20. Absorption spectra of CuPc-2T in THF.

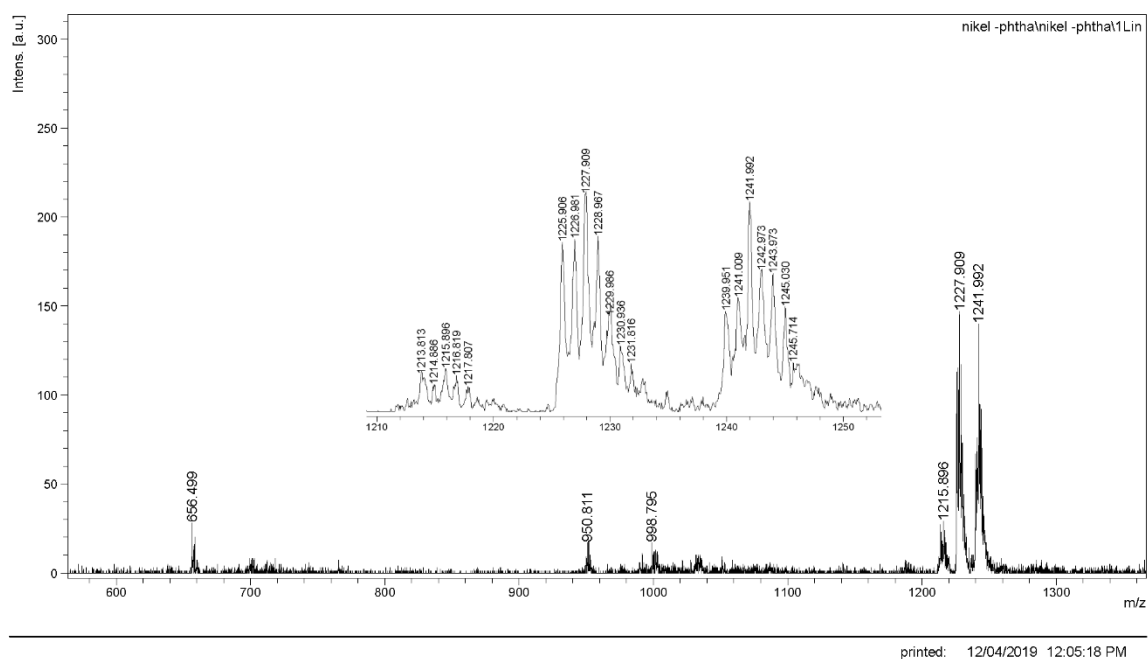
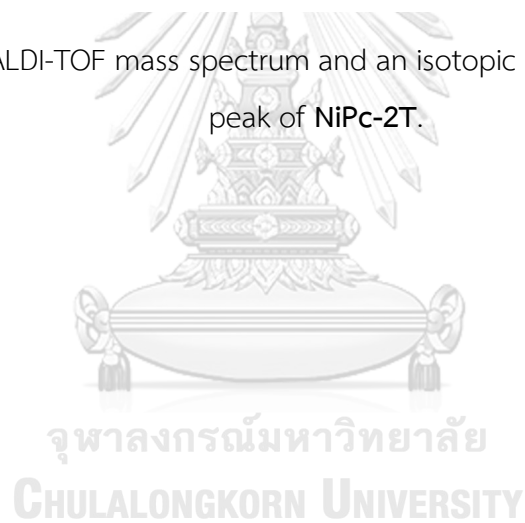


Figure A-21. A MALDI-TOF mass spectrum and an isotopic pattern of a molecular ion peak of NiPc-2T.



Electrochemical data, calculation for active surface of poly(CoPc-2T) on carbon paper

Due to the effect of hydrogen evolution in water media causing the over potential and having some interference with active surface area,^{66, 131} The experiments in N₂-saturated 0.1 M TBAPF₆ DMF solution and electrochemical setup of cyclic voltammetry in N₂-glove box were performed. The current density vs. time was plotted. And then, the background current density was subtracted in order to be able to integrate average charge (Q) for one electron reduction (**Figure A-19**). The mole of active surface area was calculated by following this equation:

Average Q = 3.64 × 10⁻³ coulombs from J/time curve

$$n = \frac{Q}{F} = \frac{3.64 \times 10^{-3} \text{ C}}{96485 \frac{\text{C}}{\text{mol e}^{-}}} = 3.78 \times 10^{-8} \text{ mol e}^{-}$$

Approximately 1 unit of **poly(CoPc-2T)** get each 1 electron with 100 % Faradaic efficiency under this range of the applied potential.

$$\text{Mole of active poly(CoPc-2T)} = 3.78 \times 10^{-8} \text{ mol e}^{-} \left(\frac{1 \text{ mol poly(CoPc-2T)}}{1 \text{ mol e}^{-}} \right) = 3.78 \times 10^{-8} \text{ mol}$$

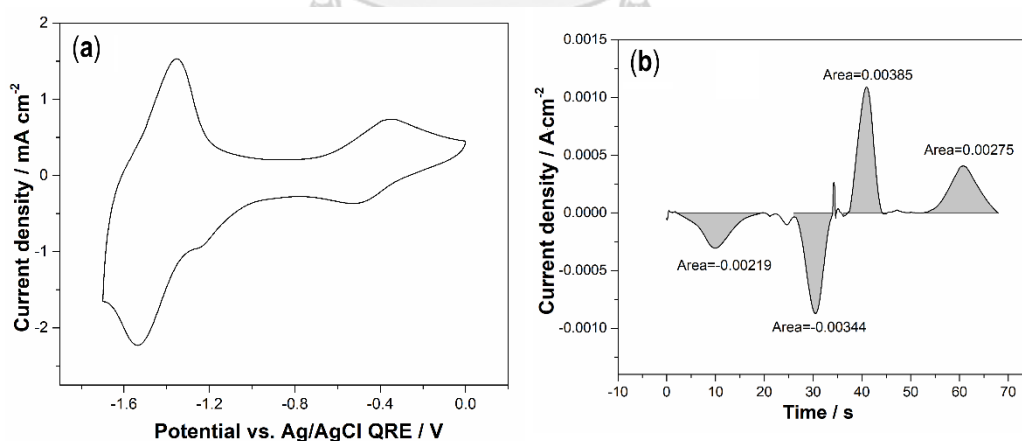


Figure A-22. a) Cyclic voltammogram (CV) of the **poly(CoPc-2T)**-modified carbon paper in N₂-saturated 0.1 M TBAPF₆ DMF solution with scan rate of 50 mV·s⁻¹ b) a Current density vs. time curve, corresponding with CV curve.

Calculation of %FE of CO formation from 2-h batch experiments.

The results from CPE measurement and batch GC analysis at best applied potential of -1.3 V vs. Ag/AgCl (3M KCl) for 2 h under CO₂-saturated 0.5 M KHCO₃ aqueous solution were used to be sample for calculation of the %FE of CO formation.

$$\% \text{ Faradaic efficiency} = \frac{e_{\text{output}}}{e_{\text{input}}} \times 100 \dots \text{ref}^{77}$$

e_{input} = The total number of moles of electrons measured during electrolysis

e_{output} = No. of moles of electrons required for reducing CO₂ to CO

$$e_{\text{input}} = n = \frac{Q}{F} = \frac{It}{F} = \frac{\text{Integrated It curve}}{\text{Faradaic constant}} = \frac{15.3 \text{ C}}{96485 \frac{\text{C}}{\text{mol e}^-}} = 1.59 \times 10^{-4} \text{ mol e}^-$$

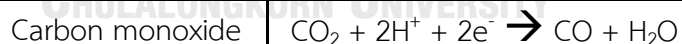
Volume of measured CO from GC = 4.92 % which was calibrated from standard gas
Head space = 38 mL which was calibrated with real volume of gas in head space without including volume of electrodes

$$\text{Volume(mL) of CO} = 38 \text{ mL} \times 0.0492 = 1.87 \text{ mL}$$

Conversion from Volume to mole by using below gas's law equation:¹³²

$$n = \frac{PV}{RT}$$

$$n = \frac{(1 \text{ atm})(1.87 \times 10^{-3} \text{ L})}{0.08206 \text{ L}\cdot\text{atm}/(\text{mol}\cdot\text{K})(298.15\text{K})} = 7.65 \times 10^{-5} \text{ mol CO}$$



$$e_{\text{output}} = 7.65 \times 10^{-5} \text{ mol of CO} \times \frac{2 \text{ mol of e}^-}{1 \text{ mol of CO}} = 1.53 \times 10^{-4} \text{ mole e}^-$$

$$\% \text{ Faradaic efficiency of CO} = \frac{e_{\text{output}}}{e_{\text{input}}} \times 100 = \frac{1.53 \times 10^{-4} \text{ mole e}^-}{1.59 \times 10^{-4} \text{ mol e}^-} \times 100 = 96.2 \%$$

In case of the concern condition of CO₂-saturated condition, the CPE measurements were conducted at least three times with fresh preparation of **poly(CoPc-2T)**-modified electrode and electrolyte solution to report in statistic value.

Calculation of %FE of CO formation from 20-h online GC experiments.

The results from CPE measurement and online GC analysis at best applied potential of -1.3 V vs. Ag/AgCl (3M KCl) for 20 h under CO₂-saturated 0.5 M KHCO₃ aqueous solution were used to be sample for calculation of the %FE of CO formation.

$$\% \text{ Faradaic efficiency} = \frac{e_{\text{output}}}{e_{\text{input}}} \times 100$$

e_{input} = The total number of moles of electrons measured during electrolysis

e_{output} = No. of moles of electrons required for reducing CO₂ to CO

$$e_{\text{input}} = n = \frac{Q}{F} = \frac{It}{F} = \frac{\text{Integrated It curve per 30 min}}{\text{Faradaic constant}} = \frac{3.25 C}{\frac{96485}{\text{mol e}^-}} = 3.37 \times 10^{-5} \text{ mol}$$

Amount of %CO measured from GC = 0.1009 (% CO is calibrated from standard gas of CO in N₂)

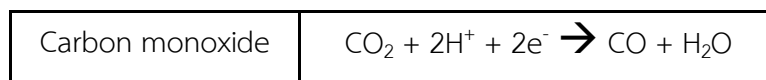
Gases in head space are measured in every 30 min.

Amount of produced CO = %CO × flow rate(ml/min.) × time(min.)

$$\begin{aligned} &= \frac{0.1009}{100} \times \frac{10 \text{ ml}}{1 \text{ min}} \times 30 \text{ min.} \\ &= 0.3027 \text{ ml} \end{aligned}$$

Conversion from Volume to mole by using below equation:

$$n = \frac{PV}{RT} = \frac{(1 \text{ atm})(0.3027 \times 10^{-3} \text{ L})}{0.08206 \text{ L}\cdot\text{atm}/(\text{mol}\cdot\text{K})(298.15\text{K})} = 1.24 \times 10^{-5} \text{ mol CO}$$



$$e_{\text{output}} = 1.24 \times 10^{-5} \text{ mol CO} \times \frac{2 \text{ mol of e}^-}{1 \text{ mol of CO}} = 2.48 \times 10^{-5} \text{ mole e}^-$$

$$\% \text{ Faradaic efficiency of CO} = \frac{e_{\text{output}}}{e_{\text{input}}} \times 100 = \frac{2.48 \times 10^{-5} \text{ mole e}^-}{3.37 \times 10^{-5} \text{ mol e}^-} = 73.5 \%$$

Calculation of turn over number (TON)

$$\begin{aligned} \text{TON} &= \frac{\text{Moles of accumulated product formed}}{\text{Moles of active surface area}} \dots\dots\dots \text{ref}^{128} \\ &= \frac{4.67 \times 10^{-4} \text{ mol CO}}{3.78 \times 10^{-8} \text{ mol CoPc-2T}} = 12,354 \end{aligned}$$

Calculation of turn over frequency (TOF)

$$\begin{aligned} \text{TOF} &= \frac{\text{TON}}{\text{Time}} \dots\dots\dots \text{ref}^{128} \\ &= \frac{12,354}{20 \times 3600 \text{ s}} = 0.17 \text{ s}^{-1} \end{aligned}$$



VITA

NAME Mr. Jirapong Luangchaiyaporn

DATE OF BIRTH 11 June 1991

PLACE OF BIRTH Kanchanaburi

INSTITUTIONS ATTENDED [Since 2014] PhD Student, Chemistry, Faculty of Science, Chulalongkorn University, Bangkok
[2009–2014] BSc, Chemistry, Faculty of Science, Slipakorn University, Nakhon pathom (GPA 3.67, First Class Honor)
[2003–2009] Visuttharangsi School, Kanchanaburi
[1994–2003] Thavorn Wittaya School, Kanchanaburi

HOME ADDRESS 232/6, Soi Bunsom, Tha Makham Sub-District, Muang Kanchaburi, Kanchanaburi, 71000

AWARD RECEIVED [2019] The 90th Anniversary of Chulalongkorn University Fund, Graduate School of Chulalongkorn University: Research Scholarship
[Jun.–Dec. 2018] Graduate School of Chulalongkorn University Fund: Overseas Research Experience Scholarship for Graduate Students (Austria)
[May–Jun. 2016] The international Promovieren an Der TU Chemnitz (InProTUC) Fund: PhD candidates to conduct research aboard (Germany)
[2004–2019] Science Achievement Scholarship of Thailand (SAST): BSc to PhD Scholarship